ELECTROLYSIS SYSTEM FOR GENERATION AND DELIVERY OF OXYGEN

ELECTROLYSIS-BASED SYSTEM FOR GENERATION AND DELIVERY OF OXYGEN TO MICROFLUIDIC OXYGENATOR UNIT FOR PRETERM NEONATES WITH RESPIRATORY DISTRESS SYNDROME

By

Melizeth Mazumdar Bolanos

A Thesis Submitted to the School of Graduate Studies in Partial
Fulfillment of the Requirement for the Degree Master of Applied Science

McMaster University

MASTER OF APPLIED SCIENCE (2017) McMaster University
(School of Biomedical Engineering) Hamilton, ON

TITLE:	Electrolysis-based system for generation and delivery of oxygen to microfluidic oxygenator unit for preterm neonates with respiratory distress syndrome.
AUTHOR:	Melizeth Mazumdar Bolanos, B.E. (UABC, Mexico)
SUPERVISOR:	Dr. Ravi Selvaganapathy
NUMBER OF PAGES:	*(xi, 151)*

ABSTRACT

Respiratory distress syndrome (RDS) is a major cause of mortality and long-term morbidity annually affecting 14% preterm infants worldwide. Therapies have been developed to overcome this common disorder; however, limitations exist with these treatments that often lead to complications including bronchopulmonary dysplasia (BPD). One approach to address RDS is to implement a microfluidic oxygenator that serves as a respiratory support system for preterm neonates while the lungs fully develop, extra-uterine. This artificial lung assist device (LAD) is characterised by its non-invasiveness (given that it is connected via umbilical vessels), pumpless configuration, ambient air operation, portability and low priming volume. Furthermore, the LAD is formed by single oxygenator units (SOU) that are stacked in a parallel array which allows for usage on different body weights.

The objective of this thesis is to design an electrochemical system to provide an in-situ enriched O_2 environment able to supply 1.9 ml O_2/min for use in the SOU while maintaining the simplicity of operation of the oxygenator. An inexpensive, electrically powered and compact device was envisioned allowing for a higher permeation flux to fully oxygenate the blood. Moreover, the system would be easy to manufacture, low maintenance and avoid the risk of gas contamination.

In the initial work, different designs of electrolytic cells were developed and tested. The two-chamber design connected by a gel membrane showed an O_2 production 10 times higher than with previous designs with 42 mg O_2/L. Subsequently, different supporting electrolytes were tested. NaOH demonstrated a better performance and no degradation of the electrode in contrast to NaCl and Na_2SO_4. Stainless steel mesh (SSM) and graphite sheet electrodes were then tested; it was observed that stainless steel produced 3.4 times more dissolved oxygen (DO) than graphite with

28.3 mg O_2/L. Experimentation with electrolysis of water showed that the DO in water reached stability 3 min after the electrolysis process was initiated measuring a change of DO of 29 mg/L at 3 A. Furthermore, an active oxygenation (AO) system was developed for in-vitro experiments via electrolysis of water and compared to a passive oxygenation (PO) system exposing blood to enriched O_2 air and ambient air, respectively. It was demonstrated that AO provided 300% greater oxygenation to blood than PO.

The electrolysis chamber designed for the microfluidic oxygenator allows the oxygenator to maintain its essential characteristics of simplicity and low cost while increasing the rate of oxygenation of blood. Preterm neonates suffering from RDS need an artificial lung that can partially support the oxygenation of their blood. Thus, combining the oxygenator with the O_2 generation in-situ system enables a greater blood O_2 uptake of 300% making possible the development of an efficient artificial lung.

ACKNOWLEDGEMENTS

All through my stay in Canada I was lucky to have people around me that offered their support and friendship. My studies at McMaster would have been different without all these people that I met along this journey. I am truly grateful for the support of my supervisor, Dr. Ravi Selvaganapathy. Thank you for your guidance and willingness to help. You are an excellent supervisor who is always devoted to your students. I would also like to thank Dr. Gerhard Fusch and Dr. Christophe Fusch who provided me with the tools and resources to successfully conduct my research. Thank you, Dr. Leslie Berry and Dr. Helen Atkinson, for your knowledge and input in the monthly meetings. Thanks to CONACYT for funding my studies.

I was lucky to work with Darren, Harpreet and Mohammad, members of the oxygenator project. You made the project enjoyable and our Friday coffee meetings are something that I will never forget. Thank you for all the input you provided to my research and for your willingness to help me move forward with the project. Thank you, guys, for your time. Darren, many thanks for all your meaningful help and support while I was writing this thesis.

My dear friend Caty, thanks a lot for being there for me, for listening my seminar rehearsal so many times. Sreekant, thanks for your endless help, I really appreciate it. Larona and Ale, Michael, Shayan, Monika, Celine, Rana, Sudip, Eric, Ian, Alex, Eduardo, Pedro, Ana Lau, Isra, Veronika, Eli, Clau and so many others, for your friendship and help.

Last, but certainly not least, I would like to thank my Mom for always being there for me, especially when I needed it the most. Mom you have always encouraged me to take whatever path I see fit. Without your love and support I would not have any of the accomplishments that I have today. Thanks Jaz for all the help and friendship you offered to me without even knowing me.

TABLE OF CONTENTS

Abstract ..... **iii**

Acknowledgements ..... **v**

List of Figures and Tables ..... **viii**

List of Abbreviations ..... **x**

Glossary ..... **xi**

Motivation and Thesis Organization **1**
1.1 Sequence of Chapters 2

Introduction **3**
2.1 Respiratory Failure 3
2.1.1 Surfactant Replacement Therapy *4*
2.1.2 Continuous Positive Airway Pressure *5*
2.1.3 Assisted Ventilation *5*
2.1.4 Extracorporeal Membrane Oxygenation *6*
2.1.5 Artificial placenta *7*

Literature Review **10**
3.1 History of Blood Oxygenation Devices 10
3.1.1 Direct Contact Oxygenators *11*
3.1.2 Indirect contact oxygenators *11*
3.2 Artificial Placenta 26
3.3 Oxygenators Performance with Ambient Air 31
3.3.1 In-vitro Experiments *31*
3.3.2 In-vivo Experiments *34*
3.4 Oxygenators Performance with Pure Oxygen 35
3.4.1 In-vitro Testing of Microfluidic Oxygenators *35*
3.4.2 In-vitro Testing of Commercial Hollow Fibre Oxygenators *39*
3.5 Alternatives to Supply Oxygen to Blood In-situ 40
3.5.1 Chemical Generation of Oxygen *40*
3.5.2 Oxygen Concentrators *41*
3.5.3 Electrolysis of water *42*
3.6 Electrolysis of Water 43
3.6.1 Electrochemistry *43*
3.7 Commercially Available Electrolysers 52
3.7.1 Dissolved Oxygen Electrolyser *52*

Materials, Fabrication, and Methods **55**
4.1 Materials 55
4.2 Fabrication 57
4.2.1 Composite Conventional SOU Fabrication *57*
4.2.2 Electrolysis Chamber Fabrication *61*
4.2.3 Agarose Gel Membrane Fabrication *62*
4.3 Methods 63
4.3.1 Dissolved Oxygen Measurement in Water *63*
4.3.2 Hydraulic Resistance Test to SOU *64*

4.3.3 Control of Blood Oxygen Level *66*
4.3.4 Blood Storage and Syringe Loading *68*
4.3.5 Hematocrit Measurement *70*
4.3.6 Blood Oxygenation *70*
4.4 Statistical Analysis 76

Results and Discussion 77
5.1 Design 77
5.1.1 Design of an Electrolysis Chamber *78*
5.1.2 Supporting Electrolyte Selection *96*
5.1.3 Electrode Material *102*
5.2 DissolveD Oxygen in Water 112
5.2.1 Effect of the Molar Concentration *113*
5.2.2 Effect of the Current Supplied *114*
5.3 SOU In-vitro Testing 117
5.3.1 Oxygen Uptake in Air and in an Excess Oxygen Environments *121*

Conclusions 124
6.1 Key contributions 124
6.1.2 Additional Key Contributions *126*
6.2 Recommendations For Future Work 126

References 130

Appendix A 140
A.1 Fabrication 140
A.2 Experimental Setup 143
A.3 Testing 147

LIST OF FIGURES AND TABLES

Figure 3.1 - Illustration of a single flat-sheet unit *13*
Figure 3.2 - Illustration of a SciMed Kolobow spiral-coil oxygenator *14*
Figure 3.3 - Terumo HFO *15*
Figure 3.4 - Illustration of a) intracapillary and b) extracapillary blood flow in an HFO *16*
Figure 3.5 - Lee et. al., microfluidic oxygenator designs *19*
Figure 3.6 - Hoganson et. al., branched vascular network design *20*
Figure 3.7 - Potkay *et. al.*, bio-inspired artificial lung *20*
Figure 3.8 - Hoganson et. al., physiologic blood flow development *21*
Figure 3.9 - Kniazeva et. al., multilayer oxygenator *22*
Figure 3.10 - Wu et. al., lung assist device (LAD) for preterm neonates *23*
Figure 3.11 - Kovach et. al., biomimetic artificial lung *24*
Figure 3.12 - Rieper et. al., double sided gas transfer oxygenator *25*
Figure 3.13 - Thompson et. al., rolled-membrane *26*
Figure 3.14 - Block diagram of an O_2 concentrator components and its operation *42*
Figure 3.15 – Illustration of a basic water electrolysis system *45*
Figure 3.16 – Cell potential for H_2 and O_2 production *47*
Figure 3.17 – Typical Tafel plot for H2 and O_2 evolution *50*
Figure 3.18 – The oxygenator electrolyser *53*
Figure 4.1 – Schematic diagram of a conventional oxygenator unit *58*
Figure 4.2 - Composite conventional SOU filled with bovine blood *60*
Figure 4.3 – Illustration of the electrolysis chamber components and its inner dimensions *62*
Figure 4.4 – Experimental setup for the hydraulic resistance test *65*
Figure 4.5 – Close up view of the vascular network being filled with water *65*
Figure 4.6 – Experimental setup used for *the* deoxygenation of blood *67*
Figure 4.7 – Experimental setup to load the syringes with blood *69*
Figure 4.8 – Experimental setup for passive and active oxygenation *72*
Figure 4.9 - Passive oxygenation timeline *74*
Figure 4.10 - Active oxygenation timeline *75*
Figure 5.1 – Diagram of an electrolytic cell *78*
Figure 5.2 - Illustration of electrolysis in a single container *80*
Figure 5.3 – Increase in the DO concentration with time in the single chamber *81*
Figure 5.5 - Illustration of electrolysis in two separate containers connected by a paper scaffold salt bridge. *83*
Figure 5.6. – Increase in the DO concentration with time in the two-chamber design with paper scaffold salt bridge *85*
Figure 5.8 - Illustration of electrolysis in two separate containers connected by an agarose gel. *86*
Figure 5.9 – Increase in the DO concentration with time in the two containers design with agarose gel salt bridge *87*
Figure 5.12 – Diagram of the electro-chamber lid and support for the SOU *90*
Figure 5.13 – Diagram of the acrylic frame separator *91*
Figure 5.14 - Illustration of the electrolysis chamber *92*
Figure 5.15 – Increase in the DO concentration with time in the two-chamber design with gel membrane salt bridge *95*

Figure 5.16 - Illustration of different supporting electrolytes using four electrodes..... *97*
Figure 5.17 - Effect of the supporting electrolyte on the degradation of the electrodes. *100*
Figure 5.18 – Increase in the DO concentration with time in the two-chamber design with gel membrane salt bridge, ... *102*
Figure 5.19 - Increase in the DO concentration using stainless-steel and graphite electrodes *103*
Figure 5.20 – (a)Applied voltage to inject a current of 1.6 A using stainless-steel and graphite electrodes *104*
Figure 5.21 – Microscopic images showing the damage to graphite electrodes. *105*
Figure 5.22 - Diagram of the three different placements of the electrodes in the acrylic chamber. *106*
Figure 5.23 – Increase in the DO concentration over time using the electro-chamber design *108*
Figure 5.24 - (a)Applied voltage to inject a current of 2 A using three different electrode placements *108*
Figure 5.25 - Magnified image of the SSM to show the changes on the mesh structure *109*
Figure 5.26 - Illustration of the areas affected on the electrode by the electrode placement *110*
Figure 5.27 – Bubble formation at the surface of the electrode using three different electrode placements. *111*
Figure 5.28 - Effect of the molar concentration in the DO measured in water, change of voltage and temperature *114*
Figure 5.29 – Increase in the DO concentration with time at different current levels using the electro-chamber design..... *115*
Figure 5.30 - Effect of the different current levels on the change of voltage and temperature..... *116*
Figure 5.33 - Oxygen uptake in air and O_2 excess environments *122*
Figure 6.1 – Modified electrolysis chamber..... *128*
Figure A. 1 - Schematic for the hollow fibres cleansing. *146*
Figure A. 2 - Setup to measure the O_2 content in blood to test the gas transfer due to the tubing used. *149*
Figure A. 3 - Change on O_2 concentration in blood because of PVC Tygon® tube. *150*
Figure A. 4- Change of haemoglobin count over 2 weeks. *151*

Table 1 - Design and performance parameters of In-vitro experiments conducted using microfluidic oxygenators in air or compressed air environments. 32
Table 2 - Design and performance parameters of In-vivo experiments conducted using microfluidic oxygenators in an air environment 34
Table 3 - Design and performance parameters of In-vitro experiments conducted using microfluidic oxygenators in a 100% O_2 environment..... 37
Table 4 - Commercial oxygenators for neonates using O_2 as the gas supplied 39

LIST OF ABBREVIATIONS

Δ	Difference operator
AO	Active Oxygenation
AP	Artificial Placenta
BPD	Bronchopulmonary Dysplasia
CO_2	Carbon Dioxide
CPAP	Continuous Positive Airway Pressure
DI	Deionized
DO	Dissolve Oxygen
ECMO	Extracorporeal Membrane Oxygenation
Hb	Haemoglobin
Hct	Hematocrit
HFO	Hollow Fibre Oxygenator
IPA	Isopropyl alcohol
LAD	Lung Assist Device
mA	Milliampere
mg	Milligram
Min	Minute
mL	milliliter
MV	Mechanical Ventilation
N_2	Nitrogen
Na_2SO_4	Sodium Sulfate
NaCl	Sodium Chloride
NaOH	Sodium Hydroxide
O_2	Oxygen
PCO_2	Partial Pressure of Carbon Dioxide
PDMS	Polydimethylsiloxane
PO_2	Partial Pressure of Oxygen
PO	Passive Oxygenation
RBC	Red Blood Cell
RDS	Respiratory Distress Syndrome
RPM	Revolutions per minute
RT	Room Temperature
SaO_2	Oxygen Saturation
Sec	Second

SOU	Single Oxygenation Unit	V	Voltage
SRT	Surfactant Replacement Therapy	W	Watts
SSM	Stainless Steel Mesh	µm	Micrometer
U	Units		

GLOSSARY

Arteriovenous access: circuit removing blood through the artery and returning it through the vein.

Hematocrit: volume of red blood cells present in blood.

Haemoglobin: protein present in the red blood cells which binds to gases such as oxygen and carbon dioxide.

Intracranial hemorrhage: bleeding within the skull that leads to increase in intracranial pressure.

Oxygen saturation: percentage of oxygen bound to hemoglobin.

Neonate: newborn infant of less than 4 weeks of life.

Red blood cell: (also known as erythrocyte) carries hemoglobin to deliver oxygen to the body tissues.

CHAPTER 1

MOTIVATION AND THESIS ORGANIZATION

Respiratory distress syndrome (RDS) is a life-threatening disorder observed with symptoms of cyanosis, grunting, chest retractions and tachypnea. This disorder is caused by lung immaturity and lack of pulmonary surfactant which leads to mortality and long-term morbidity in preterm and term infants [1]. Although several treatments exist for RDS, preterm neonates with particular low birth weight are usually assisted with mechanical ventilation (MV). MV is associated with high risks of lung damage that lead to long-term morbidities [8, 16.1]. Bronchopulmonary dysplasia (BPD) is the most common long-term complication that results in the need for supplemental oxygen (O_2) in patients [2]. It has been reported that BPD develops in 33% of the neonatal population with a low body weight [3].

One way to treat RDS and its long-term complications such as BPD, is the use of an artificial placenta (AP) type device that allows oxygenation of the neonate blood without positive air pressure that is applied in MV. The AP is to be connected to the neonate through the umbilical vessels, thereby avoiding surgery, to withdraw the blood from the body to the oxygenator device and back into the body. Microfluidic AP type devices have been recently developed using microfabrication methods to minimise the priming volume to accommodate the needs of neonates. These devices are designed to be pumpless, operating based on the arterio-venous pressure difference, and exchange O_2 with the ambient. However, the concentration of O_2 in the ambient air is not sufficient to increase the saturation level of O_2 in the blood sufficiently. Therefore, a simple yet robust method for enrichment of O_2 is required which is the main motivation of this thesis.

1.1 SEQUENCE OF CHAPTERS

The thesis is comprised of six chapters that follow the sequence described below.

Chapter 2 provides an overview of RDS followed by its current clinical treatments. The concept behind the microfluidic AP device is briefly introduced. Finally, the objective of this thesis is stated.

Chapter 3 delves into the history of oxygenators. The performance of gas transfer in the recently developed microfluidic oxygenators is compared under various exposure conditions such as ambient air and pure O_2. Subsequently, alternatives to supply O_2 in-situ are investigated. In particular, the electrochemical method for generation of O_2 is detailed with description of the electrochemistry of water electrolysis. Finally, commercial electrolysers are assessed to determine their potential to serve as the O_2 in-situ device.

Chapter 4 presents the materials used in the fabrication process and the experimental setups. The fabrication process of the microfluidic device, the acrylic electrolysis chamber and the separator gel membrane are described. The experimental setups for water-based and in-vitro experiments are then discussed. Lastly, the statistical analysis selected to demonstrate statistical significance is mentioned.

Chapter 5 reports and discuss the experimental results of the evolving designs for the electrolysis chamber followed by water experiments to characterise the O_2 production and finally, the in-vitro experiments.

Chapter 6 concludes the work done in this thesis and suggests future work that could be done to improve the electrolysis chamber efficiency and performance.

CHAPTER 2

INTRODUCTION

This chapter briefly introduces the main respiratory problem that preterm neonates face and the treatments that they may undergo to overcome this illness. The treatments, including surfactant replacement therapy (SRT), continuous positive airway pressure (CPAP), mechanical ventilation (MV) and extracorporeal membrane oxygenation (ECMO), are briefly explained and their drawbacks are highlighted. Next, the artificial placenta concept that is proposed as an alternative to current treatments is discussed. Finally, the limitations of the artificial placenta in fully oxygenating the blood is discussed, and potential solutions to overcome this issue are proposed.

2.1 RESPIRATORY FAILURE

According to the World Health Organization, 15 million babies are born prematurely (<37 weeks of gestation) every year worldwide. Unfortunately, 14% of them do not survive due to various conditions such as respiratory failure (8%) or neurodevelopmental impairments (8%) [4, 5]. Among the preterm neonates that survive (86%), extremely preterm babies (<28 weeks of gestation) have the greatest risk of suffering from a neurologic or physical impairment (e.g. respiratory disease) [5]. Lung immaturity is a major cause of morbidity and mortality in preterm neonates between week 24 and 38 of gestation as critical formations of the lung (canalicular and saccular stage) and production of surfactants happen during this period [1]. Thus, RDS develops because of this deficiency in surfactant and structural immaturity of the lung [6]. RDS is observed with cyanosis, grunting, chest retractions and tachypnea [7]. If untreated, RDS turns to hypoxia and finally to deaths.

Over the last 40 years, many strategies have been developed to treat RDS that have been accepted and used for preterm infants [6]. The first treatment, antenatal steroids, is directly given to the mother. These steroids decrease the risk of RDS progressing the lung maturation; however, the dose must be taken by the mother at least one day before birth [6]. Once the baby is born, therapies such as assisted ventilation, SRT, CPAP and ECMO are provided to assist the baby in respiration. ECMO is only an option for term infants with birth weights greater than 2 kg because of the difficult intravascular access, and high blood volume and pressure required [8, 9].

2.1.1 Surfactant Replacement Therapy

The role of pulmonary surfactant is to lower the alveolar surface tension which reduces the alveolar tendency to collapse and provides efficient gas exchange surface area [10]. SRT administers exogenous surfactants via endotracheal tube. This is crucial for the treatment of RDS and in reducing the mortality and morbidity (e.g. air leak syndromes and intraventricular hemorrhage) in preterm infants [6, 11]. Pulmonary surfactant is composed of 80% phospholipids, 8% neutral lipids and 12% proteins [11]. Synthetic surfactants are only composed of lipids which are responsible for the alveolar surface tension; however, natural surfactants (also contain proteins) have shown additional benefits including the reduction of pneumothorax [11, 10]. Studies for surfactant administration have been conducted to determine the most suitable dose and its timing for delivery which change with the age of gestation and the birth weight [6]. Furthermore, SRT is usually combined with another treatment such as MV or CPAP to assist with the lungs function during their development outside the womb [11, 12]. It has been noted that the latter technology has shown to cause less damage to the baby's lungs [11].

2.1.2 Continuous Positive Airway Pressure

CPAP is a non-invasive ventilation method that increases the air pressure to prevent alveolar collapse so that spontaneous breathing can be sustained [13, 14]. Currently, CPAP is supplied through nasal prongs [14]. It has been shown that the combination of SRT and nasal CPAP is effective at reducing the incidence of pneumothorax and the need to use MV by up to 40% [6, 11, 12]. However, an excessive CPAP can lead to the air-leak syndrome including pulmonary interstitial emphysema, pneumothorax and systemic air embolism, among others [15]. Furthermore, it has been noted that the better outcome of this therapy is observed in preterm neonates with mild RDS which generally occurs in late prematurity (32-36 weeks of gestation) [5, 14, 16]. Nevertheless, CPAP is a recommended technique to use before trying MV [6].

2.1.3 Assisted Ventilation

Assisted ventilation is an invasive method that supports the lung function. The ventilation is provided via endotracheal intubation by a mechanical ventilator that creates a positive airway pressure in patients with non-spontaneous breathing [17]. Over the years, several forms of MV have been developed to find the optimal ventilation strategy; however, all of them can induce lung injury [6, 14]. The common modes used for MV are intermittent positive pressure ventilation (IPPV) and high-frequency oscillatory ventilation (HFOV). Newborn infants suffering from RDS are usually treated with SRT and MV to overcome the alveolar collapse and gas transfer deficiency, respectively. Although MV has shown to reduce the mortality of neonates, long exposures introduce a risk of morbidity through acute lung damage that includes barotrauma, volutrauma, BPD and bronchomalacia [11, 17, 18]. Moreover, lung damage often worsens the effects of RDS in the neonate. Despite the reduction of BPD and death rates in moderately preterm infants, there

is still the risk of developing BPD among the survivors [11, 17, 19]. Furthermore, BPD and other long-term complications are associated with MV which causes stress to the vulnerable lungs under development.

2.1.4 Extracorporeal Membrane Oxygenation

ECMO is a system that does not use a ventilator to achieve gas exchange [8]. ECMO is an invasive therapy that is connected to a veno-venous (respiratory support) or veno-arterial (cardiorespiratory support) circulation to oxygenate the blood for days or even weeks to allow native organ function to return [20]. Hollow fibre oxygenator (HFO) is a type of membrane oxygenator which is the most commonly used when treating RDS [9]. The blood is usually taken from the right atrium via interior jugular vein and pumped through an artificial lung (outside the body) to allow for the gas exchange between O_2 and carbon dioxide (CO_2). The blood is then warmed up by a heat exchanger and it is returned to the neonate's body [9].

ECMO is used when the aforementioned treatments cannot successfully ventilate the neonate. The greatest risk to account for with ECMO is intracranial haemorrhage which usually occurs in neonates with extreme or moderate prematurity [9]. Thus, preterm babies with an age of gestation lower than 34 weeks and a birth body weight lower than 2 kg cannot undergo the ECMO treatment [8, 9]. The survival rate of neonates that received ECMO is 77%; however, ECMO therapy has been associated with the development of short-term and long-term complications [9, 5]. The duration of the ECMO support, the time to extubation, the cease arterio-venous bypass and the use of heparin and the poor feeding are related to development of further complications on the neonate [21, 22]. Children that have been treated with ECMO present complications within the first 6 months such as feeding problems, poor somatic growth, lung disease and re-hospitalizations

related with the respiratory system. Between 3 and 4 years old, 24% of the survivors are at risk of behavior and learning problems and 17% present delays on learning. Furthermore, these children show a lower IQ at 5 years old [9].

The development of a new technology has been proposed [8] to alleviate the negative outcomes but also to provide an extracorporeal oxygenation to younger (<34 weeks) and low body weight (<2 kg) preterm neonates suffering from RDS.

2.1.5 Artificial placenta

The concept of an artificial placenta (AP) refers to a postnatal lung assist device (LAD) that sustains the lung function of preterm and term neonates suffering from RDS. The AP is connected through the umbilical vessels (arterio-venous) to partially support the gas exchange until the neonate's lungs are fully developed [8, 19]. Microfluidic technology has been used to overcome the current constraints of ECMO so that small priming volumes suitable for neonates can be achieved.

The artificial placenta is thought to have the lowest priming volume (<10 ml/kg) among all the extracorporeal oxygenators. Preterm infants (<34 weeks of gestation) could then be treated even though their blood volume is low (≤100 ml/kg). The pumpless LAD is driven by the pressure difference between the artery and vein (30-40 mmHg) to minimise the mechanical blood damage (e.g. haemolysis) and cardiac failure [19]. Furthermore, to keep the device as simple as possible, it should be operated under ambient air conditions [19]. Lastly, the surface of the device in contact with blood would be modified so that hemocompatibility is achieved to avoid blood coagulation and thrombus formation [8]. The artificial placenta is constructed in a modular fashion with

multiple single oxygenator units (SOUs) connected together into a network to form a lung assist device (LAD). The number of units and the interconnections between them are determined by the size and weight of the neonate.

Improvements on the design of the SOU that form the LAD have been done to increase its performance [23]. However, recent studies [19, 23, 24, 25, 26] have demonstrated that exposure to ambient air was not sufficient to provide 30% of oxygen saturation (SaO_2) in blood. Therefore, there is a need of increasing the blood O_2 uptake by other means.

The most common approach to support the oxygenation of blood with ECMO and the recently developed microfluidic oxygenators is exposure to enriched O_2 environment. However, several constraints should be taken into account:

1) Pure O_2, either supplied by cylinders or pipelines in hospitals, is expensive and requires continuous monitoring and maintenance [27, 28].

    a. Developed countries usually have the financial support to maintain tanks and pipelines with O_2 readily available. Nevertheless, community hospitals still depend on medical gases supplied from cylinders [29].

    b. On the other hand, most developing countries face limitations that sometimes are taken for granted. Developing countries usually lack O_2 systems (pipelines) and rely on public infrastructure (e.g. roads) to get delivered O_2 cylinders. It has been reported [30] that up to 28.1% of the developing world does not have pure O_2 available for their patients mainly because of bad roads. Furthermore, the shortage

of financial aid is another main limitation directly affecting the O_2 gas ordering system [28]. Moreover, the price of an O_2 cylinder can be 3 times higher than in the developed world in addition to its distribution cost (e.g. vehicle, fuel) [28].

2) Although it is not common to have incidences of fires in hospitals it has happened in the past and in recent years due to O_2 cylinders (e.g. gas leakage) [31, 32].

3) It is known that human errors can occur when handling, labelling, connecting and giving maintenance to cylinders and pipelines [29, 33]. Sometimes, these errors have led to death of patients [34]. Incidences have been reported where contamination of O_2 pipelines and cylinders have been detected [35]. Furthermore, reports of accidental damage of pipelines because of external work in the surroundings have affected the centralised O_2 system for up to 15 hours [36, 37]. These issues present a critical safety issue for doctors and nurses to rely on O_2 cylinders. Regardless of the hospital stock, there is always the risk of running out of cylinders.

The objective of the work reported in this thesis was to design an electrochemical system to provide an in-situ enriched O_2 environment for high O_2 uptake while maintaining the simplicity of operation of the AP concept. An inexpensive, electrically powered and compact device was envisioned to enrich the AP surroundings with more O_2. This O_2-rich environment would allow for a higher permeation flux to fully oxygenate the blood. Moreover, the system would be easy to manufacture, low maintenance and avoid the risk of gas contamination.

CHAPTER 3

LITERATURE REVIEW

This chapter examines the history of oxygenators from the development of direct and indirect contact oxygenators to microfluidic designs that have been under research. It also introduces the concept of a microfluidic AP focused on preterm neonates with RDS and presents the early and current research in the AP field. The gas exchange rate of various microfluidic devices is compared when the gas supplied is air or pure O_2. The chapter also discusses the alternatives of supplying O_2 to blood in-situ, in particular water electrolysis. The electrochemistry behind the electrolysis of water is then discussed. Finally, commercially available electrolysers and their constraints are detailed.

3.1 HISTORY OF BLOOD OXYGENATION DEVICES

Traumas of the lung, such as pulmonary and cardiac dysfunctions, have led to the development of devices that can artificially support the oxygenation of the blood [13]. For decades [38], researchers have looked for new ways to improve the oxygenation of blood and the prevention of blood traumas. The concept of an extracorporeal oxygenator was first described by Robert Hooke in the 17th century, but it was not until the 19th century that Ludwig and Schmidt developed the first oxygenator [39]. Over the years, two types of artificial oxygenators have been developed and clinically accepted [40]. These oxygenators are categorized as direct and indirect contact which refers to the blood being in contact with air or separated by a membrane.

3.1.1 Direct Contact Oxygenators

Direct contact oxygenators do not offer a physical barrier between blood and the air surface; thus, blood is fully oxygenated with ease. However, blood in contact with air is prone to blood traumas [39]. There are two types of direct oxygenators: bubble and film oxygenator devices.

The principle behind bubble oxygenator is to directly introduce bubbles into venous blood [13, 40]. The bubbles increase the surface area of air-blood contact, thereby oxygenating the blood. This technique is inexpensive and easy to use, but it also causes the greatest trauma to the blood among all oxygenators [40]. The film oxygenator uses a pump to produce a large surface area of a thin film of blood through different techniques (e.g. inclined cylinder, rotating disc, silk screen). This thin film is exposed to air or enriched O_2 which quickly oxygenates the blood [39, 40].

The disadvantages of the direct contact oxygenators are mainly related with the damage and destruction of red blood cells (RBCs) and platelets, coagulation disorders and protein denaturation [39]. Furthermore, these oxygenators can only be used for a limited time (up to 4 hrs) making them unsuitable for the therapeutic support in adults and infants suffering from RDS. These disadvantages and limitations led to investigation of oxygenator designs that indirectly expose blood to air.

3.1.2 Indirect contact oxygenators

Indirect contact oxygenators are also termed as “membrane oxygenators” due to the use of a membrane to provide a physical barrier between blood and gases while still allowing diffusion of gases through it. Membrane oxygenators are the cutting-edge technology for respiratory care [23].

The first clinical membrane oxygenator was developed in 1957 by Clowes, Hopkins and Neville [39]. This oxygenator was a flat-sheet type oxygenator formed of ethylcellulose membranes stacked in parallel [41]. A variety of gas permeable membranes have been used in the development of indirect contact oxygenators including polyethylene (PE), polypropylene (PP), ethylcellulose and polymethylpentene (PMP), polydimethylsiloxaine (PDMS) and polycarbonate (PC) [19, 42].

For respiratory support (e.g. pulmonary insufficiency), membrane oxygenators are exclusively used. [43]. Typical membrane oxygenators were flat-sheet or spiral-coil types and both have been used clinically [44]. Currently, HFO dominate the field because of their higher compatibility with blood, their low levels of gaseous microemboli formation and a greater gas exchange efficiency [42, 45]; nevertheless, research is ongoing to overcome the limitations of the HFO using microfluidic technology. These limitations are mainly due to their high priming volume and the high pressure drop in these systems.

3.1.2.1 *Flat-sheet Oxygenator*

The flat-sheet oxygenator was based on the multilayered system of Skeggs-Leonards plate dialyzer where the gas permeable membrane substituted the dialyzer membrane. The blood flowed through microchannels located between two membranes with the outer side of one of the membranes exposed to O_2 (Figure 3.1) [40]. The flat-sheet was the first membrane oxygenator to be introduced [42]. It could achieve priming volumes of 600 mL with an exchange surface area of 2.3 m^2 which would be suitable for oxygenation needs of adults but not neonates because of the high priming volumes required [46]. Furthermore, the device required access to the central vessels which was invasive.

In addition, it had tortuous and uneven blood flow paths which resulted in a high transfer of O_2 [43, 24]. On the other hand, this flat-type oxygenator reduced the blood damage which was a major issue with the direct contact oxygenators [42].

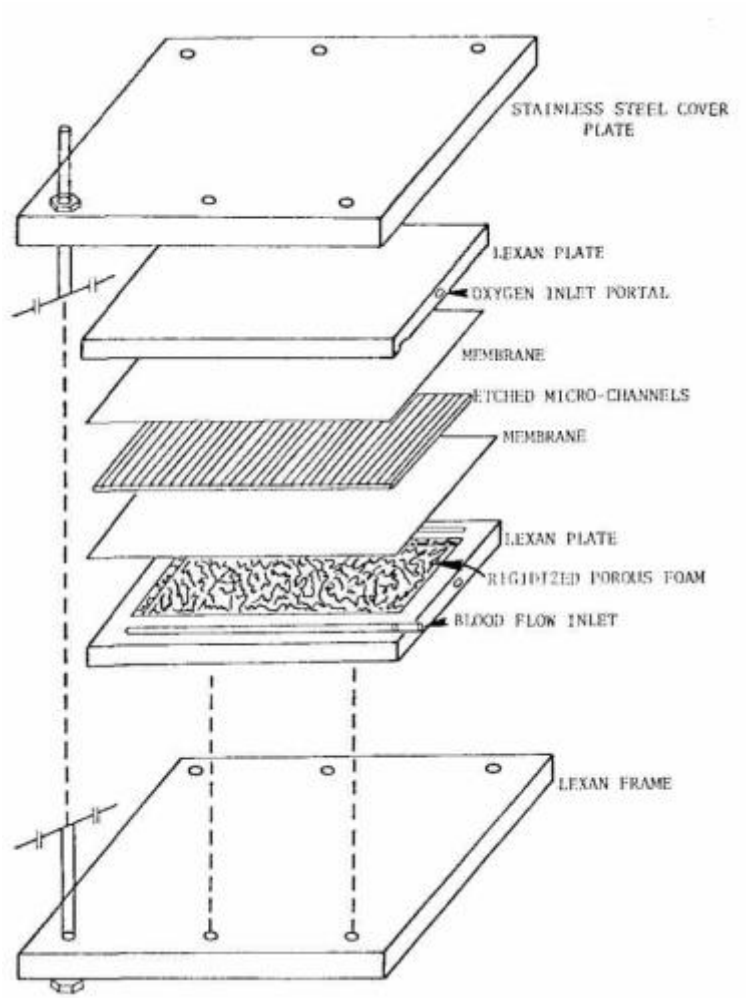

Figure 3.1 - *Illustration of a single flat-sheet unit. Blood channels are 110 µm tall [47].*

3.1.2.2 *Spiral-Coil Oxygenator*

The spiral oxygenator was first designed in such a way that the blood and the O_2, separated by a membrane, flowed in the respective manifold in a spiral direction along the axis of a cylinder. Further, Kolobow modified the spiral oxygenator design by replacing the polyethylene membrane with a silicone rubber membrane and interchanging the blood and gas flow paths. The change of

blood flow path to the outside of the membrane envelope (Figure 3.2) allowed for a dramatic improvement on the gas exchange [40]. In addition, the required priming volumes were reduced to 100 mL/m^2 [48]. This oxygenator was used in cardiac surgery, it was also successfully used as a respiratory assist device, becoming the only oxygenator available for long-term treatment [40]. The high flow resistance of 150 mL/min·kg deformed the membrane creating uneven paths for the blood which allowed for a better gas exchange [48]. However, a study in 50 children and infants was performed with this oxygenator and it was found that it resulted in an increase in lung fibrosis and a decrease in the platelet count of 31% and 51%, respectively [45]. Thus, the development of a more suitable device was sought.

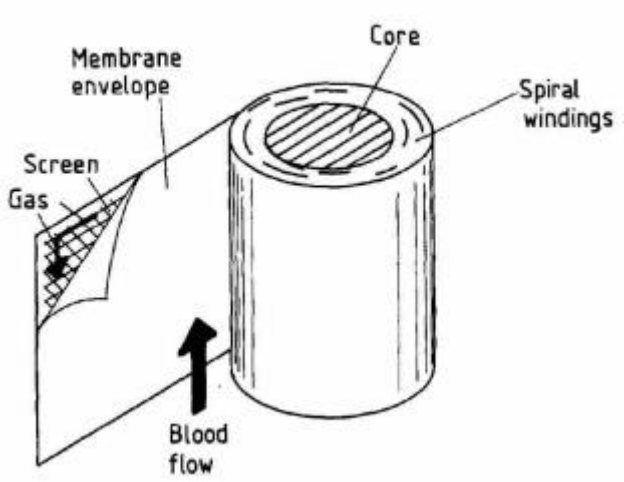

Figure 3.2 - *Illustration of a SciMed Kolobow spiral-coil oxygenator [43].*

3.1.2.3 *Hollow Fiber Oxygenator*

The HFO is a hard shell composed of bundled fibres that have a diameter ranging between 200 µm and 300 µm, as seen in Figure 3.3 [39]. Fibres, which can be porous or non-porous, allow the separation of the blood from direct contact with the gases. The first HFO was created in 1963; however, it was until 1981 when the first HFO was commercialised [39, 40].

The gas exchange efficiency, the blood compatibility and the easy usage of the HFOs eventually replaced the direct contact oxygenators in cardiac surgery [40].

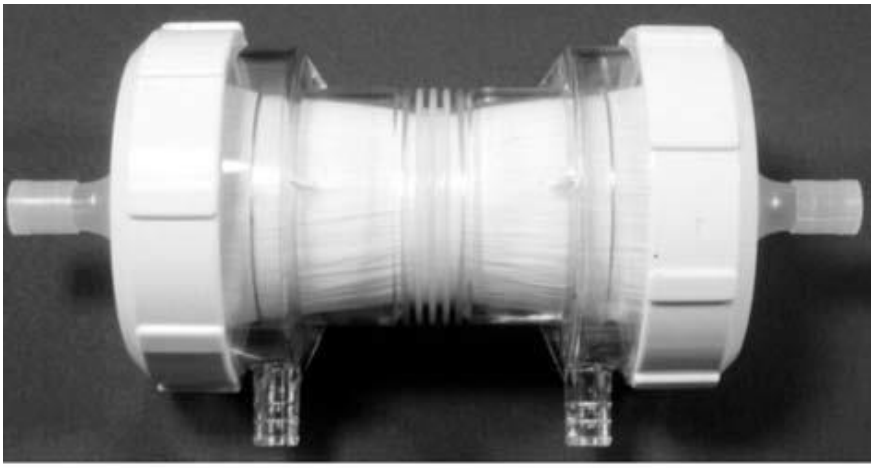

Figure 3.3 - *Terumo HFO [40].*

The HFO can be operated in two configurations: intracapillary and extracapillary blood flow mode (Figure 3.4) [40]. In the former, the blood flows inside the fibres while the gas flows on the outside, and in the latter, the gas flows in the fibres lumen and blood on the outside of the fibres. The dominant type has been the extracapillary setup because turbulent flows are introduced which enhance the gas exchange [39]. Furthermore, this extracapillary flow reduces the blood damage and pressure drop [49].

The fibres of the oxygenators can be microporous or non-microporous polypropylene [40]. The microporous is widely used for short-term application (e.g. cardiopulmonary bypass). However, for long-term applications, such as RDS therapy, the silicone-coated fibres are the preferred material to avoid plasma leakage [39, 40].

HFOs have become more compact with reductions of 10.8 times in area and 17 times in priming volume compared to the first commercially available HFOs [23]. The current priming volume required ranges between 50 mL and 300 mL with an exchange surface area of 0.5 m^2 to 2.5 m^2 [49]. The available commercial HFOs show an O_2 transfer rate in the range of 300 mL/min·m^2 [49].

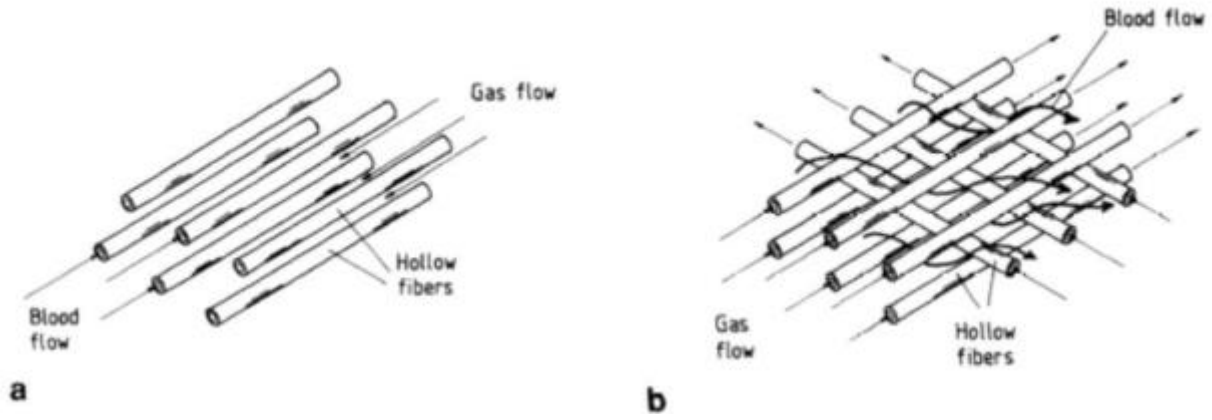

Figure 3.4 - *Illustration of a) intracapillary and b) extracapillary blood flow [43].*

The HFO is state-of-the-art technology, and it has considerable advantages over the other types oxygenators such as lower priming volumes, lower blood flow resistance, higher gas exchange efficiency and a lower manufacturing cost [40, 50]. Despite these improvements, the HFO is an invasive technology that still presents significant disadvantages for the preterm neonatal population. The HFO depends on mechanical pumps which generate high pressure drops for preterm neonates. Furthermore, it has been shown that for a baby of less than 2 kg body weight and less than 34 weeks of gestational age, the incidence of intracranial hemorrhage is higher and the intravascular access is more difficult than for term neonates [9, 51]. Lastly, the acceptable

priming volume for a preterm neonate of less than 2 kg body weight and less than 34 weeks of gestational age is 10 mL/min·kg [8.1]. The HFO technology has a larger volume than this design criteria making them unsuitable for the neonatal population. Given the limitations of the HFO, it was predicted by Federspiel and Svitek in 2004 that the next step for the oxygenator device was in the micro-scale [52].

3.1.2.4 *Microfluidic oxygenator*

Microfluidic devices are designed to manipulate fluids and gases in microchannels and typically have high surface to volume ratios. The miniaturization of systems enables a broad range of chemical, biological and medical applications [24, 52]. Microfabrication and microtechnology developments have allowed the manufacturing of ultra-thin membranes and blood channels with sizes in the micrometer scale, from 1 to 100 µm [18]. These micrometer dimensions have made it possible to build smaller oxygenators that, could potentially overcome many of the issues associated with the realization of a compact oxygenator for neonates.

Microfluidic oxygenators have thin membranes (as small as 6 µm [19]) similar in dimension to human lungs (2 µm [18]) that reduce the resistance to gas transfer, increase the flux of gases and thereby the oxygenation capacity. They also allow a laminar flow characterised by smooth flow paths for the blood and reduce the dead zones and high shear areas which is important in reducing blood trauma [18]. The reduction in shear forces is especially important in the case of blood which is a non-Newtonian shear hardening fluid [134]. Priming volumes can also be reduced to volumes as low as 4.8 mL, as reported by Rochow *et. al.* [25], which are extremely low compared to the HFOs (~41 times lower) [18].

3.1.2.4.1 Historical Development of Microfluidic Oxygenators

In 2007, Gilbert *et. al.,* proposed the use of PDMS for the microfluidic device so that gas diffusion and hemocompatibility limitations could be addressed. The channel height and width were 0.1 mm and 1.197 mm, respectively. They tested four devices at a flow rate of 0.25 mL/min for 6 hours. They obtained a uniform flow and a hemolysis rate of less than 5% and no thrombus deposition was observed [53].

In 2008, Lee *et. al.,* proposed several designs and showed theoretical calculations for the O_2 uptake [54]. In the same year, they tested their screen-filled wide rectangular channels design where the channel height was created by the thickness of the stainless-steel screen. The screen was sandwiched between a rectangular PC support and a silicone rubber membrane. The channel heights tested were 40 µm and 82 µm, and the membrane thickness was 100 µm. This device was easy to fabricate and maintained uniformity in the channel height. However, the channel height was limited by the availability of screen sizes. Most importantly, the blood was exposed to more foreign surfaces [55]. They also tested two other designs that presented open rectangular microchannels with a 130 µm thick membrane in two different configurations (Figure 3.5). These two designs were more efficient in the O_2 uptake than with the screen-filled wide rectangular channels design; however, these designs only partially oxygenated the blood. Thus, further improvements that are comparable with the lung's natural efficiency were needed [56]. Moreover, the device was designed for a priming volume greater than 15 mL, not accounting for the manifolds or connectors. This volume of blood is high for the intended application with early preterm infants whose total volume is 100 mL/kg [8].

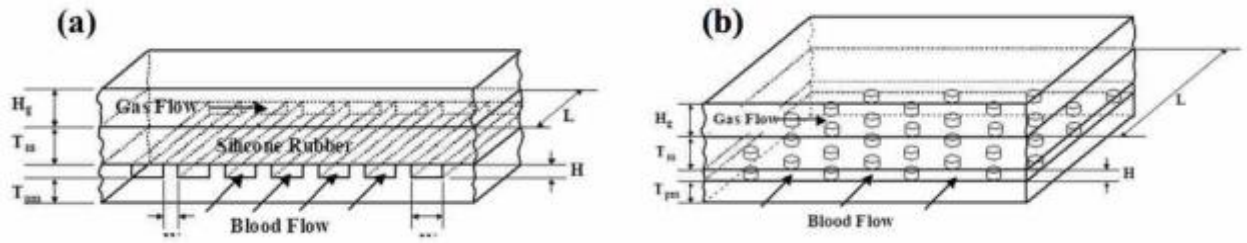

Figure 3.5 - *Lee et. al., microfluidic oxygenators tested. a) straight, parallel rectangular microchannels, b) wide rectangular microchannels with support posts [54].*

In 2009, Burgees *et. al.*, proposed a 33 µm tall by 100 µm wide semi-circular blood channels design, incorporating a 64 µm thickness PDMS membrane [57]. The device had a surface area of 4.72 cm^2 and a volume of 4.56 µl. The device was tested to measure the gas permeability through the membrane by submerging it in a water bath. Pure O_2 was supplied through the inlet of the device and the pressure drop was increased to 250 mmHg. The membrane resistance to O_2 diffusion was $109x10^3$ $mL/min \cdot m^2$. In the same year, Potkay *et. al.*, designed a microfluidic oxygenator comparable in sizes to the human lung, achieving a membrane thickness of 15 µm which became the thinnest membrane available at that time. The channel height was 30 µm and the volume was 29 mL. The device was tested with water to measure the permeability of the membrane to O_2. Pure O_2 was supplied with a pressure of 250 mmHg and the resistance obtained to O_2 diffusion was $27x10^3$ $mL/min \cdot m^2$ [58].

In 2010, Hoganson *et. al.* [59], designed and fabricated a capillary-like network oxygenator of 200 µm channel height (*Figure **3.6***). They also tested three different thicknesses in three different membrane materials [59]. A porous PC membrane with a 12µm thickness was used as the control. Silicone-coated porous PC and silicone with 15 µm and 63 µm thickness, respectively, were tested and compared with the control. The microfluidic oxygenator showed a similar O_2 uptake (57 mL/min) as a HFO; nevertheless, no difference in gas exchange was observed among the three

different membranes used [59]. Although a comparable oxygenation to HFOs was shown, the device was designed to work with pure O_2 which makes it unsuitable for the envisioned device for preterm neonates.

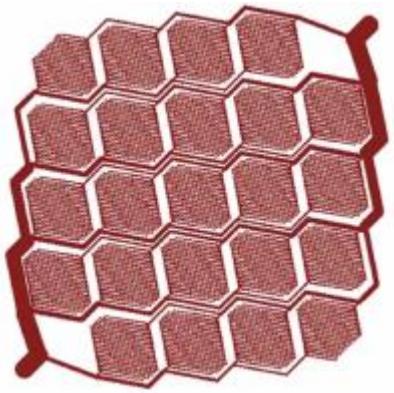

Figure 3.6 - Hoganson et. al., branched vascular network design [59].

In 2011, Potkay *et. al.* [60], fabricated a device that was designed to work with air (***Figure 3.7***). It contained a non-porous membrane with a thickness of 15 µm. The channel was 88 µm wide, and it was designed and tested with two different heights: 10 µm and 20 µm. Gas exchange efficiencies were comparable with commercially available oxygenators that use pure O_2 [18]. Although the efficiency of this oxygenator is promising, the pressure drop was extremely high compared to human blood pressure necessitating the need for an external pump for perfusion [58].

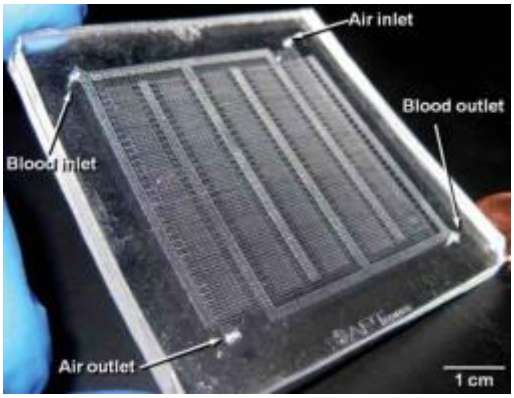

Figure 3.7 - Potkay et. al., *bio-inspired artificial lung [60].*

In 2011, Hoganson *et. al.,* also proposed and tested a new design where they tried to emulate the physiologic blood flow in the natural lung [61]. They fabricated a membrane with a thickness of 9 µm. The microchannels had a rectangular shape of 100 µm tall and wide. The shear stress at different flow rates was within the limit of the shear stress in arteries (53 dyne/cm^2 and 43 dyne/cm^2) [62]. However, the device presented a low efficiency to transfer O_2 and CO_2 even when the gas source was pure O_2 [61].

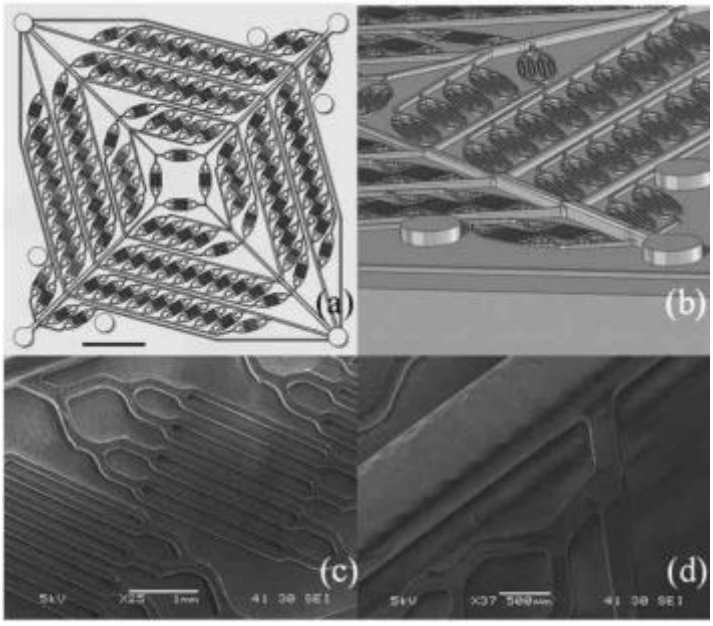

Figure 3.8 - Hoganson et. al., physiologic blood flow development [61].

In 2012, Kniazeva *et. al.,* tested a 10-stack parallel plate multilayered oxygenator built with PDMS. The membrane thicknesses were 30 µm and 117 µm with channel heights of 50 µm and 100 µm. It was found that decreasing the membrane thickness and the channel height increased the gas transfer rate. However, further work in the geometry of the device needs to be done to optimize the priming volume while maintaining the O_2 transfer efficiency [63]. Furthermore, this device works with pure O_2 which is undesirable for use with early preterm infants.

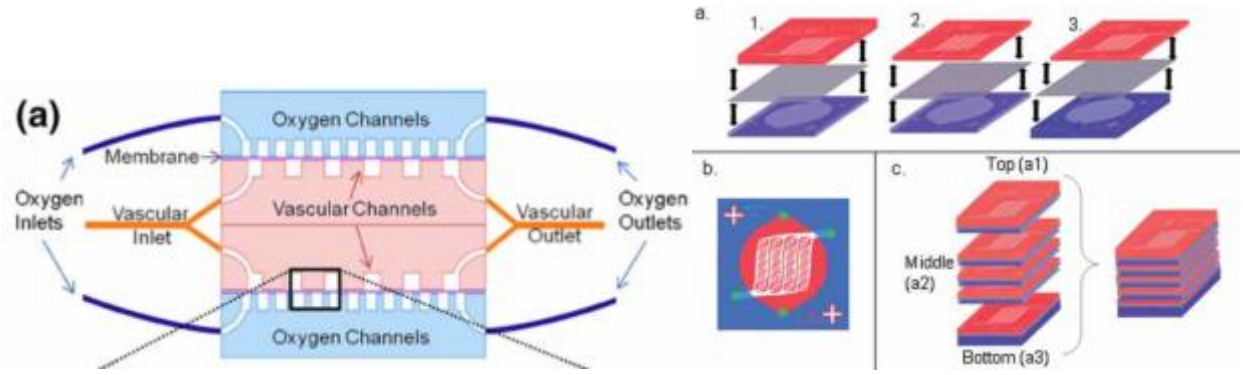

Figure 3.9 - Kniazeva et. al., multilayer oxygenator [65, 63].

In 2011, Wu *et. al.* [64], introduced a new concept for a microfluidic oxygenator targeted for usage as an AP. They proposed a non-invasive PDMS device for preterm neonates younger than 34 weeks of gestation and less than 2 kg body weight [8, 26, 64]. The device would be connected through the umbilical vessels, the blood flow driven by the heart (pumpless) and the blood would obtain the O_2 from air (~21%) [26]. The microfluidic device was composed of a vascular network with channels that were 80 µm high and 500 µm wide (*Figure **3.10***). Two membrane materials, nonporous and porous PDMS membranes 15 µm thick and porous PC membranes 6 µm thick (0.1 µm and 0.05 µm pore sizes), along with the vascular network, were tested [19]. The porous PDMS membrane oxygenator showed a 367% greater O_2 uptake than commercially available HFOs. The pressure drop was as low as 30 mmHg at a flow rate of 4 mL/min and the priming volume was also kept low (4.8 mL/min) [8]. In 2014, Rochow *et. al.* [25], performed in-vitro and in-vivo experiments using the previously mentioned microfluidic device. Ten microfluidic units stacked in parallel sustained the oxygenation of blood of 1 kg baby with ambient air. In-vivo experiments showed promising results on the O_2 gas exchange rate (3 µl/min·cm^2) and demonstrated the feasibility of a pumpless device [25]. In spite of the PDMS showing the best performance among other membrane materials, the increase in the gas transfer can be further improved by modifying

the membrane elasticity so that the channels do not expand in height. Thus, this microfluidic device is suitable for preterm infants. Nonetheless, further improvements in the microfluidic device need to be done to achieve a 30% change in O_2 saturation required to fully oxygenate the venous blood of neonates.

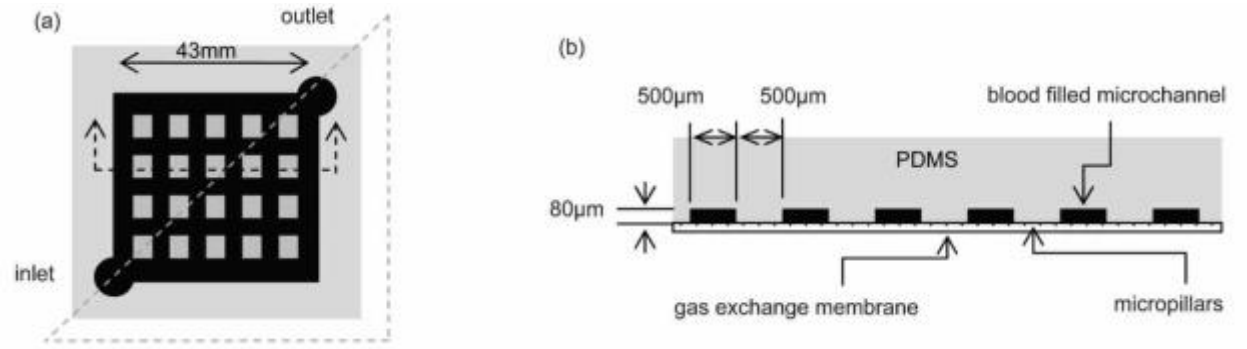

Figure 3.10 - Wu et. al., lung assist device (LAD) for preterm neonates [64].

In 2015, Kovach *et. al.*, introduced a new design that mimics the physiology of the natural lung so that pressure drop and shear stress are reduced [65]. The device was designed with three different channel heights: 200 µm that branches to 60 µm to 10 µm capillaries (*Figure **3.11***). The widths varied from 60 µm to 300 µm. The membrane was fabricated with a thickness of 15 µm. The device was tested showing a low pressure drop (2-10 mmHg) across the device; however, the O_2 uptake was 2 times lower than with Wu's device [19] despite pure O_2 being supplied for the Kovach's device [23]. Thus, the device does not fit the gas transfer nor the gas supply (ambient air) requirements to be used in a preterm infant.

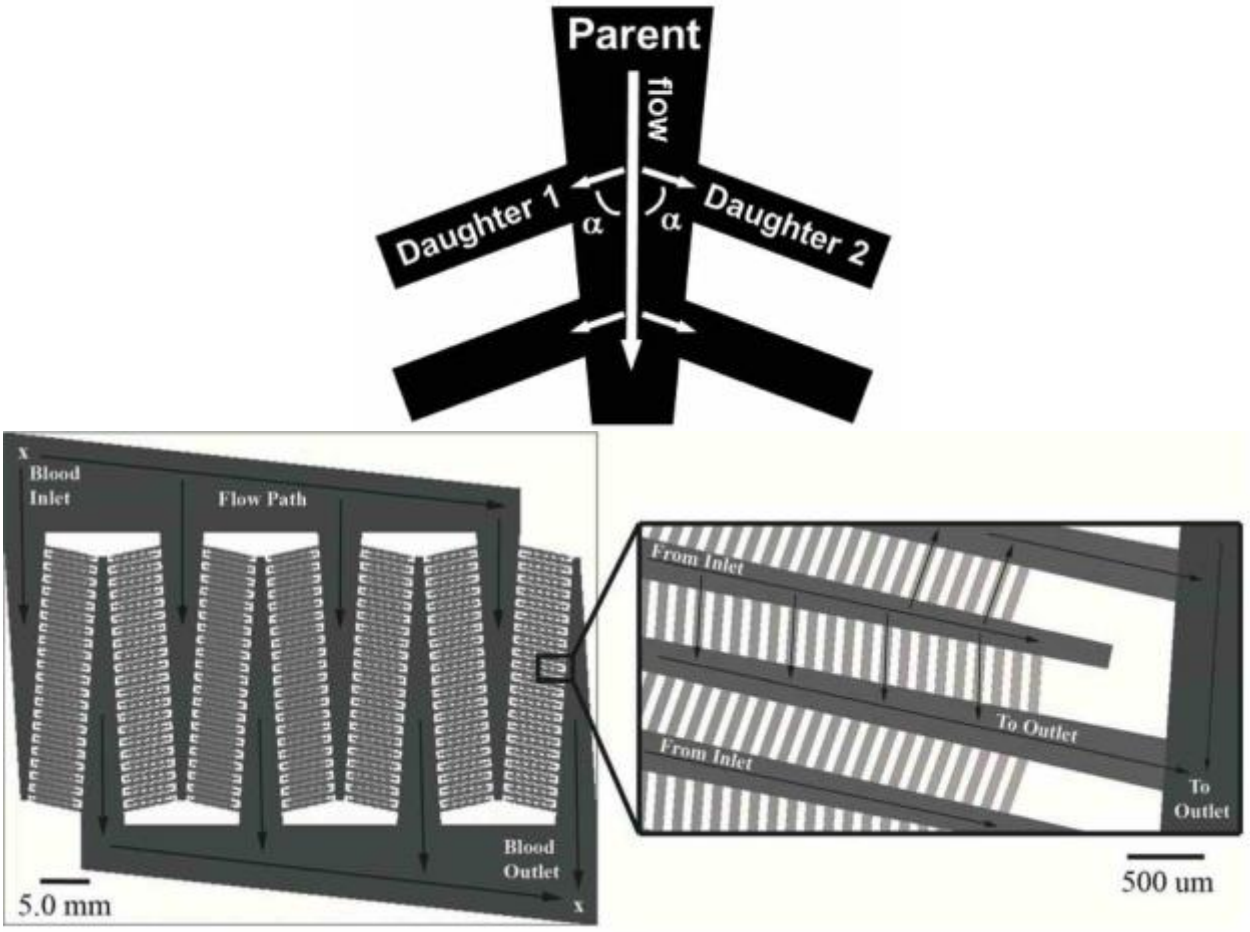

Figure 3.11 - Kovach et. al., biomimetic artificial lung [65].

In 2015, Rieper *et. al.,* proposed an all PDMS (including the housing) double sided gas exchange oxygenator [66]. The design is such that a stack of layers form the device so that the microchannels present a highly integrated blood path. Blood and gas ventilation compartments are alternated with the PDMS membranes (Figure 3.12). The microchannels were 1 mm wide and 100 µm tall. The membrane thickness was 90 µm. The 10 layered device showed the largest rated blood flow to date (83 mL/min) [67]. However, it showed a poor gas exchange performance using O_2 as the supplied gas and the fabrication of the device was labor intensive. Although this device had a low priming volume (16.3 mL plus manifolds) when compared with other oxygenators [66], it is not suitable for use in premature neonates [8].

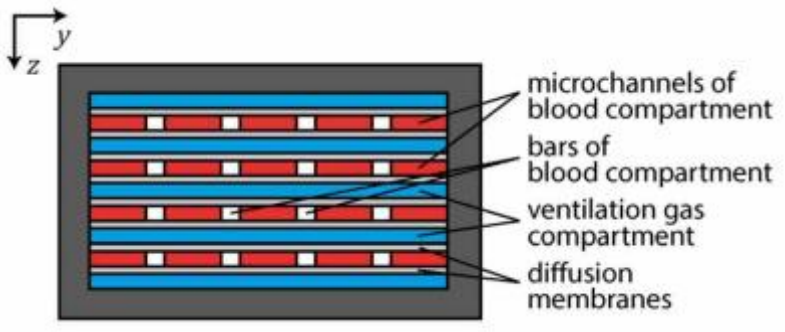

Figure 3.12 - *Rieper et. al., cross sectional view of a double sided gas transfer oxygenator [66].*

In 2017, Thompson *et. al.* [62], introduced a new microfluidic design aiming for a larger surface area. The microfluidic rolled-membrane (Figure 3.13) follows a similar biomimetic branching introduced by the same group in 2015 (*Figure **3.11***). The microchannels were 100 µm tall and the capillaries are 40 µm wide and 10 µm tall with a membrane thickness of 66 µm. The design was conceived to have a 4-layer structure where a PDMS flat layer is patterned with blood and gas layers and rolled in a substrate (capping layer). The gas and blood layer were separated by a PDMS membrane. This rolled-membrane allows for a double-sided gas exchange and increasing the exposure of the blood area. The device showed good performance when blood was exposed to air. It outperformed Rochow *et. al.* [25], device in both gas exchange and priming volume. However, at a flow rate of 1.25 mL/min there was an extreme increase in pressure drop to 120 mmHg, 250% higher than the pressure driven by a preterm infant heart [19]. Thus, it cannot be used for a preterm neonate.

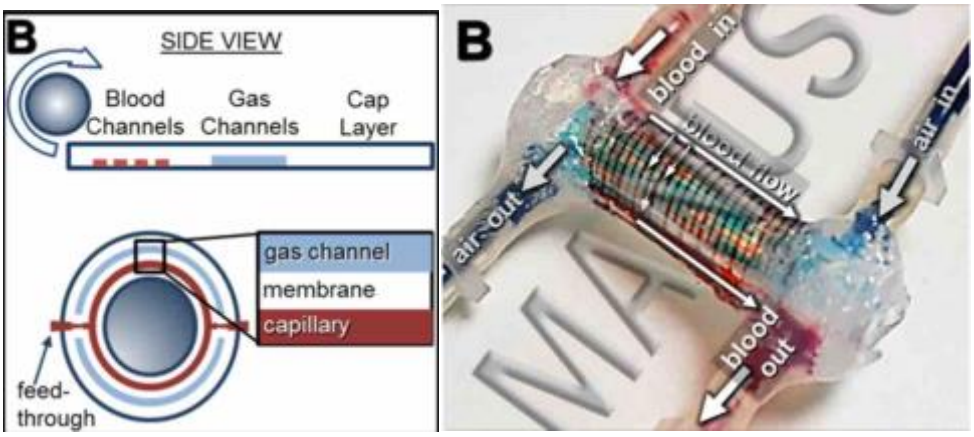

Figure 3.13 - *Thompson et. al., rolled-membrane [62].*

Although microfluidic oxygenators are closer to mimicking the natural lung dimensions and its functionality, most of the groups developing microfluidic oxygenators have shown high pressure drops in their designs which make them unsuitable for pumpless operation. In addition, some also have high priming volumes. Very few groups have focused on developing low priming volume and low pressure drop oxygenators that are suitable for AP like application for term and preterm neonates with RDS.

3.2 ARTIFICIAL PLACENTA

Extracorporeal lung support or AP is a concept under development for preterm and term infants as a bridge to allow the development of native lung function in an extra-uterine environment. The AP model connects an ECMO through the fetal circulation via umbilical vessels. The blood flow can be assisted by a pump (veno-venous) or be pumpless (arterio-venous). The inner surfaces in contact with blood would be hemocompatible so that intracranial hemorrhage risk is diminished [68]. Lastly, the AP does not contribute to the exchange of nutrient and metabolic products.

The AP was also proposed for the use on preterm neonates with low birth weight (<2 kg) and low gestational age (<37 weeks). The specific characteristics of this placenta device to decrease the mortality and long-term morbidity in preterm infants were defined by Rochow *et. al.* [8.1]. The priming volume must be below 10 mL/kg body weight (~10%, typically 8-10 mL) 8.1. The blood is taken from the umbilical artery, moved across the LAD, and brought back to the body using the umbilical vein. The blood is then driven by the pressure difference between the artery and the vein (30-40 mmHg). The oxygenation of blood is achieved using the O_2 present in ambient air (~21%). Lastly, a flow rate of 30 mL/min should be sustained to reproduce the fetal blood flow.

The AP concept has been investigated for more than 50 years [68]. In 1958, the first cannulation via umbilical vessels was performed in human fetuses, however, the concept of AP was first introduced in 1961 by Callaghan *et. al.* [68]. In 1962, Callaghan *et. al.*, conducted an experiment with a rotating disc oxygenator in a veno-venous circuit and kept alive mongrel dogs for 2.5 hours. Although promising, the survival time needed to be increased. In the same year, a pumpless gas exchanger and a small dialyzer was developed by Lawn *et. al.* [69], and connected in an arterio-venous circuit. This device was a film-type (rotating discs) oxygenator with a priming volume on the range of 200 to 250 mL and gas exchange area of 0.25 m^2. They tested the device on pig fetuses which were kept alive for up to 7 hours. Although the duration of the support was extended they required stabilisation of the arterial pressure continuously. In 1964, Alexander *et. al.* [70], oxygenated the blood of lamb fetuses using a rotating disc oxygenator and a pump. The arterio-venous circuit required a blood volume of 150-200 mL. The lambs were kept alive for up to 8 hours. The flow rate varied from 60-180 mL/min·kg with a mean pressure drop ranging from 30-60 mmHg. The lambs survived the entire perfusion period; however, it was observed that for long-

term oxygenation (beyond 2 hours) the blood flow dropped significantly which led to a constant control of the flow. Thus, stabilisation of the flow rate for longer periods was required. The same year, SenGupta *et. al.* [71], tested a flat-sheet oxygenator comprised of a silicone elastomer membrane that required the use of a pump. A priming volume of 400 mL to 500 mL was required with a gas transfer area of 0.3 m^2. They reported a survival rate of 69% where dogs were connected to the umbilical vessels for up to 5 hours. However, a better control of the flow rate and a reduction of hemolysis were needed. In 1969, Zapol *et. al.* [48], used a spiral-coil ECMO to maintain a premature lamb fetus alive for up to 55 hours. A constant priming volume of 70 mL was required with a gas transfer area of 0.4 m^2. All lambs underwent cardiac arrest and showed an increase in peritoneal fluid. In 1979, positive pressure mechanical ventilation showed a dramatic increment in the survival rate of preterm infants; thus, from then on the AP concept was not as intensively investigated. Nevertheless, in 1987, Kuwabara *et. al.* [72], introduced a new system for the AP where a blood reservoir, a silicone HFO and a pump were used. The functional surface area ranged from 0.1 to 0.3 m^2 and the priming volume was 100 mL. They experimented with goat fetuses and reported the first long-term survival of 7 days (in 1 of 8 goats). The major cause of death was intraperitoneal hemorrhage. In 1989, Kuwabara *et. al.* [73], included a dialyzer in their setup which showed an increase in the survival time of goat fetuses. The functional surface area ranged from 0.3 to 0.5 m^2 and the priming volume was 160 mL. One of the six goats survived for up to 10 days. The major cause of death was circulatory failure which might be related with poor O_2 supply to the organs. In 1993, Unno *et. al.* [74], used a pump, silicone HFO and a heat exchanger to perfused goat fetuses. The circuit was connected via arterio-venous access with a priming volume of 230 mL and a surface area of 0.5 m^2. Two goat fetuses were studied and maintained alive for up to 3 weeks. Through different experimental setups, they proved that the resistance to flow was a main

factor in the long-term perfusion. In 1998, Sakata *et. al.* [75], used a polyolefin HFO and a centrifugal pump in an arterio-venous circuit with a priming volume in the range of 105 mL. They tested goat fetuses and kept them alive for an average of 6 days, one for up to 9 days. The designed setup achieved lower resistances and higher flow rates compared to previous setups. However, the material of the fibres allowed for low gas transfer [24].

More recently, in 2011, Arens *et. al.* [76], built a pumpless, miniaturised HFO that had a priming volume of 19 mL and a gas exchange area of 0.09 m^2, reducing the surface area while decreasing the thrombin formation and inflammation. In-vitro experiments showed an O_2 gas transfer of 53 mL/L_{blood} at a blood and O_2 flow rate of 80 mL/min and 160 mL/min, respectively. In-vivo experiments were also performed in lambs connecting the device via arterio-venous. The lambs were kept alive for up to 3 hours at a maximum flow rate of 33 mL/min·kg (91 ±35 mL). The pressure drop reported was greater than 35 mmHg. Blood clots at the inlet were observed at a flow rate of 28.1 mL/min. Furthermore, pure O_2 was supplied to achieve higher gas exchange rates.

In 2012, Gray *et. al.* [77], used a polypropylene HFO with a surface area of 0.5 m^2 and a priming volume of 200 mL. The circuit consisted of a pump, HFO and a heat exchanger. Lamb fetuses were connected via veno-venous, of which five of nine survived for 24 hours. A flow rate of 94 ±20 mL/min·kg with a pressure drop of 69 ±10 mmHg were achieved. The mean ΔPO_2 was 17 mmHg. The major cause of death was multi-system organ failure. In 2013, they [123] incubated 6 lambs in a dry heated waterbed for up to 3 days with efficient gas exchange. No signs of intraventricular hemorrhage were present but haemodynamic instability was observed in some of the lambs. The mean ΔPO_2 was 95 mmHg and the reported blood flow rate was 25±7.5mL/min·kg.

In 2012, Miura *et. al.* [78], used a pumpless HFO with arterio-venous access to premature lambs. The surface area of the device was 0.3 m^2 with a priming volume of the circuit was 60 mL. It showed an efficient O_2 transfer of 10.5 to 12.2 mL/min at flow rates of 25 to 125 mL/min·kg. Five lambs survived for approximately 18.2 hours. Although the priming volume is lower than previous ECMO designs, it is still too high to be used in preterm neonates.

In 2013, Wu *et. al.* [19], developed a pumpless microfluidic oxygenator which comprised of multiple modular units so that it could be adjusted to the body weight of the preterm baby. The device was tested in a piglet for up to 4 hours with an arterio-venous access. The priming volume was 4.8 mL/kg including manifolds and connectors with a surface exchange area of 0.008 m^2. The pressure drop was 88 mmHg with a maximum flow rate achieved of 24 mL/min. The O_2 gas transfer was 30 mL/min·m^2 [25]. This device seems suitable for preterm neonates; however, a lower pressure drop, higher flow rates and longer periods of perfusion need to be achieved.

In 2015, Bryners *et. al.* [79], used extremely premature lambs (<26 weeks of gestation) to undergo treatment with ECMO or mechanical ventilation (MV). The ECMO device was connected with a veno-venous access, the flow rate range between 28.1 to 100 mL/min·kg, and the priming volume was 200 mL. Results showed that lambs were sustained for 1 week with an AP whereas with MV they were maintained alive for less than 4 hours.

Improvements in the cannulation configuration, the O_2 uptake and priming volume have been observed over the years with the ECMO devices. However, the priming volumes are still too high for preterm neonates. Wu *et. al.* [19], showed a pumpless microfluidic device that used a priming volume as low as a 4.8 mL and was sufficient enough to support up to 15% of the total O_2

consumption of a neonate of 1 kg. This oxygenator device [24] was further developed by Matharoo [23] showing an improvement of 44% in blood O_2 uptake with an O_2 uptake of 26 µL/min at a flow rate of 1.2 mL/min [23]. However, this value is still below the O_2 uptake needs which is 1.9 mL/min·kg for a preterm neonate. Furthermore, at higher flow rates the oxygenation of blood is less efficient. One approach that can be adopted is to expose this oxygenator to enriched O_2 environment in order to improve its performance and achieve high blood oxygenation under the same operating conditions. An in-situ method that can generate O_2 without external gas lines is desirable.

3.3 OXYGENATORS PERFORMANCE WITH AMBIENT AIR

This section shows the performance of microfluidic oxygenators tested with ambient air in-vitro and in-vivo conditions. The microfluidic oxygenators that have been developed in the literature and discussed in the Chapter 3, Section 3.1.2.4 are shown in a comparative table (**Table 1** and **Table 2**).

3.3.1 In-vitro Experiments

The performance parameters and the designs of several microfluidic oxygenators in which in-vitro experiments have been performed are compared in **Table 1**. Parameters such as the maximum blood O_2 uptake, flow rate, pressure drop and their designs are reported. The experiments reported were performed with animal and human blood and under ambient air conditions.

Table 1 - *Design and performance parameters of In-vitro experiments conducted using microfluidic oxygenators in air or compressed air environments. Surface area (SA) and surface-to-volume-ratio (SAV) represent the effective gas exchange area. Priming volume is defined as the amount of blood that can be contained in the oxygenator. The pressure drop is the difference in pressure between the inlet and outlet of the device. PDMS membrane was non-porous unless otherwise specified. "*" represents calculated values.*

Research group	Lee 2008 [56]		Potkay 2011 [60]		Wu 2013 [19]				Rochow 2014 [25]	Kovach 2015 [65]	Thompson 2017 [62]
Channel type	Rectangular	Rectangular with support posts	Rectangular		Rectangular with support posts				Rectangular with support posts	Branched	Rolled-membrane
Channel Height (µm)	15		10	20	80				80	200-10	10
Membrane Thickness (µm)	130		15		15		15	6	20	15	66
Membrane material	PDMS		PDMS		PDMS		PC porous (µm)		PDMS	PDMS	PDMS
					Porous	Normal	0.5	1	139*	15.3*	4.3*
SA (cm^2)	0.83	1.16	1.67	2.34	13.9*				126*	77*	158
SAV (cm^{-1})	669*	667*	800	400	126*				1.1*	0.2	0.027
Priming volume (mL)	0.00124	0.00174	0.002*	0.006*	0.11*				3	1.3*	4.4
O_2 Exchange (µL/min·cm^2)	8.2		22.8	13.7	1.8	1.3	1	0.9	10	5	12.7
CO_2 Exchange (µl/min·cm^2)	-		30	34.2	7.8	6.8	5.8	5.5	10	5	12.7
Blood Flow (mL/min)	0.8		1.5	1.5	2				40	0.2	1.25

Pressure Drop (mmHg)	2-4	>300	500	20	28	35	40	62	2	120
Type of Blood	Bovine	Porcine		Human				Human	Bovine	Bovine
Gas supplied	Ambient air	Ambient air		Ambient air				Ambient air	Ambient air	Ambient air

Although the Potkay device [60] has shown to have an outstanding performance with air and is comparable to HFOs working with pure O_2, the pressure drop is extremely high. The Rochow device [25] has shown a good performance at higher flow rates; however, it was not able to provide higher O_2 transfers using just ambient air.

3.3.2 In-vivo Experiments

In this section, the performance of microfluidic oxygenators that have reported in-vivo experiments are compared. Rochow [25] and Kovach [65] groups have performed in-vivo experiments and the design and performance are compared in **Table 2**. Parameters such as the maximum blood O_2 uptake, flow rate, pressure drop and their designs are reported. The experiments were performed on a single animal and under ambient air conditions.

Table 2 - *Design and performance parameters of In-vivo experiments conducted using microfluidic oxygenators in an air environment. Surface area (SA) and surface-to-volume-ratio (SAV) represent the effective gas exchange area. Priming volume is defined as the amount of blood that can be contained in the oxygenator. The pressure drop is the difference in pressure between the inlet and outlet of the device. PDMS membrane was non-porous unless otherwise specified. "*" represents calculated values.*

Research group	Rochow 2014 [25]	Kovach 2015 [65]
Channel type	Rectangular with support posts	Branched
Channel Height (µm)	80	200-10
Membrane Thickness (µm)	20	15
SA (cm^2)	83.4*	15.3*
SAV (cm^{-1})	126*	77*
Priming volume (mL)	0.66	0.2
Membrane material	PDMS	PDMS-PEG
O_2 Exchange ($\mu L/min \cdot cm^2$)	3	5.7

CO_2 Exchange (µl/min·cm^2)	-	5.9
Blood Flow (mL/min)	24	0.5
Pressure Drop (mmHg)	88	6
Animal	Piglet (1)	Sprague-Dawley (1)
Gas supplied	Ambient air	Ambient air

The in-vivo experiments show that the Rochow device [25] was capable of a blood O_2 uptake of half the oxygenation obtained with the Kovach device [65]; however, the flow rate is 12 times higher using the Rochow oxygenator [25]. Thus, the Rochow device seems to have a better performance. Nonetheless, the experiments do not use the same animal model nor the same body weight of the animal. Furthermore, in Kovach's in-vivo experiment, they ventilated the rat with pure O_2 (98% after accounting for isoflurane) [65]. Thus, the blood already came fully oxygenated to the lung device where the blood SaO_2 level decreased with its exposure to air. The reported O_2 transfer was that of the decrease of O_2 in blood. Rochow [25] designed the experiment so that blood O_2 uptake was taking place. Thus, these experiments are not comparable.

3.4 OXYGENATORS PERFORMANCE WITH PURE OXYGEN

This section shows the performance of microfluidic oxygenators tested with pure O_2 in-vitro conditions. The under development microfluidic oxygenators mentioned in section 3.1.2.4 are shown in a comparative table (**Table 3**). This is followed by a comparative table of the performance of the gas transfer in commercial HFO for the term neonate population (**Table 4**).

3.4.1 In-vitro Testing of Microfluidic Oxygenators

Table 3 summarises the work of several groups that have tested microfluidic oxygenators in an 100% O_2 environment. Parameters such as the maximum blood O_2 uptake, flow rate, pressure drop and their designs are reported. The experiments reported were performed with animal and human blood and under an enriched O_2 environment using pure O_2.

Table 3 - Design and performance parameters of *In-vitro experiments conducted using microfluidic oxygenators in a 100% O_2 environment. Surface area (SA) and surface-to-volume-ratio (SAV) represent the effective gas exchange area. Priming volume is defined as the amount of blood that can be contained in the oxygenator. The pressure drop is the difference in pressure between the inlet and outlet of the device. PDMS membrane was non-porous unless otherwise specified. "*" represents calculated values.*

Research group	Lee 2008 [56]		Hoganson 2010 [59]			Hoganson 2011 [61]	Kniazeva 2011 [63]	Rochow 2014 [25]	Rieper 2015 [66]	Thompson 2017 [62]
Channel type	Rectangular	Posts	Branched			Rectangular	Branched multilayered	Rectangular with support posts	Rectangular double-sided gas	Rolled-membrane
Channel Height (µm)	15		200			746-100	100	80	100	10
Membrane Thickness (µm)	130		12	15	11	20	90	66	90	66
Membrane material	PDMS		PC	PDMS-PC	PDMS	PDMS	PDMS	PDMS	PDMS	PDMS
SA (cm^2)	0.83	1.16	30.8 (18)			17*	139*	1200	4.3*	4.3*
SAV (cm^{-1})	669*	667*	45			100	126*	100	158	158
Priming volume (mL)	0.00124	0.00174	0.6*			0.17*	1.1*	12	0.027	0.027
O_2 Exchange ($\mu L/min \cdot cm^2$)	26.2	24.7	4.9 (8)			0.3*	10.4	2.5	6.6	6.6
CO_2 Exchange ($\mu l/min \cdot cm^2$)	-		4.5 (7.8)			17	-	10	3	13
Blood Flow (mL/min)	0.4	2	4			0.5*	40	50	1.25	1.25

Pressure Drop (mmHg)	2-4 mmHg	72	20	-	62	80	120
Type of Blood	Bovine	Porcine	Sheep	Phosphate buffer saline	Human	Porcine	Bovine
Gas supplied	Pure O_2	Pure O_2	Pure O_2	Pure O_2	Pure O_2	Pure O_2	Pure O_2

3.4.2 In-vitro Testing of Commercial Hollow Fibre Oxygenators

Table 4 summarises the performance of three different AP commercially available. Parameters such as the maximum blood O_2 uptake, flow rate, pressure drop and their designs are reported. The experiments reported were performed with animal blood and under an enriched O_2 environment using pure O_2.

Table 4 - *Commercial oxygenators for neonates using O_2 as the gas supplied. Surface area (SA) and surface-to-volume-ratio (SAV) represent the effective gas exchange area. Priming volume is defined as the amount of blood that can be contained in the HFO and the arterial filter. The pressure drop is the difference in pressure between the inlet and outlet of the device.*

Product Name	Maquet Quadrox-i Neonatal [80]	CAPIOX FX 05 Baby [81]	Dideco D100 [82]
Channel type	Hollow fibres	Hollow fibres	Hollow fibres
SA (cm^2)	3800	5000	2200
SAV (cm^{-1})	95*	116*	25.1.8*
Priming volume (mL)	40 (15 mL minimal operating volume)	43 (15 mL minimal operating volume)	47 (10 mL minimal operating volume)
Membrane material	Microporous polypropylene	Microporous polypropylene	-
O_2 Exchange ($\mu L/min \cdot cm^2$)	23.7	20	21.8
CO_2 Exchange ($\mu l/min \cdot cm^2$)	18.7	16	14
Blood Flow (mL/min)	1500	1500	700
Pressure Drop (mmHg)	70	90	175
Blood	-	Bovine	Bovine

The blood O_2 uptake from microfluidic devices that have low priming volume are comparable with commercial HFO when they are ventilated with pure O_2. All of the microfluidic devices show a better performance at releasing CO_2 gas. It is then desirable to increase the O_2 content in the environment while maintaining a compact and inexpensive AP. Therefore, a new approach to oxygenate the blood in-situ should be investigated.

3.5 ALTERNATIVES TO SUPPLY OXYGEN TO BLOOD IN-SITU

Although 100% O_2 environment provide an advantage in terms of oxygenation, they require gas cylinders that are bulky. This section introduces alternatives to generate O_2 in-situ that are more compact and portable than compressed gas cylinders. Possible mechanisms to supply O_2 in-situ include electrochemical devices, O_2 concentrators and chemical methods [83]. These alternatives are explained in more detail in the subsections below.

3.5.1 Chemical Generation of Oxygen

The chemical generation of O_2 occurs when a solid oxidant is combined with a catalyst. Chemical generators of O_2 (CGO) usually use solid compounds such as sodium chlorate ($NaClO_3$), sodium perchlorate ($NaClO_4$), potassium superoxide (KO_2), sodium percarbonate ($Na_2CO_3 \cdot 1.5\ H_2O_2$) and percarbamide peroxide ($CH_6N_2O_3$) [84]. Catalysts are used to initiate or accelerate the decomposition reaction of the aforementioned solid compounds to produce gaseous O_2. Commonly used catalysts include catalase, peroxidases, manganese dioxide and iron [85]. CGO is an exothermic reaction that can reach temperatures as high as 800ºC as a result of the generation of O_2 [86]. Insulators can be used to protect the outside environment from such high tempertures and to dissipate away the heat; however, the temperature at the surface could still reach 80ºC [82]. Moreover, COGs have a limited lifetime of less than 30 min.

Although O_2 generators do not need electricity to work nor maintenance, the flow rate of the O_2 generated cannot be controlled. This approach is widely used in aircraft, spacecraft, submarines, combat zones and mine rescue [85, 86] for emergency purposes but is not suitable for delivering O_2 to an AP.

3.5.2 Oxygen Concentrators

An O_2 concentrator (OC) is a machine that can generate 90% to 95% enriched O_2 using ambient air [87]. The OC compresses the air that it takes from the surroundings and passes it through zeolite sieves that adsorb the nitrogen present in air. The concentrated O_2 in the equipment can be then delivered to the patient (Figure 3.14). A stationary and portable OC can deliver between 5-10 L/min and 3 L/min of O_2, respectively, at a lower cost than with the previously mentioned technologies [84, 87]. The stationary OC requires direct connection to an electrical outlet whereas the portable OC uses a rechargeable battery than can run for up to 5.4 hours. OCs require day-to-day maintenance. The staff needs to be trained to give a proper maintenance to the equipment and maximize its functionality. Extensive training is also required to properly use the stationary OC system. Furthermore, adequate infrastructure is needed to install the O_2 system [87]. The OC, either portable or stationary, has a lifespan of 5 to 10 years depending on the maintenance given [88].

Although the continuous flow output supplied of O_2 by the OC is more than enough for an AP, some limitations are observed with this technology. These systems are expensive and even the portable systems are bulky and may not be suited for integration with the AP technology.

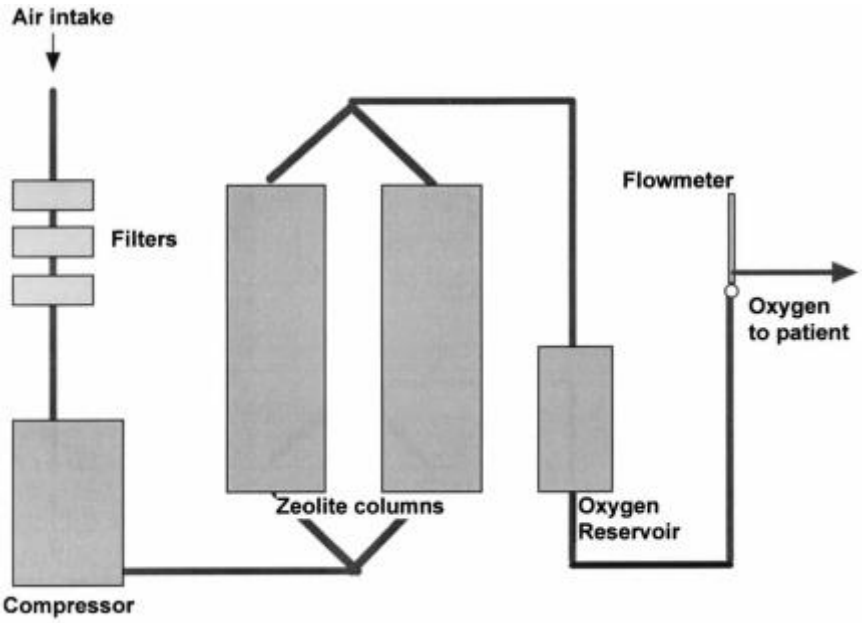

Figure 3.14 - *Block diagram of an O_2 concentrator components and its operation [28]. After filtration air is compressed and then passed alternately through columns of zeolite, in which nitrogen is adsorbed. A small O_2 reservoir prevents outlet flow from varying during pressure swings. A flow meter controls the outlet flow to the patient.*

3.5.3 Electrolysis of water

Water electrolysis is an electrochemical process that separates water molecules into gaseous O_2 and H_2. The decomposition of these two gases is driven by the potential applied at the electrodes. The electrochemical reaction produces O_2 with a high purity [89]. The O_2 production is dependent on the current that flows through. The electrolysis efficiency depends on the electrolytes and electrode materials used [90].

This technology can be customized so that the amount of O_2 being produced can be regulated by adjusting the electricity supplied [90]. It can also be made compact with no requirement for additional infrastructure to install it. Furthermore, minimum maintenance would be required given that most of the materials used are low cost and can be made disposable. Hence, this technology is suitable for the AP.

3.6 ELECTROLYSIS OF WATER

In this section, the electrochemistry behind the electrolysis of water is discussed, including the basic thermodynamic and electrochemical principles of operation of an electrolytic cell. The electrochemical reactions involved in the production of O_2, Faraday's Law of electrolysis that relates the current to the amount of O_2 produced, and the electrochemical potentials required to initiate the reaction are discussed. Finally, the electrode kinetics, and the efficiency of the generation O_2 process are discussed.

3.6.1 Electrochemistry

Electrochemistry studies the relationship between the transfer of electrical charges (electrons) across a medium (solution) and its chemical reaction [91]. Typically, the chemical reaction that occurs at the electrode due to transfer of charge from it, is an oxidation (at one electrode) - reduction (at the other electrode) reaction. The electrochemical reaction occurs in an electrochemical cell that is composed of conductive electrodes (anode and cathode) and an electrolyte solution in which the electrodes are immersed. The electrochemical cell can be galvanic or electrolytic. A galvanic cell is characterized by a spontaneous reaction while an electrolytic cell uses the energy supplied from an external power source to drive the reaction [92].

Electrolysis of water is a non-spontaneous reaction that decomposes water molecules into gaseous H_2 and O_2. The following section will focus on describing the electrochemical process.

3.6.1.1 *Electrochemical Reaction*

Electrochemical reactions occur when a current is imposed on an electrolytic cell. This reaction comprises of simultaneous reduction at the cathode and oxidation at the anode. The anode (positive electrode) loses electrons which are gained by the cathode (negative electrode). Water consists of hydrogen ions (H+) and hydroxyl ions (OH^-) present in equilibrium as shown in equation (3.1) [93]. When an electrical current is applied these ions migrate to the cathode and anode respectively.

$$H_2O\ (l) \leftrightarrow H^+(aq) + OH^-(aq) \quad \textbf{(3.1)}$$

The OH^- ions react at the anode to give away electrons to form gaseous O_2, and the H^+ ions react at the cathode consuming the electrons from the electrode to produce gaseous H_2 (Figure 3.15). Theoretically, 4 electrons (e-) are needed to split two molecules of water into two molecules of H_2 and one molecule of O_2 [90]. The half reactions occurring at the anode and cathode can be written as:

Cathode: $2H^+(aq) + 2e \rightarrow H_2\ (g)$ **(3.2)**

Anode: $4OH^- \rightarrow O_2\ (g) + 2H_2O + 4e$ **(3.3)**

The overall chemical reaction of water can be written as:

$$\boldsymbol{H_2O \rightarrow H_2\ (g) + \frac{1}{2} O_2\ (g)} \quad \textbf{(3.4)}$$

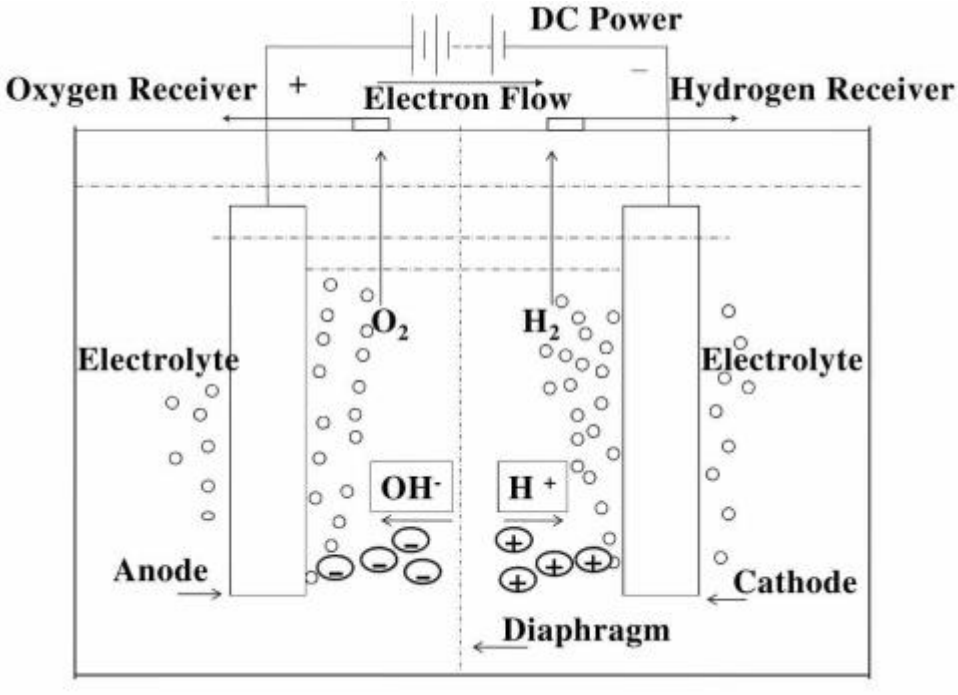

Figure 3.15 – *Illustration of a basic water electrolysis system [93].*

3.6.1.2 *Faraday's Law*

Faraday's law of electrolysis states that the amount of chemical change that happens at an electrode depends on the amount of electricity flowing through the electrolytic cell [94]. Therefore, the mass of substance produced by the anodic and cathodic reactions increases with the current supplied. In the case of water electrolysis, the amount of O_2 produced can then be calculated using equation (3.5) developed by Faraday.

$$\mathrm{I} = \frac{\frac{m}{M} \times F \times z}{t} \tag{3.5}$$

M is the molar mass, *z* is the number of electrons involved per molecule, *m* is the mass of the substance generated at an electrode and *F* is the Faraday constant (representing the amount of electric charge in 1 mole of electrons = 96485 C/mole) [92].

3.6.1.3 *Critical Voltage*

In the previous subsection, it was mentioned that the amount of gas evolved is proportional to the current supplied. However, for this reaction to start, the presence of a critical voltage is required. The critical voltage then represents the minimum voltage in the electrochemical cell (E^o_{cell}) to decompose water into H_2 and O_2 [95].

The change in Gibbs free energy (ΔG), at standard temperature and pressure (STP), measures the minimum of work needed so that electrolysis of water can happen [96]. Thus, to ensure that the electrochemical reaction takes place E^o_{cell} can be related with ΔG by the following equation:

$$E^o_{cell} = \frac{-\Delta G^o}{nF} \tag{3.6}$$

ΔG^o is the change in the Gibbs free energy under STP, n is the number of electrons transferred and F is the Faraday constant (96485 C/mole) [90].

The heat of formation of water at STP is then governed by the difference between enthalpy and entropy within the system which has been established as 237.2 kJ/mol [95].

$$\Delta G^o = \Delta H^o - T\Delta S^o \tag{3.7}$$

Therefore, based on equation **(3.6)** the theoretical critical voltage needed to decompose one molecule of water the is $E^o_{cell} = 1.229\,V$.

An electrochemical cell achieves 100% efficiency when the reaction is endothermic which is considered below 1.47 V [95]. However, in practice an overpotential is needed of 1.8 V to overcome the reaction resistances generated in the system [93]. These resistances depend on the electrolyte properties, the design of the electrolytic cell and the electrode form and material.

Figure 3.16 summarizes the concepts above mentioned. Moreover, it shows that when electrolysis of water occurs at higher temperatures, the voltage to start splitting the water molecules decreases [97]. However, it is not just the thermodynamic laws that affect the performance of the system. It is of great importance to consider parameters such as the electrode materials and electrolyte properties.

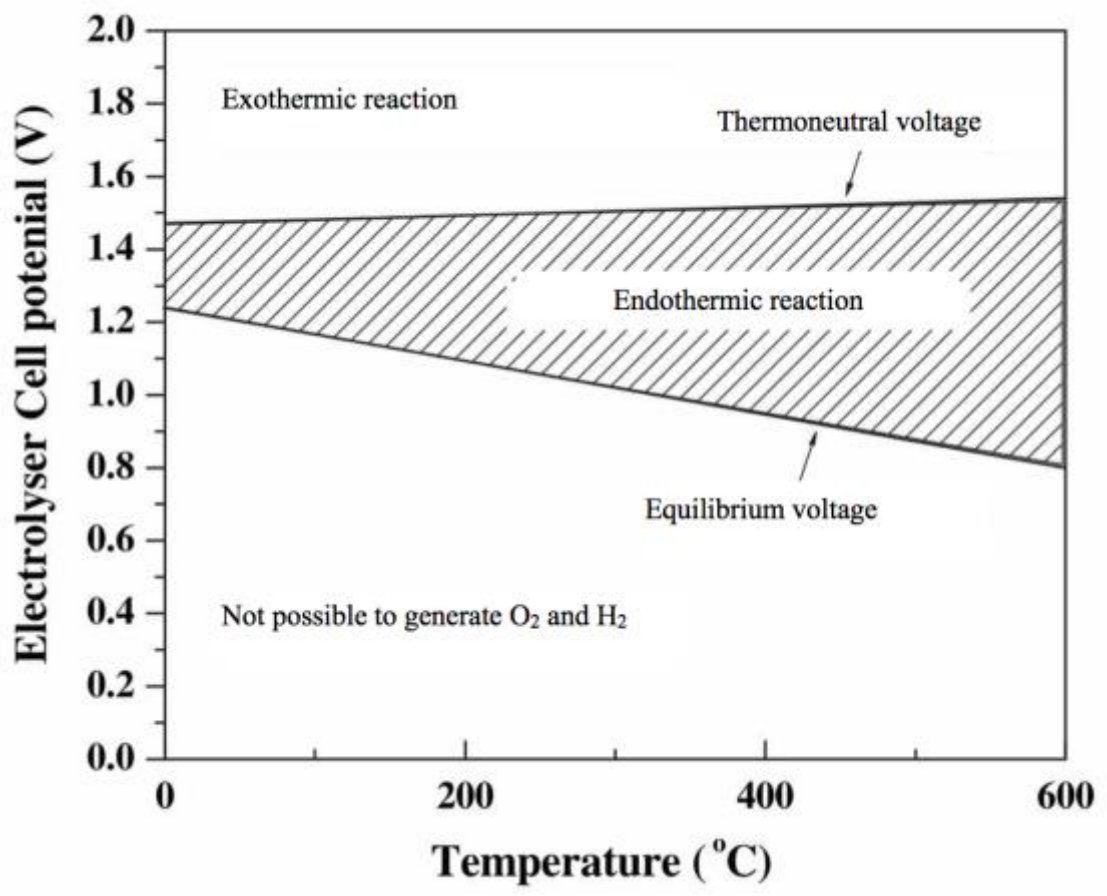

Figure 3.16 – *Cell potential for* H_2 *and* O_2 *production [93].*

3.6.1.4 *Electrode Kinetics*

Electrode reactions obey the kinetic law that directly affects the rate of production of the gas. The rate of the reaction at the electrode will depend on the material, surface, shape (e.g. rough, porous) and activation energy of the electrode, and the current density and composition of the

electrolytic solution. Thus, although the critical voltage is reached, an overpotential is required to start the electrolysis. Furthermore, the aforementioned factors are associated with the electrode's ability to sustain the reaction and maintain the flow of the current in the entire cell [93, 94]. Note that the electrode reaction is also intertwined with the electrolyte and its mechanisms to transport the current and the ions [94].

The reaction happening at the surface of the electrodes is associated with the current density (*j*). This *j* can be correlated with the rate at which electrolysis happens with equation **(3.8)** [93].

$$Rate = \frac{j}{nF} \tag{3.8}$$

Where *j* is the current density, *n* the number of electrons transferred and *F* is the is the Faraday constant (96485 C/mole).

The rate constant of the chemical reaction is determined by the activation overpotential which is associated with the activation energy (E_A = E-E^o) and is, in turn strongly related with the electrode material [93]. Arrhenius equation can express the rate constant of a chemical reaction (3.9) .

$$k = Ae^{\frac{E-E^O}{RT}} \tag{3.9}$$

Where E_A is the activation energy, *A* is the frequency factor, *R* is the gas constant and *T* is the temperature.

Equations **(3.8)** and (3.9) can then be associated using the transition-state-theory to obtain the Butler-Volmer equation for one-electron reaction [93,94]:

$$i = i_{cathode} - i_{anode} = FAk^0(C_0(0,t)e^{-\alpha\frac{F}{RT}(E-E^O)} - C_R(0,t)e^{\frac{F}{RT}(1-\alpha)(E-E^O)}) \tag{3.10}$$

Where A is the surface area of the electrode affected by the current, K^0 is the standard rate constant, α is the transfer coefficient, t is the specific time at which this current occurs, 0 is the distance from the electrode, R and F are the gas and Faraday's constants respectively, T is the temperature. $C_0(0,t)$ represents the concentration of ions (OH^- or H^+) at the electrode and $C_R(0,t)$ represents the concentration of the reaction product (O_2 or H_2).

The over potential needed to initiate the chemical reactions at the electrode is dependent on a number of factors such as the solution resistance, temperature of the cell, bubble formation at the electrode and the activation energy required at that temperature [93]. All of these are affected by the current density imposed at the electrodes (Figure 3.17). In general, higher overpotential is required at higher current density as the potential drop required to move the ions across the solution increases. Furthermore, the formation of gas bubbles at the electrodes also increase the resistance of the system and therefore increase the overpotential required to impose the same current density. Finally, the flow of the current through the solution causes joule heating which increases the temperature. The activation overpotential reduces with temperature. Therefore, to improve the efficiency in the cell a reduction of the solution resistance overpotential is required. The right selection of the electrodes and suitable design of the electrochemical cell can significantly lower the solution resistance and enhance the efficiency [93].

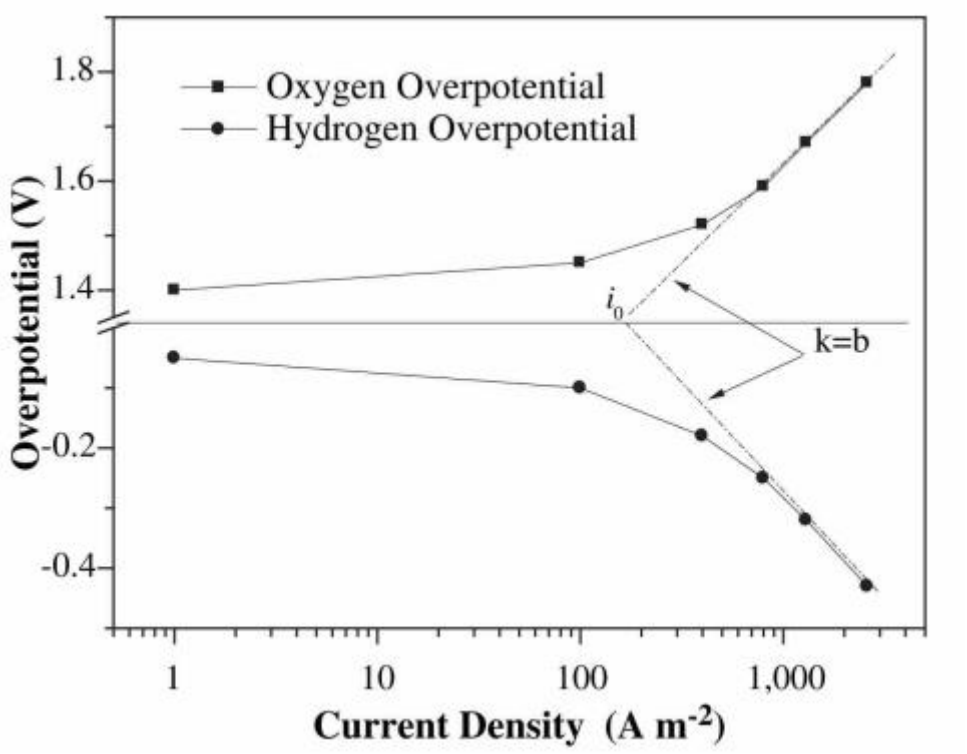

Figure 3.17 – *Typical Tafel plot for* H_2 *and* O_2 *evolution [93].*

3.6.1.5 *Electrolyte Solution and Membrane Separator Resistances*

The main reasons for electrical resistance are related to the electrolyte solution, the membrane that separates the cathode and the anode, wires and electrodes used in the system [93]. The electrical resistance in the connections and electrodes can be attenuated by using more conductive materials and by varying their dimensions.

The ionic transfer is a mass transport phenomena that is determined by the molar concentration of the electrolyte solution, the inter-electrode spacing and the membrane that separates the anode and cathode [93]. The mass transfer rate of the ions is primarily dependent on the concentration of the electrolyte. An empirical relationship can be made between the molar conductivity and the concentration of electrolytes (strong electrolytes) based on Kohlrausch's Law [93]:

$$\Lambda = \Lambda_0 - K\sqrt{C} \tag{3.11}$$

Where Λ_0 is the molar conductivity extrapolated to infinite dilution, K is the Kohlrausch coefficient and C is the electrolyte concentration. Thus, the conductivity of the electrolyte can be increased by increasing its ionic concentration.

Furthermore, the formation of bubbles in the electrolyte solution and on the electrodes surface is the major cause of resistance [93]. These bubbles greatly affect the ionic transfer rate and the reaction rate at the electrode. The influence of bubbles on the electrode and the electrolyte can be represented by the following equations:

$$k_g = k(1 - 1.5f)$$

(3.12)

Where g stands for each component of the circuit, k is the specific conductivity (of the gas-free electrolyte solution) and f is the volume fraction of the gas in the solution.

$$\rho = \rho_0(1 - \theta)^{-3/2}$$

(3.13)

Where ρ_0 is the specific resistivity (of the gas-free electrolyte solution) and θ is the percentage of the electrode covered by the bubbles.

As mentioned above the membrane (diaphragm) that separates the production of gases (O_2 and H_2) also introduces a resistance to the system. The apparent conductivity can be expressed using the following equation by MacMullin and Muccini equation [93].

$$k_d = 0.272\frac{km^2}{p}$$

(3.14)

Where *m* is the membrane hydraulic radius, *p* is the membrane permeability and *k* the specific conductivity.

The energy losses translated to Joule heating can be calculated based on Ohm's law by dividing the overpotential by the current density. The overall electrical resistance in the system is then obtained.

3.7 COMMERCIALLY AVAILABLE ELECTROLYSERS

Commercially available electrolysers are usually targeted towards generation of pure H_2, sodium hypochlorite (ClO^-) or O_2. The applications of these electrolysers are in treatment of wastewater, disinfection via ClO^-, O_2 production for cell culture, maintaining high levels of O_2 in aquatic environments, hydroponics and electrolysis for hair removal. The following subsection discuss the application and the basic principles of operation of a DO commercial electrolyser.

3.7.1 Dissolved Oxygen Electrolyser

The oxygenator is a commercial electrolyser that is focused on increasing the content of O_2 dissolved in water to create a supersaturated environment [98]. A current is supplied (<1 A) to the electrodes which are positioned at close proximity from each other. The rate of current flow is set such that a slow gas evolution occurs which is just sufficient to generate bubbles is in the range of 0.1 to 100 µm so that they do not break the surface tension of the medium [99]. This micrometer size then allows the bubbles to quickly dissipate away and the gas to stay dissolved in the water providing a constant source of O_2 to bait and catch fish while maintaining their healthy levels and reducing their stress (Figure 3.18) [98]. Furthermore, this concept could be used for other aquatic animals, hydroponic culture and as a wastewater treatment [99]. It has been observed that if the

water contains salts such as NaCl, a production of Cl^- is also present which is an undesirable byproduct that reduces the amount of DO produced [100]. Although this electrolyser is portable and works with a 12V DC power supply, it is restricted to currents of less than 1 A which limits the production of O_2. Furthermore, the oxygenator is designed to increase the DO content rather than produce large bubbles that can enrich the supernatant space above the water with higher O_2 content. This electrolyser is not suitable for the AP which needs an O_2 enriched environment.

Figure 3.18 – *The oxygenator electrolyser.*

In this chapter, the history of oxygenators from the development of direct to indirect contact oxygenators was introduced. The major drawbacks observed for the clinically used oxygenators was the damage caused to blood, high pressure drop and high priming volumes. Later, microfluidic oxygenator designs that are under development were presented. These devices showed advantages over the clinically used oxygenators such as smaller priming volumes and higher surface area. However, the O_2 gas exchange was reported to be lower when using ambient air as the source of

O_2. Therefore, alternative methods of supplying higher concentrations of O_2 to blood in-situ were investigated to increase the blood O_2 uptake. It was found that electrolysis of water can fulfill this requirement by enriching the environment with an excess of O_2 while maintaining a compact design. The following chapter presents the design of the electrolysis cell and the methods developed to perform the in-vitro experiments.

CHAPTER 4

MATERIALS, FABRICATION, AND METHODS

This chapter presents the materials used, fabrication methods used to construct the device and the experiment setup and procedures used in the testing of the device. First, the fabrication process for the SOU devices is discussed. Next, the design of the electrolysis chamber and the incorporation of the agarose gel membrane as a salt bridge is detailed. The setups for various experiments are described. In particular, these setups were used to produce O_2 via electrolysis of water and to measure the DO in water as well as the blood O_2 uptake. The setup to measure the hydraulic resistance of a SOU for water and to set the O_2 level of blood are also discussed. Finally, the statistical analysis methods used to process the oxygenation data obtained are discussed.

4.1 MATERIALS

The moulds for the fabrication of the microfluidic oxygenators were fabricated using a silicon wafer substrate and SU-8 100 negative photoresist patterns. The SU-8 100 negative photoresist and SU-8 developer were purchased from MicroChem (Westborough, MA). The silicon wafers were purchased from University Wafer (Boston, MA). The wafers were cleansed with 2-isopropanol (IPA) purchased from Caledon Laboratory Chemicals (Halton Hills, ON). The oxygenators were fabricated by casting Polydimethylsiloxane (PDMS) on the moulds. The PDMS (Sylgard® 184 Silicone Elastomer Kit) was obtained from Dow Corning (Midland, MI).

The electrolysis chamber for O_2 generation was constructed using acrylic pieces that were joined with acetone purchased from Caledon Laboratory Chemicals (Halton Hills, ON), and the 3D printed supports were glued with cyanoacrylate from Elmer's Products Inc. (Westerville, OH).

Electrolysis of water was performed using stainless steel electrodes Asada Hardmesh® (MS-400/19) purchased from DynaMesh (Batavia, IL) and graphite electrodes (EYG-S121803) from Panasonic (Newark, NJ). The supporting electrolytes used for water electrolysis were sodium hydroxide (NaOH), potassium nitrate (KNO_3) and sodium chloride (NaCl) which were purchased from Caledon Laboratory Chemicals (Halton Hills, ON), and sodium sulphate (Na_2SO_4) from VWR (Mississauga, ON). The anode and cathode side of the electrolytic chamber was separated by agarose gel filter paper membranes which were made with agar powder from Bioshop (Burlington, ON), potassium chloride (KCl) and potassium nitrate (KNO_3) from Caledon Laboratory Chemicals (Halton Hills, ON), Whatman® paper filters grade 1 from Sigma-Aldrich (Oakville, ON) and microscope slides from VWR (Mississauga, ON).

The oxygenators were tested using bovine whole blood (7200807) with K2-ETDA anticoagulant which was purchased from Cedarlane Labs (Burlington, ON). The blood was heparinized using heparin sodium injection USP (10,000 U/mL) which was obtained from Sandoz (Boucherville, QC) and glucose monohydrate from EMD Millipore (Etobicoke, ON). The hematocrit (Hct) measurement in blood was performed employing plastic microhematocrit tubes and capillary tube sealant Critoseal™ from Fisher Scientific (Ottawa, ON).

The cleansing of blood from equipment and surfaces was done with Valsure® enzymatic cleaner which was purchased from Steris (Mississauga, ON) and Lavo® Pro6 bleach from Lavo Inc. (Montreal, QC).

4.2 FABRICATION

The fabrication process of the microfluidic device consists of three main steps which are discussed in the following subsection. Furthermore, details of the methods used in the design and fabrication of the electrolysis chamber and the manufacture process of the agarose gel membrane are discussed below.

4.2.1 Composite Conventional SOU Fabrication

The fabrication method used in this thesis for the fabrication of a SOU builds on the work done previously in our group [23]. The SOU was fabricated in three steps: the vascular network, the composite membrane, and the bonding of this membrane with the vascular network by O_2 plasma treatment.

4.2.1.1 *PDMS Microfluidic Network*

The mould to create the vascular network was fabricated using photolithography. A silicon wafer of 3 in (7.62 cm) was spun at 4000 rpm with a negative photoresist SU-8 100 on top creating a thickness of 100 µm. A mask was placed on top of the photoresist and exposed to UV light to create the desired pattern. After being on a hot plate for 45 min, the wafer was exposed to a SU-8 photoresist developer. The SU-8 developer dissolved the unexposed photoresist and preserved the fluidic network previously imprinted with the UV light. Once the mould was ready, the thickness of the features formed was verified using a polarising microscope (Eclipse LV100, Nikon, Melville, NY). The silicon wafer was then placed on a Pyrex® petri dish to provide support and contain the subsequently poured PDMS.

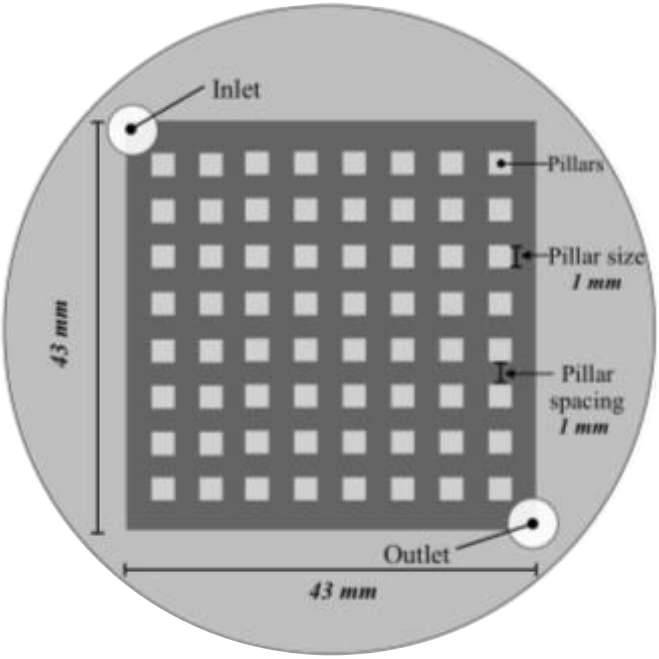

Figure 4.1 – *Schematic diagram of a conventional oxygenator unit. Top view showing the inlet and outlet and the array of uniformly spaced square pillars [23].*

PDMS was prepared using the silicone elastomer kit by mixing the elastomer base and curing agent in a mass ratio of 10:1, respectively. A 25 g mixture was stirred for one minute and then placed in a vacuum desiccator to extract the air bubbles (see Appendix A for detailed procedure). Two 1 cm length silicone tubes (Masterflex platinum-cured silicone tubing, L/S 16, Cole-Palmer, Montreal, QC) with a 3.1 mm inner diameter were positioned facing each other on opposite corners of the mould (Figure 4.1). PDMS was slowly poured into the mould (Figure 4.1), and the mould was placed in a preheated furnace (vo-1b020 vacuum oven, Across International, Sparks, NV) at 100ºC for 25 to 30 min. The cured cast was cut in a circular shape using a scalpel, leaving a fair distance between the edge of the petri dish and the inlet and outlet tubes. Subsequently, the PDMS network was peeled off from the mould and the inlet and outlet tubes were completely cleaned from any debris using a punch (Miltex Dermal Punch, Integra, Oakville, ON).

The vascular network was stored in a clean plastic petri dish (Fisherbrand™ 431761, Fisher Scientific, Ottawa, ON) with a clean tissue paper (Kimtech Kimwipes, Kimberly-Clark, Mississauga, ON) covering the bottom to prevent deposition of dust particles that could jeopardize the integrity of the vascular network.

4.2.1.2 *Composite Membrane*

The composite membrane was a modified PDMS membrane that had an embedded SSM. The composite membrane with the mesh is stiffer than a simple PDMS membrane, which in turn prevents its delamination under the operating conditions that was a problem in earlier oxygenators. This membrane also has the role of blocking the direct contact of blood with air; thus, the blood does not undergo denaturation of plasma proteins or impairment of erythrocytes [8].

The composite membrane was fabricated on a silicon wafer as the substrate. First, one side of the silicon wafer prepared by attaching an anti-adhesive fluorinated ethylene propylene film (Bytac® FEP Film General Purpose with Vinyl Back, US Plastics Corp.®, Lima, OH) on to the substrate. Second, the wafer was thoroughly cleaned using tissue paper (Kim wipes) moistened with IPA. Then, the wafer was placed centred onto the chuck of the spin coater (6800 Spin Coater Series, Specialty Coating Systems™, Indianapolis, IN). Next, 1 mL of PDMS was dispensed at the centre of the wafer using a syringe. The wafer was spun at 4000 rpm, after which an 8 cm by 8 cm stainless steel zero-wrinkle mesh was placed on top of the PDMS layer. The substrate was cured in a preheated furnace at 100ºC for 3 min. The wafer was taken out of the oven and another layer of PDMS was spun at 4000 rpm and cured. The resulting membrane was covered with a KimWipe and stored in a petri dish (see Appendix A for further details on the procedure).

4.2.1.3 *Plasma Bonding*

The bonding of the microfluidic network with the composite membrane was the final step of the fabrication of the SOU. A handheld corona generator (BD20-AC, Electro-Technic Products®, Chicago, IL) was used to activate both surfaces (see Appendix A for details).

First, the surfaces to be exposed were cleansed using compressed air. Second, both the clean surfaces were treated with the plasma, then pressed together and left undisturbed in the oven at 80ºC for up to 12 hours to make a strong bond. Finally, the fabricated SOU was carefully peeled off of the silicon wafer and stored in a petri dish protecting the membrane side with a KimWipe.

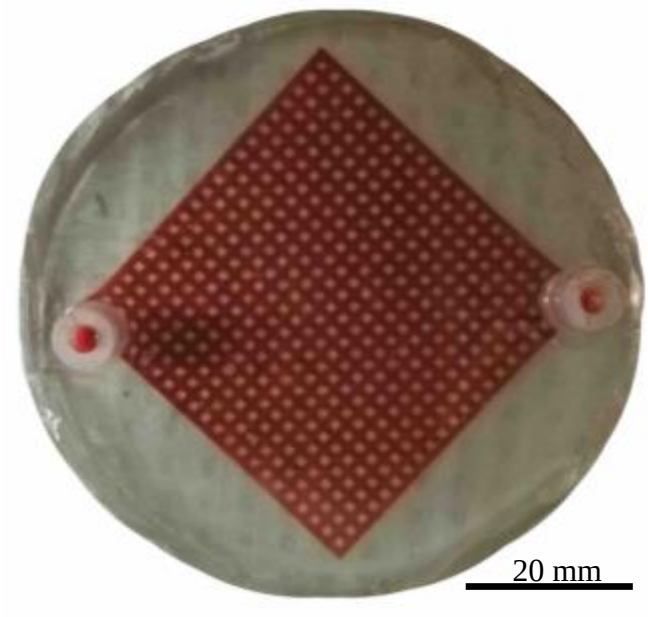

Figure 4.2 - *Composite conventional SOU filled with bovine blood. Pillar dimensions 100 µm x 100 µm x 100 µm. The pillars and composite membrane are bonded by* O_2 *plasma treatment.*

4.2.2 Electrolysis Chamber Fabrication

An acrylic chamber was designed and fabricated to perform experiments with water and blood. The chamber was designed using Autodesk® 123D Design for visualization purposes. It was made of transparent acrylic to observe any changes related with the electrolysis process or the blood flow across the SOU. It was built in a rectangular shape with inner dimensions of 16 cm × 8 cm × 6 cm so that a volume of 400 mL could be contained. Figure 4.3 shows the inner dimensions of the chamber in detail. The chamber was composed of a lid, an acrylic frame and 2 supports.

The chamber 3D design was converted into a two-dimensional (2D) drawing using Inkscape software. Then, a 3 mm thick acrylic sheet was cut into several pieces with a laser cutter (Speedy300, Trotec®, Mississauga, ON) available at the McMaster Engineering Research Machine Shop (JHE-115). The chamber was divided in two with the frame that held a filter paper membrane with agarose gel to connect the two sides of the chamber. The holders were designed with dimensions of 6 cm by 0.5 cm to support the SOU. The holders were 3D printed (Fortus 450mc, Stratasys, Eden Prairie, MI) at the McMaster Manufacturing Research Institute (JHE-109A).

The chamber was assembled and held in position by partially dissolving the acrylic surface with acetone attaching them and letting it dry so that a complete seal of the chamber joints was achieved. The holders were attached to the acrylic with cyanoacrylate glue (Krazy Glue®, High Point, NC).

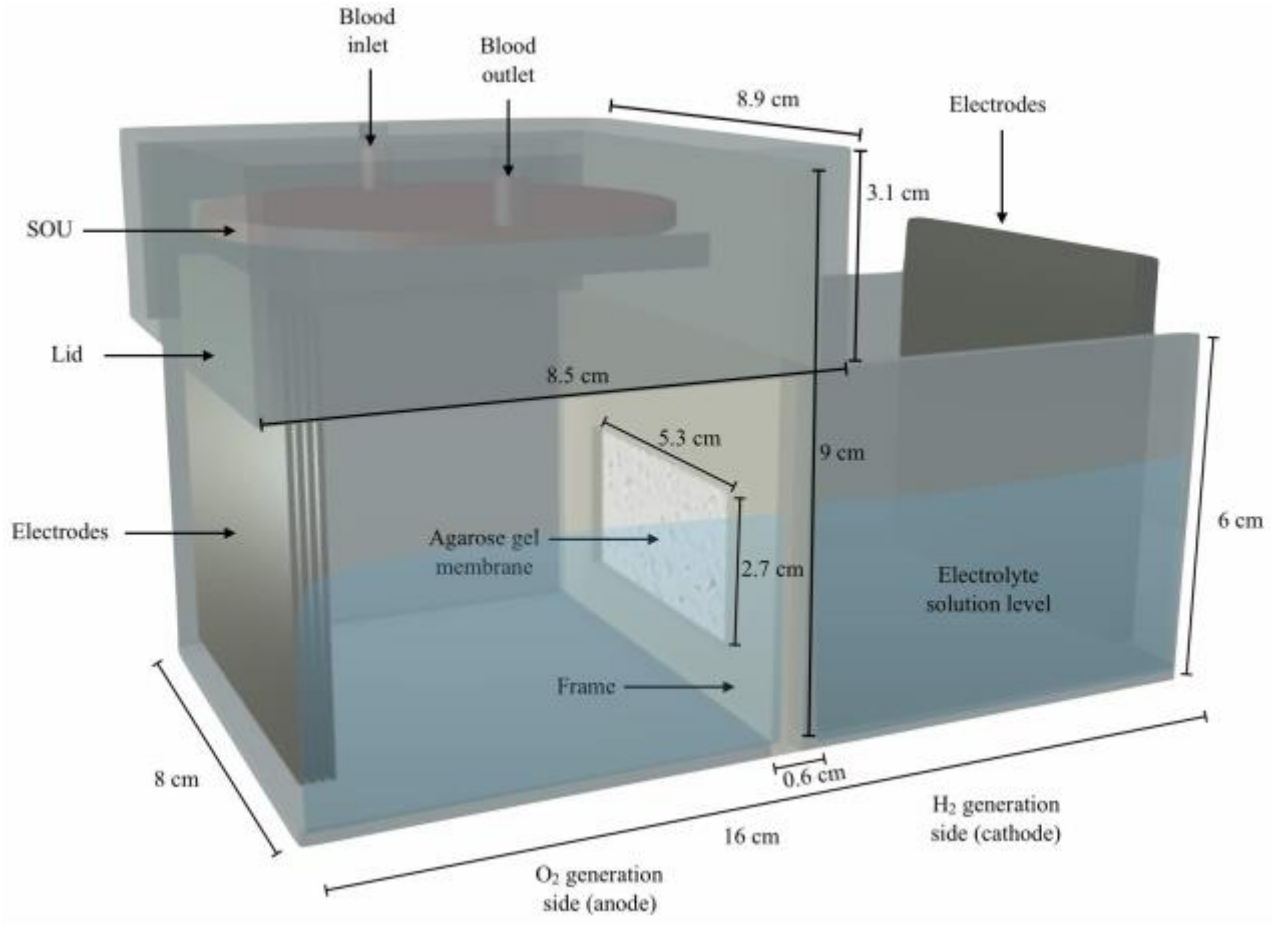

Figure 4.3 – *Illustration of the electrolysis chamber components and its inner dimensions. The lid holds the SOU and confines the generated* O_2*. The current is supplied by two sets of electrodes immersed into the electrolyte solution. The anode and the cathode chambers are separated by a gel membrane grasped by a frame.*

4.2.3 Agarose Gel Membrane Fabrication

A gel membrane was fabricated to separate the anode and cathode side of the electrolysis chamber. Agar gel was prepared with KNO_3 as the electrolyte and used to coat a filter paper membrane grade 1. The gel filled up the pores and enabled good electrical contact but prevented any gas transfer. The paper membrane served as the support to hold the agarose gel mixture.

The paper membrane was cut in a rectangular shape measuring 6.5 cm by 5 cm. A mixture of 2% agar powder and 1 M KNO_3 was heated up to the melting point of agar (85ºC). The mixture was then kept on a hot plate to maintain the temperature above 40ºC (solidification point of agar), and to gently mix it. The previously cut membrane was then immersed in the agarose gel, taken out and place it on a flat surface covered with plastic wrap. Next, a microscope slide was used to gently push the agarose gel into the pores and to remove the surplus gel from the surface. A smooth surface was then obtained. Finally, the membrane was completely wrapped in the plastic and stored in the fridge to maintain the humidity and its life span (Appendix A). From now on the agarose gel filter paper membrane is referred as the gel membrane.

4.3 METHODS

4.3.1 Dissolved Oxygen Measurement in Water

The DO in the water was measured as an indicator of the O_2 production. At room temperature (25ºC) and when it is in equilibrium with the ambient atmosphere containing 21% O_2, water can dissolve 8.3 mg/L of O_2 [101]. Under certain conditions, such as when water is close to a waterfall [102], algal bloom [103, 104] or because of an electrochemical reaction (e.g. electrolysis) [105], where the water is either sparged with O_2 or there is a generation, the concentration dissolved in water can reach a higher value. In the particular case of an electrochemical reaction, one can tune the amount of O_2 to be produced by varying the current supplied.

The experimental setup to investigate the effect of electrolysis current on DO levels in water involved two electrodes, introduced into a container with water, both of which were connected to either terminals of a DC power supply (1670A, BK Precision, Yorba Linda, CA). A power supply was operated in a constant current mode with a pre-determined current set for a defined period of

time. The power supply was turned off every time a measurement of DO in water was taken. An electrochemical sensor (550A, YSI, Yellow Springs, OH) was used to measure the DO. The container was moved to a magnetic stirrer (PC-420D stirring hot plate, Corning ®, Corning, NY). A 1 cm stir bar (stir bar with spinning ring, Cole-Parmer) was placed inside the sample, and the magnetic stirrer was set to mix at 240 rpm. The sensor probe was introduced into the water sample and was located close to the stir bar. If bubbles were seen blocking a section of the sensor, they were removed with a KimWipe tissue, and the sensor was reintroduced. The DO value was recorded once the readings stabilized. Additionally, the temperature of the water was recorded with a thermometer, at the beginning and end of the experiment.

4.3.2 Hydraulic Resistance Test to SOU

The hydraulic resistance was measured in the fabricated SOUs to characterise the resistance to flow of every single device and establish whether they would sustain the pressure encountered during the in-vitro experiments. Devices which showed similar hydraulic resistances were selected for oxygenation experiments. Additionally, this test was used to observe the homogeneous filling of the device and detect any defects such as membrane delamination. In order to make the delamination more visible water was mixed with food colouring (red food colour preparation, Club House) and used to fill the SOU.

The setup comprised a peristaltic pump (ISM832C, Ismatec®, Wertheim, Germany), a pressure transducer (TruWave transducer, Edwards, Irvine, CA), a pressure monitor (90369 Patient Monitor, SpaceLabs Medical Inc, Mississauga, ON) to read the average pressure drop, an SOU, and the aforementioned food colouring-water mixture.

First, the pump was calibrated. Then, the inlet of the SOU was connected to the outlet of the transducer, and the outlet of the SOU was placed in the same beaker so that the liquid returned to the reservoir (**Figure** 4.4). The peristaltic pump was then set at the maximum flow rate (25 mL/min), so the water flowed through the device at full speed for 5 min. Meanwhile, the pressure drop was monitored. Also, a close inspection for any sign of delamination or leakage was performed during the test. At the end of this 5min, the pump was turned off, and the pressure drop and flow rate were recorded (further details in Appendix A).

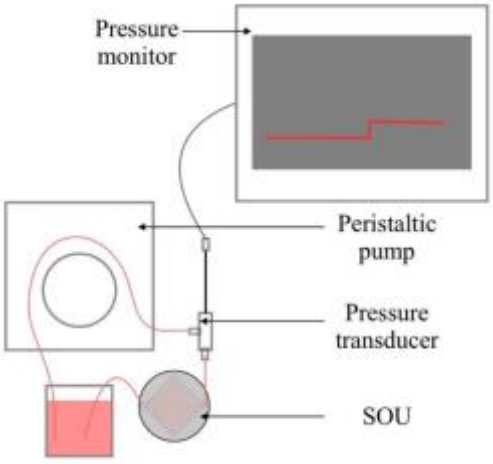

Figure 4.4 – *Experimental setup for the hydraulic resistance test. Food colour was diluted in water and pumped through the SOU and back to the reservoir for 5min.*

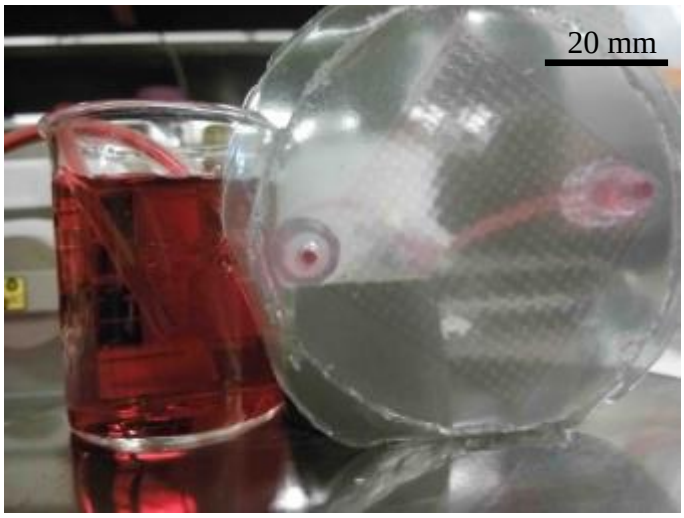

Figure 4.5 – *Close up view of the vascular network being filled with water to test its resistance to flow and delamination.*

4.3.3 Control of Blood Oxygen Level

Bovine blood was stored upon receipt in a refrigerator overnight before deoxygenation of it so as to equilibrate the SaO_2, pO_2 and partial pressure of carbon dioxide (pCO_2) to normal venous levels [38].

The setup (shown in **Figure** 4.6) for O_2 level control was prepared prior to exposure of the blood to room temperature (RT). The setup consisted of a blood reservoir attached to a magnetic stirrer, a peristaltic pump connected to the blood reservoir and the inlet of the HFO, a gas mixture cylinder of 95% nitrogen (N_2) and 5% CO_2 connected to the HFO's gas inlet and, lastly, a reservoir connected to the HFO's outlet. The magnetic stirrer was used to mix the blood during the entire process of deoxygenating the blood. The peristaltic pump attached to the magnetic stirrer was used to pump the blood through the gas exchange system. A HFO downstream from the pump (Mera Silox-S0.3, Senko Medical Instruments Mfg., Tokyo, Japan) was used to expose the blood to defined ratio of gases to control its SaO_2. It was held in a vertical position using a support stand with clamps to ensure that every single fibre would be filled up with blood. By nature, O_2 dissolves in plasma and binds with haemoglobin (Hb) that releases CO_2 [111]. The mixture of 95% N_2-5% CO_2 produces a rapid decrease in the O_2 content in blood while maintaining pH homoeostasis [106, 107]. Thus, a gas cylinder with 95% N_2-5% CO_2 mixture was connected to the gas inlet/outlet of the HFO in the counter current mode which was found to be the best mode for control of SaO_2 in blood. The other inlet/outlet gas connection of the HFO was left open so that the unbound O_2 could be cleared out from the HFO. A 3-way valve placed downstream of the HFO was used to connect a branch line that can be used to extract blood for monitoring its gas composition.

The deoxygenated blood from the HFO was collected in a polyethylene terephthalate (PETE) container (the original container sent along with the blood). The container's mouth was sealed with Parafilm® M (Bemis Company, Neenah, WI) and transparent tape to reduce the gas transfer.

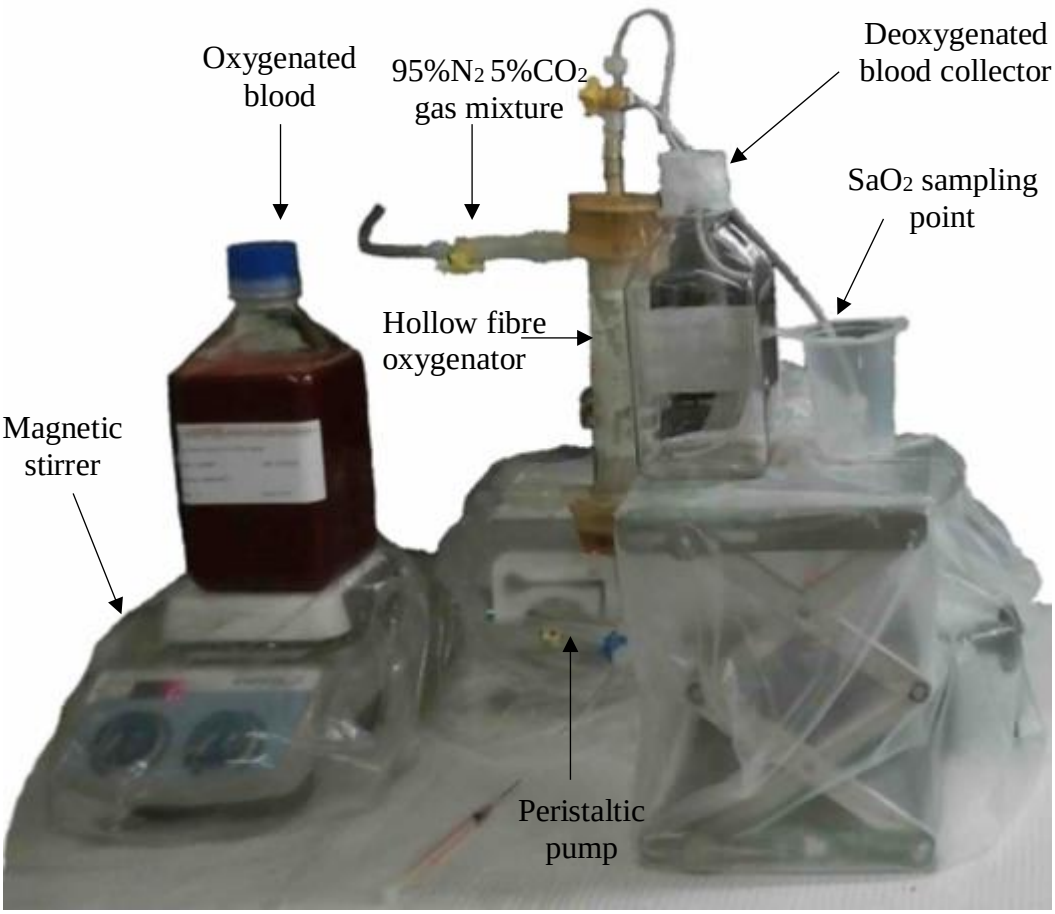

Figure 4.6 – *Experimental setup used for* the *deoxygenation of blood. The blood in the reservoir was slowly and constantly stirred while blood was forced through the HFO. Blood was exposed to the N_2-CO_2 gas mixture and then collected in another container.*

Once the setup was ready, the HFO was flushed with water to ensure all the subtilisins enzymes that were used to clean the oxygenator after prior use were removed (see Appendix A HFO cleaning process). The blood was then taken out of the refrigerator and a stir bar was added into the container. Heparin (3 U/mL) [19, 68] was added to the blood as an anticoagulant to avoid a clot formation in the sensor chamber [109]. Glucose was also added in a concentration of 1.5 mM/L to supply nutrition to the cells and prevent the lysis of the RBCs [110]. The blood was

moderately mixed by manually swirling the container. The container was set on top of the magnetic stirrer, and the blood was mixed at 100 rpm to maintain blood properties uniform all through the entire deoxygenation process. Next, the gas valve was opened, and the N_2-CO_2 gas mixture flowed through the oxygenator. Then, the pump was switched on which perfused the blood across the fibres allowing the exposure of the blood to the gas. Samples were taken to measure the SaO_2 level. Adjustments to the flow rate were made accordingly so that the desired SaO_2 levels were obtained in the blood. Once the collector container became full, the pumping was stopped. The Parafilm® M and tape sealing were left in place, and the tubing was removed. Then, the cap was tightly closed and the container stored in the refrigerator to decrease the metabolism of the red blood cells (RBCs) and minimise any changes to the SaO_2. See Appendix A for extended details on the procedure.

4.3.4 Blood Storage and Syringe Loading

The blood was placed in a PETE container when the desired SaO_2 was obtained, and the container was stored in the refrigerator. To run passive and active oxygenation experiments (Section 4.3.6) a syringe pump (Space Infusion Pump, 8713030U, B. Braun's Perfusor ®, Bethlehem, PA) was employed. The 60 mL Polypropylene (PP) syringes (BD syringes, Franklin Lakes, NY) that were loaded with blood were used on the same day, so that the integrity of the blood was not compromised. A peristaltic pump was used to load the syringes at the maximum flow rate so that the blood in the bottle had the least chance of exposure to the environment and possible gas exchange (Figure 4.7). This procedure led to a more stable loading were the risk of introducing air bubbles into the syringe was diminished.

Before loading the syringes, the blood was well mixed by gently spinning it around. Then, the inlet of the tube was introduced to the bottle, and the outlet was connected to the syringe. The syringe was held in a vertical position using a support stand to ensure that it was homogeneously filled from bottom to top and the air trapped in the syringe stayed at the top. Thus, the air bubbles did not significantly change the O_2 content in blood. Once the syringe was fully filled it was quickly unscrewed, the small bubbles were expelled and a cap was screwed to close the syringe. Lastly, the syringe was stored in the refrigerator.

Figure 4.7 – *Experimental setup to load the syringes with blood. Blood with low* O_2 *concentration was pumped into a 60 mL syringe at maximum speed.*

4.3.5 Hematocrit Measurement

The RBCs count was determined by spinning the blood in a micro-centrifuge (Microhematocrit Centrifuge StatSpin® CritSpin™, Beckman Coulter Inc., Mississauga, ON) to separate the RBCs from plasma. Then, the packed cells were measured with a digital reader (Digital Hematocrit Reader, Beckman Coulter Inc., Mississauga, ON) to determine the Hct percentage (see Appendix A). Also, the reading of Hct from the gas analyser (GEM Premier 3000, Instrumentation Laboratory, Bedford, MA) was recorded; however, this equipment is designed to analyse human blood. Hence, the micro-centrifuge Hct reading was the one reported.

4.3.6 Blood Oxygenation

In order to test the effect of active oxygenation through electrolytic generation of O_2 and to compare it with oxygenation from ambient air, the following setup was used. The setup (shown in Figure 4.8), comprised of an acrylic chamber filled with 400 mL of NaOH electrolyte solution using deionized water (PURELAB® Ultra, ELGA LabWater, Mississauga, ON). A gel membrane was held up in a frame and slid into the designated grooves in the acrylic chamber. The SSM electrodes had an open area of 49%, so four 7.5 cm by 8cm electrodes were connected together by alligators to make each of the electrodes (anode and cathode). The SSM total area in contact with the electrolyte solution was 205 cm^2. Thus, the current density at applied current of 1-3 A was ~ 4.9-15 mA/cm^2. Then, the anode and cathode were placed at the extreme ends of the acrylic chamber, away from the membrane with a gap of 14.5 cm between them. The electrodes were attached to external wires through alligator clips and insulated using electrical insulation tape (GTP-607 Tape, Gardner Bender, Mississauga, ON). The SOU was then placed inside the anodic side of the acrylic chamber and the inlet and the outlet PP male taper seal connectors with an outer

diameter of 4.75 mm and length of 1 cm were fed through the appropriately positioned holes on the lid to provide access outside. The lid was capped, and the small gaps between the chamber and the lid were sealed with strong packing tape (Staples® Heavy-Duty Shipping Tape, Staples, Hamilton, ON) to minimise the movement of air between the inside of the chamber and the outside ambient. A syringe was placed in a syringe pump and was connected to the inlet of the SOU, and a pressure transducer was added in between them, followed by a 3-way valve to monitor the initial SaO_2 condition of the blood. The pressure transducer was fixed to the pressure monitor to read the mean arterial pressure obtained at a given flow rate. One control sample was taken at the beginning and end of the experiment to observe if the SaO_2 initial setpoint was maintained throughout the experiment. The outlet was connected to a plastic container that was used to collect the oxygenated blood. The oxygenated blood samples were taken directly from the outlet tube using a needle (BD needles, Franklin Lakes, NY) with blunt tip to avoid cutting the tube; this needle was also used to take the control samples. The entire length of the needle was introduced into the tube to ensure that the sample taken was not exposed to the outside air. Polyvinyl chloride (PVC) is known for its low permeability to gases. Thus, all the experiments used Tygon™ PVC tube (Fisherbrand™ Tygon™ Flexible Tubings, Fisher Scientific, Ottawa, ON) to connect the oxygenators to reservoirs and avoid any changes to the blood O_2 content.

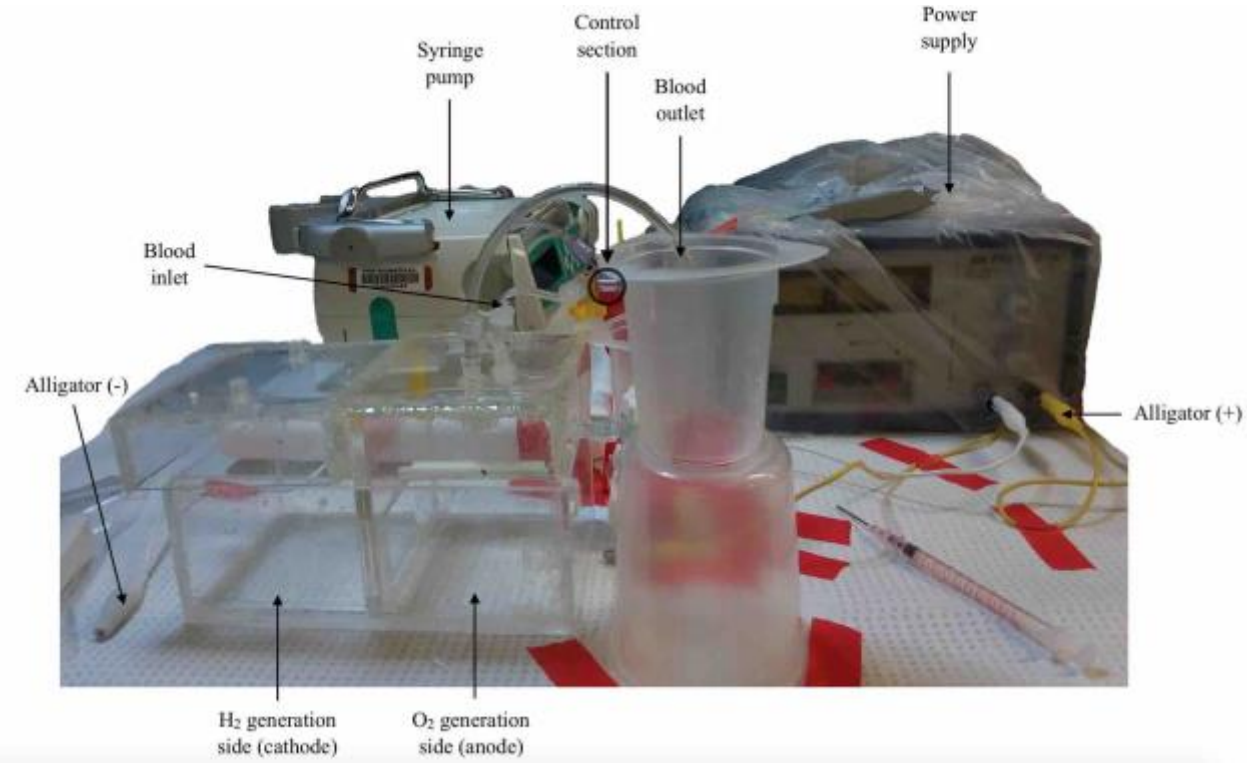

Figure 4.8 – *Experimental setup for passive and active oxygenation. The initial SaO_2 in blood is measured at the control section (before SOU) and the change in SaO_2 because exposing blood to O_2 at the blood outlet (after SOU).*

Bovine blood was the blood of choice to run the in-vitro experiments because it is readily available, less expensive and most importantly biosimilar to human blood (the erythrocytes have similar shape, size, and water permeability as human cells) [129]. A 60 mL syringe, previously loaded with deoxygenated blood, was taken from the refrigerator. The syringe was gently mixed by inversion. It was loaded onto the syringe pump and the appropriate flow rate set. The first sample was taken at the control section to establish the baseline SaO_2 of the blood. Subsequent samples were taken at the outlet every 4 min to determine the oxygenation performance of the oxygenator over time. Lastly, a second control sample was taken at the inlet (on the control section) to ensure that the O_2 level in the syringe had not changed. Refer to **Figure** 4.8 for more details.

A microhematocrit centrifuge was used to measure the Hct levels in blood to observe if Hct changed after the experiment was performed. Samples at the control section and the outlet were taken, at beginning of the experiment in the control section and at the end of the experiment in the control section again and at the outlet of the SOU.

The temperature of the blood was measured before and after the experiment to observe the change in temperature because of the experiment. A thermocouple type J (MQSS series, Omega® Engineering, Laval, QC) and a handheld thermometer (52 series II, Fluke, Mississauga, ON) were used to measure and read the blood temperature. The blood samples were measured at the beginning of the experiment in the control section and the end of the experiment in the control section again and at the outlet of the SOU.

4.3.6.1 *Passive Oxygenation*

Currently, PO is performed by exposing the SOU to ambient air. The O_2 from air diffuses through the PDMS membrane and oxygenates the blood flowing inside the oxygenator. Since, PO by exposure to ambient air is simple and does not require additional electrical power, it was used as the baseline to determine whether the AO improved oxygenation performance. The experimental procedure is described in Chapter 4, Section 4.3.6. A timeline of the experiment is shown below (**Figure** 4.9).

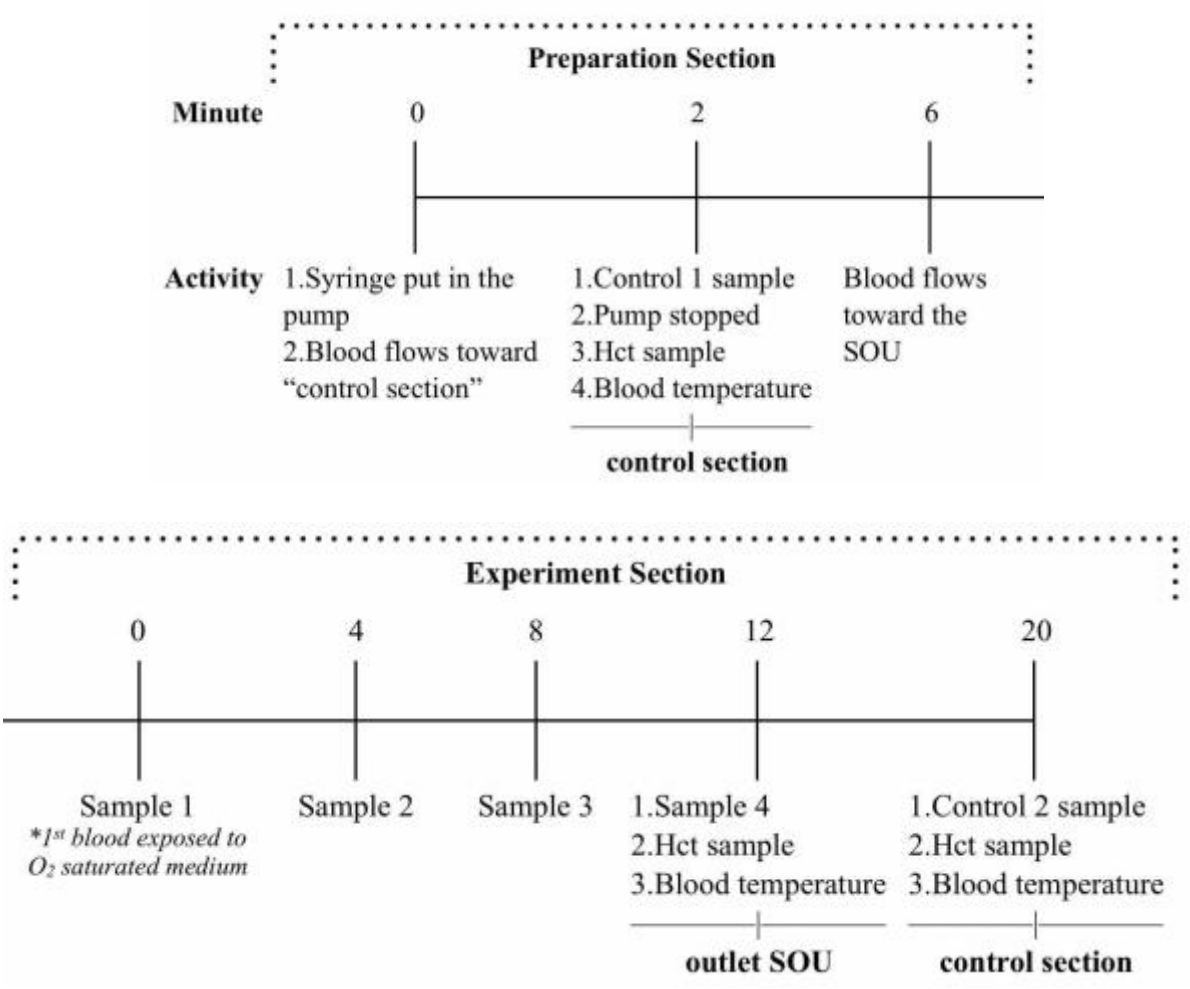

Figure 4.9 - *Passive oxygenation timeline. Steps followed and measurements taken to complete the entire PO experiment.*

4.3.6.2 *Active Oxygenation*

Electrolysis of water was used to increase the O_2 concentration in the ambient and thereby improve the O_2 uptake of blood and the SaO_2. A fixed current was applied to the electrolyte, so gaseous molecules of O_2 were generated from water at the anode. The generated O_2 gas was confined to the anode-side of the chamber with the help of an acrylic lid. Hereafter, enriching the environment with O_2 via electrolysis is referred to AO.

The AO was run with the setup earlier explained (Section 4.3.6). The current was switched on 30 min before the start of the blood oxygenation experiment in order to ensure that the ambient O_2 levels in the anode chamber were at stable levels, typical of normal operation of the device. After 30 min had passed, the blood flow was initiated and the experiment run as per procedure described in Section 4.3.6

A similar sampling method, as in Section 4.3.6, was executed. In addition, the temperature of water and blood was also measured. A timeline of the experiment is shown below (**Figure** 4.10).

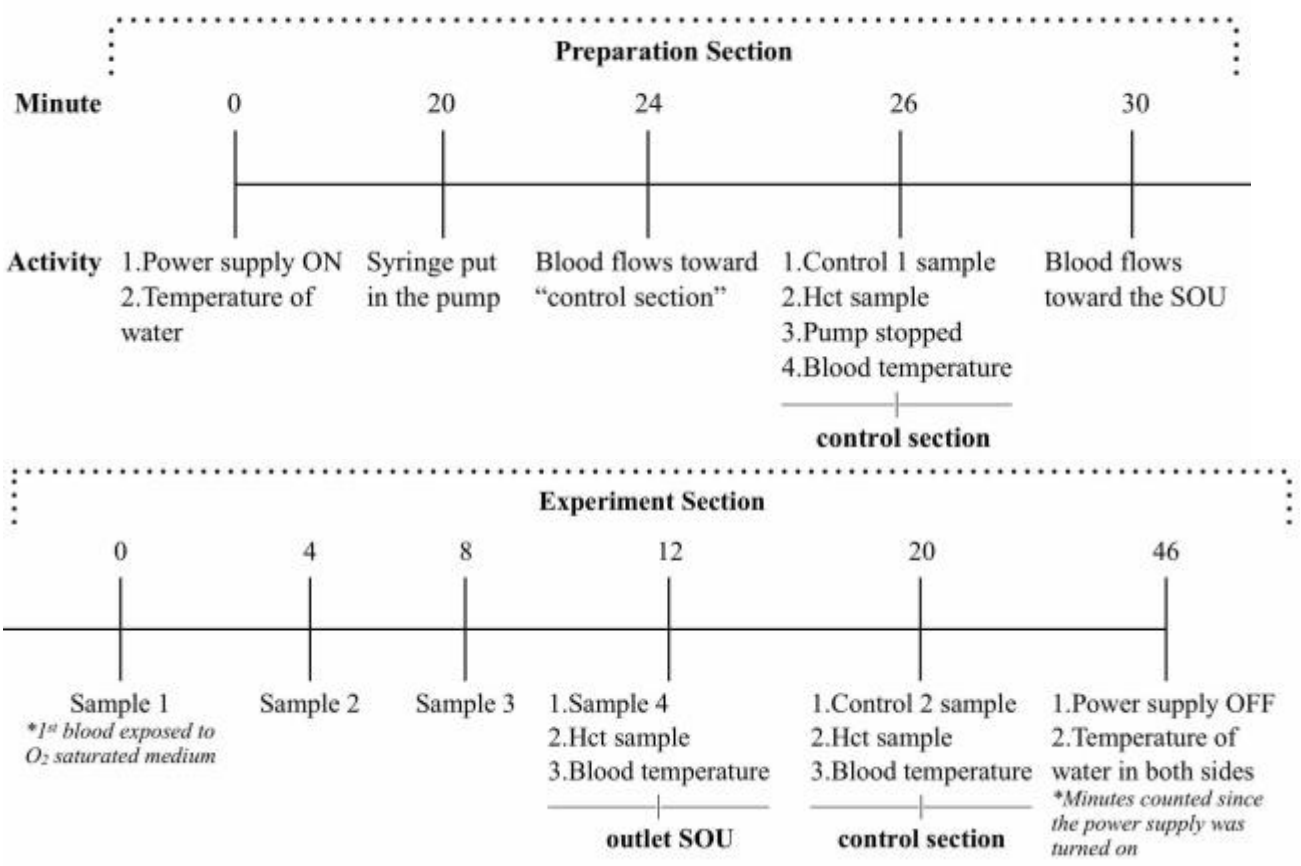

Figure 4.10 - *Active oxygenation timeline. Steps followed and measurements taken to complete the entire AO experiment.*

4.4 STATISTICAL ANALYSIS

Welch's T-test was used to determine whether the means of the two sample groups were statistically different ($p < 0.05$) from each other. A t-distribution was performed using equation (4.1) and (4.2) to accept or reject the null hypothesis and determine whether the evidence was strong.

$$t = \frac{\bar{X}_1 - \bar{X}_2}{\sqrt{\frac{s_1^2}{N_1} + \frac{s_2^2}{N_2}}} \tag{4.1}$$

Where *t* is the Welch's t-test, $\bar{X}_n$ is the sample mean, s_n^2 is the variance, N_n is the sample size of the group (n=1 or 2).

$$d.f. = \frac{\left(\frac{s_1^2}{N_1} + \frac{s_2^2}{N_2}\right)^2}{\frac{s_1^4}{N_1^2(N_1 - 1)} + \frac{s_2^4}{N_2^2(N_2 - 1)}} \tag{4.2}$$

Where d.f. are the degrees of freedom, s_n^2 is the variance, N_n is the sample size of the group (n=1 or 2).

CHAPTER 5

RESULTS AND DISCUSSION

This chapter presents the results obtained from the different experiments performed with the experimental setups discussed in the previous chapter. The experiments are divided into three main sections: design of the electrolysis chamber including the supporting electrolyte, gel membrane and electrodes design; characterization of the DO in water; and finally, the SOU in-vitro experiments. The main results are highlighted in each experiment section followed by a discussion and a brief conclusion.

5.1 DESIGN

This section introduces various designs of the electrolytic cell that were investigated in this thesis in order to achieve a configuration for sufficient O_2 generation. Parameters such as the configuration of the electrolytic cell, the material and placement of the electrodes, the supporting electrolyte efficiency and the gel membrane design were optimized.

The O_2 generator is an electrolytic cell (Figure 5.1) formed by a container that holds an electrolyte solution and two electrodes (an anode and a cathode) immersed in it. A power supply was used to apply a current to the electrodes so that electrolysis of water can occur. Furthermore, the electrolytic cell termed “electrolysis chamber” can be divided into two containers which are connected by a salt bridge in order to separate the electrochemical reactions occurring at the anode and the cathode.

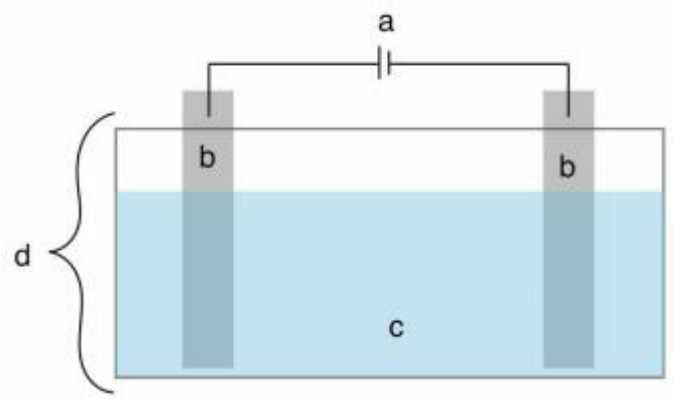

Figure 5.1 – *Diagram of an electrolytic cell. (a) Power supply, (b) Electrodes (anode and cathode), (c) Supporting electrolyte and d) Electrolysis chamber.*

5.1.1 Design of an Electrolysis Chamber

Several designs including single container; two containers; and electrolysis chamber were investigated for their suitability for generation of O_2 and integration with the oxygenator. The results and discussion of these experiments are presented in the following subsections. The experiments performed to test the electrolysis chamber and the gel membrane are also discussed.

Preterm neonates with RDS have partially developed lungs and are unable to meet their O_2 requirement. Therefore, a blood saturation of 70% was assumed [25] for venous blood which is typical in utero [19]. In order to achieve full oxygenation, the SOU that forms the LAD has to increase oxygenation level by another 30%. Given that 1 g of Hb has the capacity to transport 1.34 mL of O_2 (1.34 mL O_2/g Hb) [18], it was estimated [19] that 6.4 mL O_2/min·kg can completely saturate the Hb with blood. Thus, an O_2 supply of 1.9 mL/min• Kg (2.72 mg O_2/min·kg) would increase blood SaO_2 by 30% [19]. PO can oxygenate the blood to some extent but has not been able to provide the aforementioned amount [23, 25]. AO aims for this requirement through electrolysis of water so that an enriched O_2 medium can be provided to the blood flowing across the SOU.

The current required to supply 2.72 mg O_2/min can be calculated using Faraday's Law of electrolysis as discussed in Chapter 3. Using equation (3.5), 2.72 mg O_2/min can be produced by applying a current of I = 0.55 A to an electrolytic solution assuming 100% efficient conversion of the current. Choice of a supporting electrolyte to enable low potential drop across the solution and avoid any secondary reaction to O_2 generation is crucial to achieve high efficiency [92]. Thus, a supporting electrolyte of NaCl, Na_2SO_4 or NaOH were considered.

On the other hand, the designs have been designed so that they do not confine H_2, which is constantly released to the atmosphere. H_2 being lightest element, rapidly diffuses into the surrounding atmosphere, quickly diluting into a non-flammable concentration [136]. Despite, the H_2 production being twice the O_2 (5.4 mg/min), the flammability limits of H_2 in air are in the range of 4% to 74% [136] while that obtained during these experiments was found to be <0.0006%, which is insufficient for ignition. Hence, the production of H_2 is not considered hazardous.

5.1.1.1 *Single Container*

The first design of the electrolytic chamber (90 mL volume) that was investigated consisted of a single chamber with two electrodes inserted into an electrolytic solution as shown in Figure 5.2. The supporting electrolyte used consisted of deionized (DI) water mixed with 11.7 g/L of NaCl dissolved in it. Two stainless-steel mesh (SSM) electrodes were submerged into this solution. Another 100 mL beaker was filled with the same aqueous solution and used as a control (Figure 5.2). Each electrode had a contact area of 40.1 cm^2 with the solution. A current of 0.5 A was applied so that the low electric current density generated (12.4 mA/cm^2) would prevent significant amount

of side reactions. The DO and temperature of water was monitored every minute for 15 min. This experiment was repeated 3 times. The change in DO in the container with time for both the electrolysis case and the control is shown in Figure 5.3.

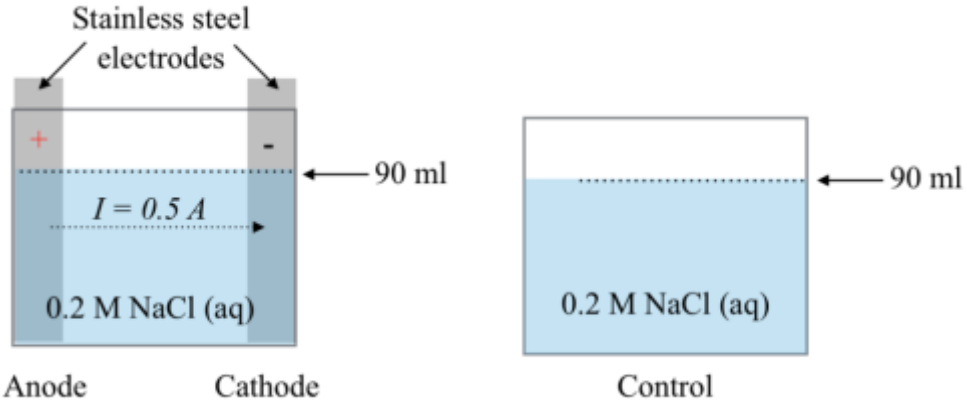

Figure 5.2 - *Illustration of electrolysis in a single container. The electrolytic cell was supplied with 0.5 A and filled with 90 mL of 0.2 M NaCl (aq) solution. The control beaker was filled with the same electrolyte solution.*

The initial condition of O_2 dissolved in water was found to be 6.3 mg/L. The potential needed to supplied 0.5 A was 7.45 ±0.2 V. The maximum increase in O_2 concentration was found to occur in the first minute (ΔDO= 2.5 mg/L) and the increase progressively became smaller. After ~ 6 min, the DO concentration was found to stabilise. The ΔDO concentration after 15 min was found to be 6.6 mg/L resulting in a DO of 12.9 mg/L (Figure 5.3). It can also be seen that the concentration of DO in the control chamber did not increase at all over the same duration time. This experiment demonstrates that the O_2 generated by the electrochemical reactions occurring at the stainless-steel electrode is capable of increasing the DO levels significantly in the water and presumably increases the O_2 concentration in the supernatant space.

Another consequence of application of a current through the electrolytic solution is the increase in temperature due to Joule heating. The initial temperature of the electrolytic chamber was 21.5ºC, the temperature was measured again after 15 min of application of 0.5 A and was found to have

increased to 24.1ºC which represents an increase of 2.5 ±0.4ºC. According to Joule's first law (5.1), the energy dissipated in the solution is proportional to square of the current and the resistance of the system.

$$P = I^2 R \tag{5.1}$$

With a resistance of 15 Ω, the resistive loss was found to be 3.75 W for a current of 0.5 A.

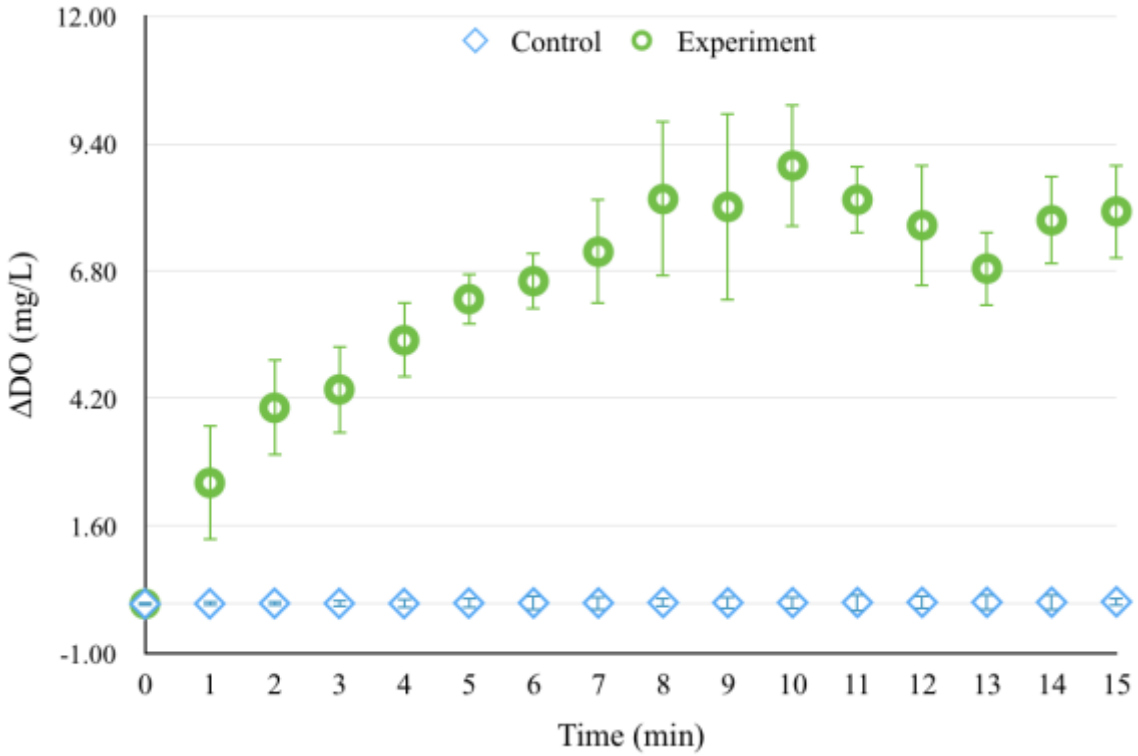

Figure 5.3 – *Increase in the DO concentration with time in the single chamber, electrolysis of 0.2 M NaCl (aq) solution at 90 mA. Graph shows the DO increase in water over time when supplying 0.5 A. J= 12.4 mA/cm^2. ΔDO= 100 µg/min (average).*

According to calculations, 100% efficiency of water electrolysis would have produced 2.72 mg of O_2/min at a current of 0.5 A. However, the average O_2 increase measured in water was only 100 µg O_2/min for the first 6 min. A number of factors could be involved in this low measurement.

First, the DO represents a fraction of the O_2 production because some O_2 is in the bubble form and is then released into the atmosphere. Second, H_2 and O_2 are produced in the same container which could lead to a change in the concentration of O_2 in water. H_2 might be acting as a purging gas which would reduce the solubility of O_2 in water, thus reducing the concentration of DO in water [113, 114]. Therefore, the mix of H_2 and O_2 should be prevented by separating the electrochemical reaction in two containers.

5.1.1.2 *Separated Chambers*

As discussed in the section above, H_2 generation in the same chamber could potentially deplete the DO in water. In addition, the H_2 gas is also permeable through the PDMS membrane and can potentially come in contact with the blood if the oxygenator is exposed to it. Thus, there is a need to separate the production of H_2 and isolate it from the oxygenator. Usually, two-chambers each containing their respective electrodes with a salt bridge connecting them is used for this purpose allowing movement of ionic current through the system while preventing the exchange of the contents of the two-chambers [92]. In this section, three designs of salt bridges were studied to identify the appropriate one for this application.

5.1.1.2.1 Salt Bridge using a Paper Scaffold

In the first design, a rectangular piece of absorbent paper was used as a salt bridge. The experimental setup consisted of two 100 mL plastic beakers connected by 0.25 m^2 of a scaffold made with 33 cm by 76.8 cm paper soaked in the electrolytic solution. One SSM electrode was placed in each beaker which were then filled with 90 mL of 0.2 M (11.7 g/L) NaCl aqueous solution. (Figure 5.4). Another 100 mL beaker was filled with the same electrolyte solution as a

control. The electrode contact area with the solution was 40.1 cm^2. The applied current was set to 0.5 A with a limiting voltage of 21 V. Measurements of the concentration of DO and temperature of water were taken every 10 min for 30 min at the anode side where O_2 was produced. The DO in the control beaker was also measured every 10 min. Finally, the DO at the cathode was measured at the beginning and end of the experiment. This experiment was repeated 3 times. The change in DO with time for anode, cathode and control is reported in Figure 5.5.

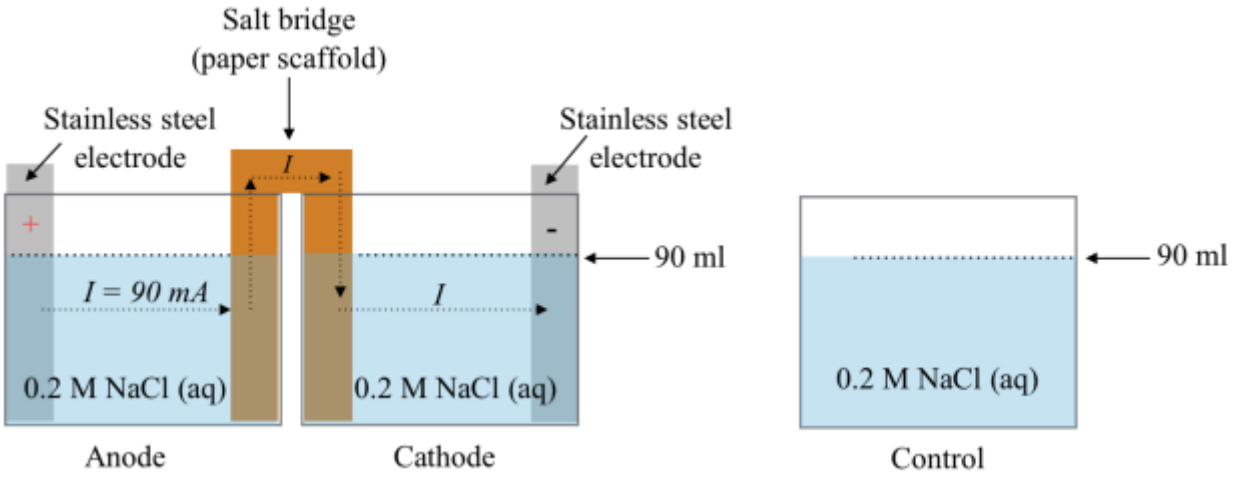

Figure 5.4 - *Illustration of electrolysis in two separate containers connected by a paper scaffold salt bridge. The electrolytic cell was supplied with 90 mA and filled with 90 mL of 0.2 M NaCl (aq) solution. The control beaker was filled with the same electrolyte solution.*

The two-chamber electrolytic cell separated by the paper salt bridge had a high resistance resulting in the power supply reaching the limiting voltage. At steady state, a voltage of 21 V was required to produce a current of only 90 mA.

The initial concentration of O_2 dissolved in water was found to be 7 mg/L. The concentration of DO in the solution was found to increase steadily to 30 mg/L in 30 min which represents an increase of ~ 22.8 mg/L (Figure 5.5). In comparison, the DO concentration in the control chamber did not change. Finally, the DO measurement in the cathode side using the electrochemical DO

measurement probe showed a decrease to 2.3 mg/L (ΔDO= -4.8 mg/L) after 30 min (Figure 5.5). This decrease demonstrates the displacement of O_2 by the H_2 generated in that chamber. The initial temperature in water was 23.7ºC. Measurements made at the end of the experiment showed that the temperature increased to 24.8ºC which represents a change of 0.9 ±0.1ºC over 30 min.

These results demonstrate that the separation of the H_2 and O_2 gas evolution into separate chambers enables the O_2 level dissolved in water to reach a higher value even at a lower current. It also showed that the concentration of O_2 at the cathode was below the original value in the water indicating that H_2 production was responsible for sparging the solution of O_2 and lowering its concentration.

Even though the resistance of the solution and the salt bridge (233 Ω) was higher than on the previous experiment (5.1.1.1), the resistive loss was lower (1.9 W) because the current applied was lower (90 mA). Consequently, a temperature increase of less than 1ºC was observed at the anode.

Although the paper scaffold for the salt bridge allowed separation of the anode and cathode chambers and demonstrated an increase in O_2 concentration in water over time, the resistance in the system was more than 15 times higher than that with the single container design which restricted the maximum current that could be applied, making this design unsuitable for the intended application

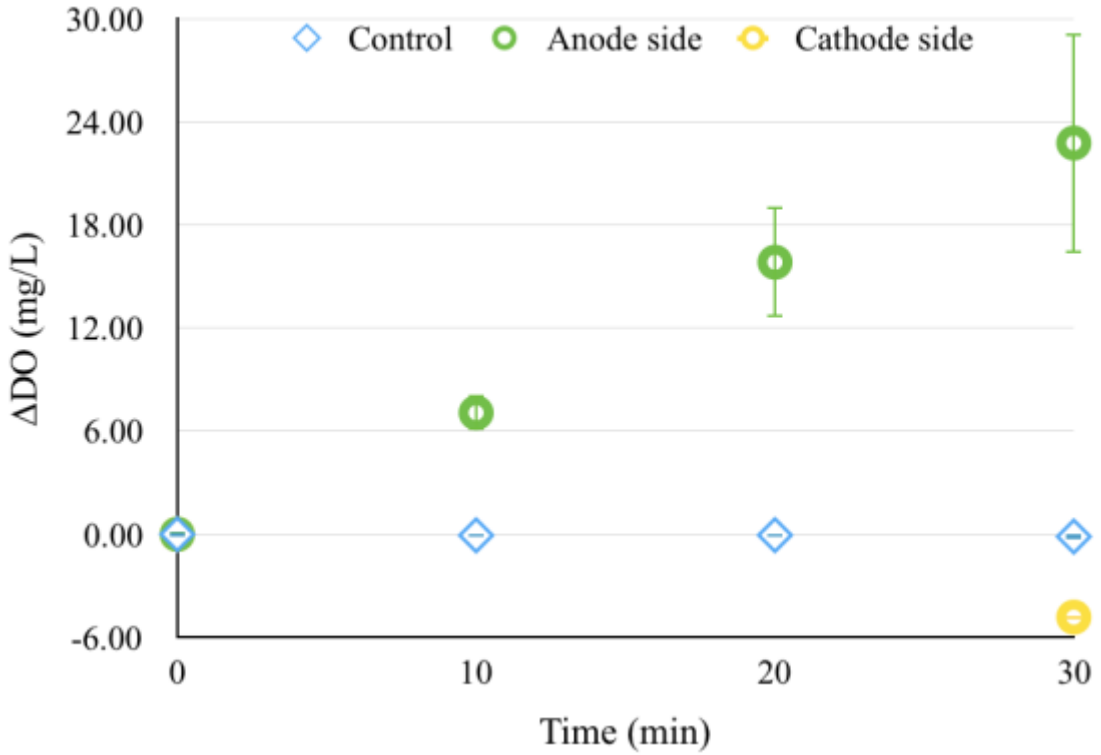

Figure 5.5. – *Increase in the DO concentration with time in the two-chamber design with paper scaffold salt bridge, electrolysis of 0.2 M NaCl (aq) solution at 90 mA. DO in water increase and decrease measured at the anode and cathode respectively. J= 2.3 mA/cm^2. ΔDO= 140 µg/min (average).*

5.1.1.2.2 Salt Bridge using Agarose Gel

The increase in resistance in the previous design was primarily due to the thin paper salt bridge that was dipped in the electrolyte solution. In order to lower the resistance of the salt bridge, an alternative was made using agarose gel. The salt bridge was prepared mixing 2% agar powder in 1 M KCl (28.1 g/L) so that the agarose gel formed had conductive properties. Once the agarose gel was prepared (see Appendix A for more details on the procedure), a silicone tube with an inner diameter of 1 cm was filled with the mixture. The sides of the silicon tube were placed into two 100 mL plastic beakers to give a path to the ions to move the current (Figure 5.6). Two SSM electrodes were used, one in each beaker. The supporting electrolyte solution was prepared using

11.7 g/L (0.2 M) of NaCl dissolved in DI water and used to fill the beakers. Simultaneously, a beaker filled with the same electrolytic solution was maintained as a control. The electrode contact area with the solution was of 40.1 cm^2. The initial current was set at 0.5 A. Measurements of the concentration of DO and temperature of water were taken every 5 min for 30 min from the anode side where the O_2 was produced. The DO in the control beaker was also measured every 5 min. Finally, the DO at the cathode was measured at the beginning and end of the experiment. The experiment was repeated 3 times. The measured values of DO over time for the anode, cathode and control are shown in Figure 5.7.

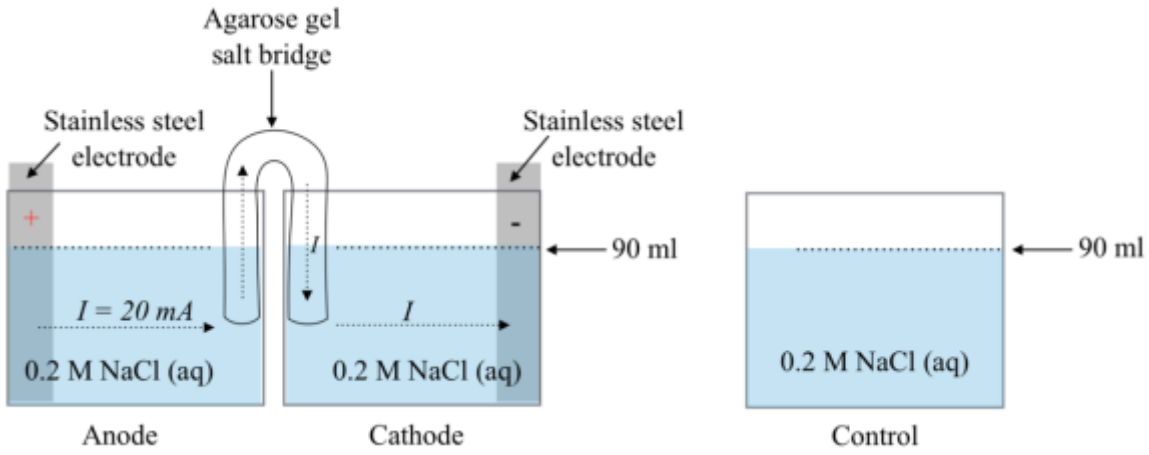

Figure 5.6 - *Illustration of electrolysis in two separate containers connected by an agarose gel. The electrolytic cell was supplied with 20 mA and filled with 90 mL of 0.2 M NaCl (aq) solution. The control beaker was filled with the same electrolyte solution.*

The salt bridge constructed using this method was still found to have a high resistance of (~805 Ω). Therefore, the intended setpoint of 0.5 A current was not reached and a modified current of 20 mA was then applied. This modified setpoint resulted in an applied voltage of 16 ±0.3 V which was within the limits of the power supply.

The initial condition of O_2 dissolved in water was found to be 7 mg/L. The concentration of DO in the solution was found to increase steadily to 20.9 mg/L in 30 min which represents an increase

of ~ 13.8 mg/L (Figure 5.7). The maximum production of O_2 was measured at 10 min (ΔDO= 4.9 mg/L). In comparison, the DO concentration in the control chamber did not change. Finally, the DO measurement in the cathode side using the electrochemical DO measurement probe showed a decrease to 4 mg/L (ΔDO= -3 mg/L) after 30 min (Figure 5.7). This demonstrates the displacement of O_2 by the H_2 generated in that chamber.

The initial temperature in water was 23.8ºC. The temperature measurements made at the end of the experiment showed that it increased by 24.4ºC, nearly a change of 0.4 ±0.2ºC in 30 min. The low overall temperature increase was expected due the low resistive loss (0.32 W).

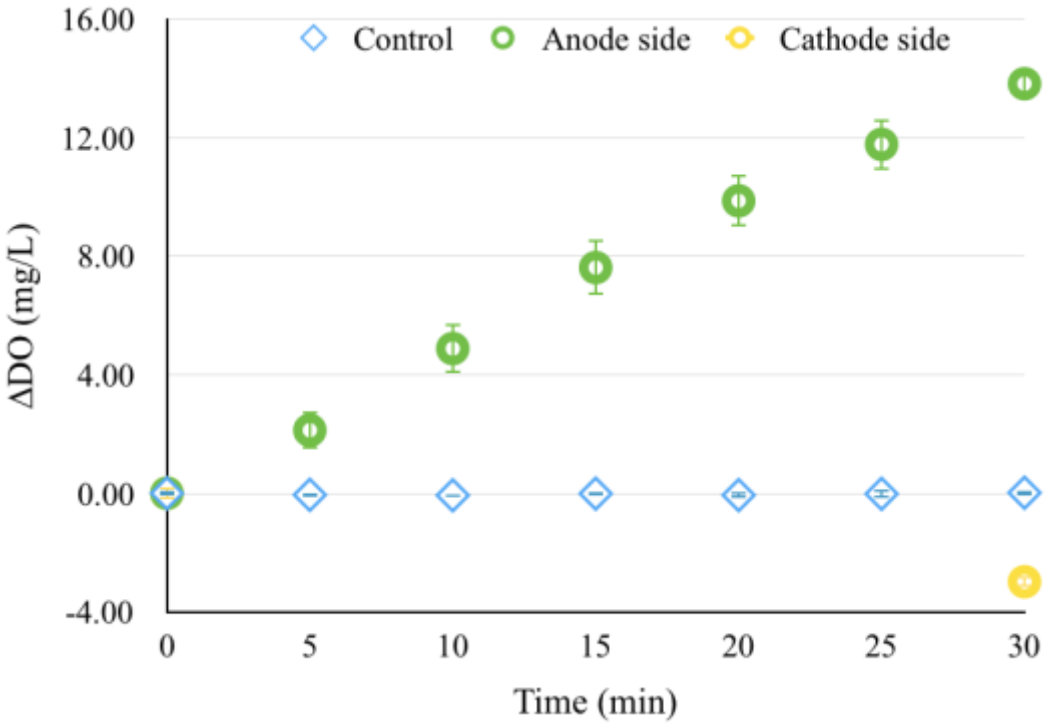

Figure 5.7 – *Increase in the DO concentration with time in the two containers design with agarose gel salt bridge, electrolysis of 0.2 M NaCl (aq) solution at 20 mA. DO in water increase and decrease measured at the anode and cathode respectively. J= 0.5 mA/cm^2. ΔDO= 80 µg/min (average).*

As discussed in the previous experiment, these results demonstrate that the separation of the H_2 and O_2 gas evolution into separate chambers enables the O_2 level dissolved in water to reach a

higher value even at a lower current. As expected, the concentration of O_2 at the cathode was below the original value in the water indicating that H_2 production was responsible for sparging the solution of O_2 and lowering its concentration.

The agarose gel salt bridge did not provide the expected conductivity to the system. The aim was to reach a higher and stable current, more precisely 0.5 A; however, steady supply was given at 20 mA. This setup (Figure 5.6) had 98% higher resistance than the single container setup; therefore, a reduction on the resistance of the salt bridge is needed. In order to achieve a lower resistance, a gel membrane with large surface area and small thickness was subsequently investigated as a suitable salt bridge. A higher current would then be feasible and the electrolysis efficiency would also improve.

5.1.1.2.3 Salt Bridge using a Gel Membrane

Given the previous results, the next design used a gel membrane to join two acrylic chambers (electro-chamber). The design and dimensions of the electro-chamber and gel membrane are discuss followed by the experiments performed to test the gel membrane performance and the efficiency of the chamber.

5.1.1.2.3.1 Electrolysis Chamber Design

The electro-chamber dimensions (shown in Chapter 4, Figure 4.3) were chosen to have the SOU fit inside in one-half of the chamber; on the O_2 generation side (anode). The H_2 generation side (cathode) was designed with the same dimensions as the anode side so that the electrolyte solution and its ions were proportionally distributed on both sides of the chamber. These dimensions were also chosen to make the device portable while containing a volume of 400 mL (**Figure 5.8**).

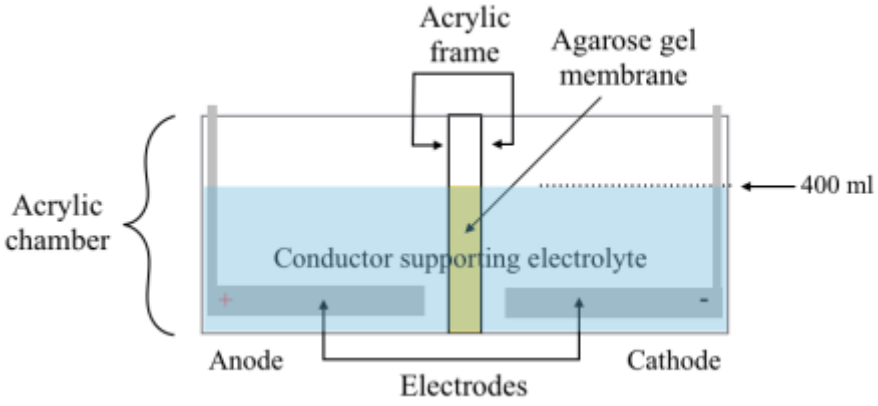

Figure 5.8 – *Diagram of the electrolysis chamber.*

Based on Faraday's law (3.5), the consumption rate of the water to produce 2.72 mg O_2/min is 2.8 µL/min. Since the oxygenation device is used as a short-term support for 2 weeks [19, 8], the total consumption would be 57 mL. Therefore, a volume of 400 mL was chosen so that there is no significant change in the operating characteristics of the electrolysis system. For longer operations, the system is designed in such a way that it is capable of being refilled. This can extend the lifetime of operation indefinitely. If this conceptualized system proves to be suitable for the oxygenation of blood, it will make the device sufficiently portable for hospitals and ultimately for homes.

Two 3D printed supports were attached 3.6 cm above the water level so that the SOU could sit on the supports and be lifted 4 cm above the water level (Figure 5.9). The anode side chamber had higher walls than the cathode side to create a support for a lid that can enclose the supernatant space above the electrolyte and prevent the generated O_2 from diffusing into the ambient.

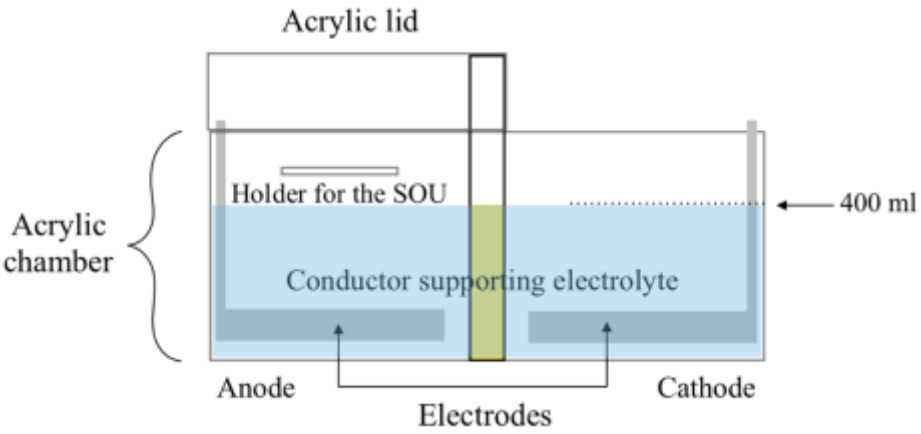

Figure 5.9 – *Diagram of the electro-chamber lid and support for the SOU.*

According to the ideal gas equation (5.2) and Faraday's law (3.5) the time required to fill the supernatant space with O_2 will be 64 min at 0.5 A, after oversaturation of O_2 in water is reached.

$$P = \frac{nRT}{V} \tag{5.2}$$

Where P is the pressure, n is the amount of substance (n= m/M), T is the absolute temperature, V is the volume of the gas, and R is the gas constant ($8.2057338X10^{-2}$ L·atm/K·mol).

The electro-chamber also had an acrylic frame to hold the gel membrane that separates the gases produced at the two electrodes but allows the ions to freely flow while conducting electricity. The separator (acrylic frame) had an open area of 15.1 cm^2 so that 2.8 cm by 5.4 cm of the gel membrane were exposed to the electrolyte solution (Figure 5.10). These dimensions were chosen to allow most of the volume of water to make contact. If the dimensions of the open area were bigger, the membrane that goes in that area would not have enough support to be held in place. The separator had a thickness of 5.78 mm with a gap of 0.22 mm so that the gel membrane tightly fit in.

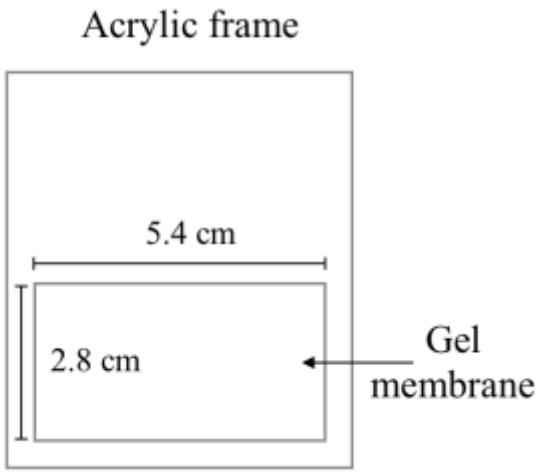

Figure 5.10 – *Diagram of the acrylic frame separator.*

5.1.1.2.3.2 Gel Membrane Design

In order to overcome the high resistance of the salt bridge encountered in the previous designs, a paper membrane infiltrated with gel was used as the separator. This design provides a large surface area of interaction between the two-chambers and therefore lower resistance.

As explained in Chapter 4 (Section 4.2.3), 101.1 g/L of potassium nitrate (KNO_3) was mixed with agar powder to form a gel that would become the membrane to join the two-chambers. However, the gel by itself is not strong enough to maintain its shape; therefore, to provide support to the gel a filter paper membrane was utilised.

The membrane chosen was a cellulose filter paper of 180 µm thickness and 11 µm pore size. The membrane was thin enough to ensure low resistance but with sufficient wet strength to avoid mechanical failure. The large pore size allowed for the agarose gel to easily penetrate the pores and fill them in order to prevent the transport of gases through the membrane. The filling procedure is described in Chapter 4, Section 4.2.3. The total membrane thickness obtained after coating with the agarose gel cover was 507 ±56 µm.

Next, a series of experiments were performed to test the electro-chamber design, the efficiency of the system and the robustness of the gel membrane. The DO generation in water was expected to increase because the low resistance of the membrane would allow for higher current to be achieved.

The experimental setup to test the O_2 generation capability of the new design consisted of two SSM electrodes placed horizontally at the bottom of each chamber with an inter-electrode spacing of 1 cm as shown in Figure 5.11. The surface area of each electrode was 90 cm^2. A solution of 0.2 M NaCl (400 mL) was poured into the chamber to fill it. A gel membrane was placed in the frame to divide the anode and cathode sides. Finally, a control beaker was filled with 90 mL of the same electrolyte solution (Figure 5.11). Measurements of the O_2 production were taken every 3 min for 18 min using an electrochemical DO probe. This experiment was repeated 3 times for each current applied. Current at various levels (20 mA, 100 mA and 500 mA) were applied to compare the results with the previous electrolysis setups.

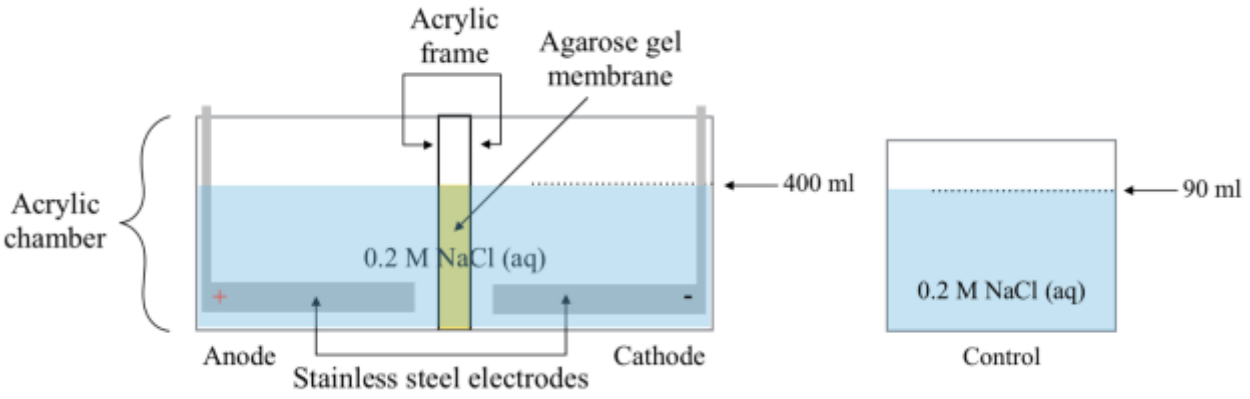

Figure 5.11 - *Illustration of the electrolysis chamber. The electrolytic cell was supplied with 20, 100 & 500 mA and filled with 400 mL of 0.2 M NaCl (aq) solution. The control beaker was filled with the same electrolyte solution.*

A current of 500 mA was applied to the two-chamber design with membrane separator to compare it with the single chamber design (Figure 5.2) which also had the same applied current. The initial DO measured in water was 6.8 mg/L. The potential required to apply a steady current of 500 mA was found to be 8.9 ± 0.6 V which indicates that the resistance of the electrolyte along with the gel membrane was ~17.8Ω. The results upon application of the current show a steady linear increase in the DO concentration over a period of 15 min to reach a value of 42 mg/L which represents an increase of 35 mg/L (Figure 5.12). This value was more than 10 times that reached at the same time in the single container. This can be attributed to the separation of the H_2 and O_2 in the two-chamber design which prevented the H_2 generated from sparging the DO in water. At the same time, a temperature change of only 0 ±0.4ºC was observed. The decrease in temperature rise compared to the 2.5ºC previously observed in the single chamber design was due to the increase in total volume of water, from 180 mL to 400 mL. Thus, having a greater area to transfer the heat.

Next, a current of 100 mA was applied to the two-chamber design with membrane separator to compare it with the two-chamber separated by a paper scaffold salt bridge (Figure 5.4) which also had applied a current of the same range (90 mA). The potential required was 4 V. The initial DO measured in water was 6.8 mg/L. The results show that the DO concentration steadily increased over a period of 18 min and reached a value of 18.7 mg/L which represents an increase of 12 mg/L (Figure 5.12). This value was more than twice that reached at nearly the same running time in the two-chamber paper scaffold design. This can be attributed to several factors: a higher current of 100 mA throughout the duration of the experiment; a larger volume of aqueous solution which allows for the dissolution of more O_2; and a better electrode reaction efficiency due to a larger surface area. At the same time, a temperature change of 0 ±0.1ºC was observed. The decrease in

temperature rise compared to the 0.9ºC previously observed was due to the increase in total volume of water, from 180 mL to 400 mL. Furthermore, the resistive loss (0.4 W) was almost 5 times lower than that observed in the paper scaffold design which is the reason for lower temperature increase.

Finally, a current of 20 mA was applied to the two-chamber design with membrane separator to compare it with the two-chamber design with agarose gel salt bridge (Figure 5.6) which also had the same applied current. The potential required was 2.9 V. The initial DO measured in water was 6.5 mg/L. The results upon application of the current show a steady increase in the DO concentration over a period of 18 min to reach a value of 9.3 mg/L which represents an increase of 2.8 mg/L (Figure 5.12). This value was more than 2.8 times that reached at nearly the same time in the agarose gel salt bridge design. This increase in DO can be attributed to the differences in bubble formation. Given that the surface area of the electrode was larger compared to that in the agarose gel salt bridge design it was expected that less layers of bubbles would form at the surface increasing the area of the electrode available for electrolytic reactions. Thus, the better electrode reaction efficiency led to a greater production of O_2. At the same time, a temperature change of 0 ±0.1ºC was observed. The temperature rise was four times lower compared to the 0.4ºC previously observed in the agarose gel salt bridge design. The reasons for it are twofold. First, the resistive loss (0.06 W) was more than 5 times lower than that observed in the agarose gel salt bridge setup. Next, the total volume of water in the chambers was larger (from 180 mL to 400 mL) which enabled the energy dissipated to be distributed over a larger volume.

Given that the temperature increase during the experiments was low, it was expected that currents in the range of 500 mA would not significantly increase the temperature of water;

therefore, when performing in-vitro experiments the temperature in blood would not be significantly changed.

The experiment also showed that the rate of production of O_2 is steady and related to the applied current. It should be noted that the DO does not represent the entire amount of O_2 produced as some in the form of bubbles rise to the surface and escape to the atmosphere. Rather, the DO is an indicator which is proportional to the amount of production. Also, the steady rise in the concentration of DO is only due to the absence of the oxygenator with blood flowing through it to consume the O_2. In its presence when the generation and consumption rates are balanced, a steady state DO concentration is expected.

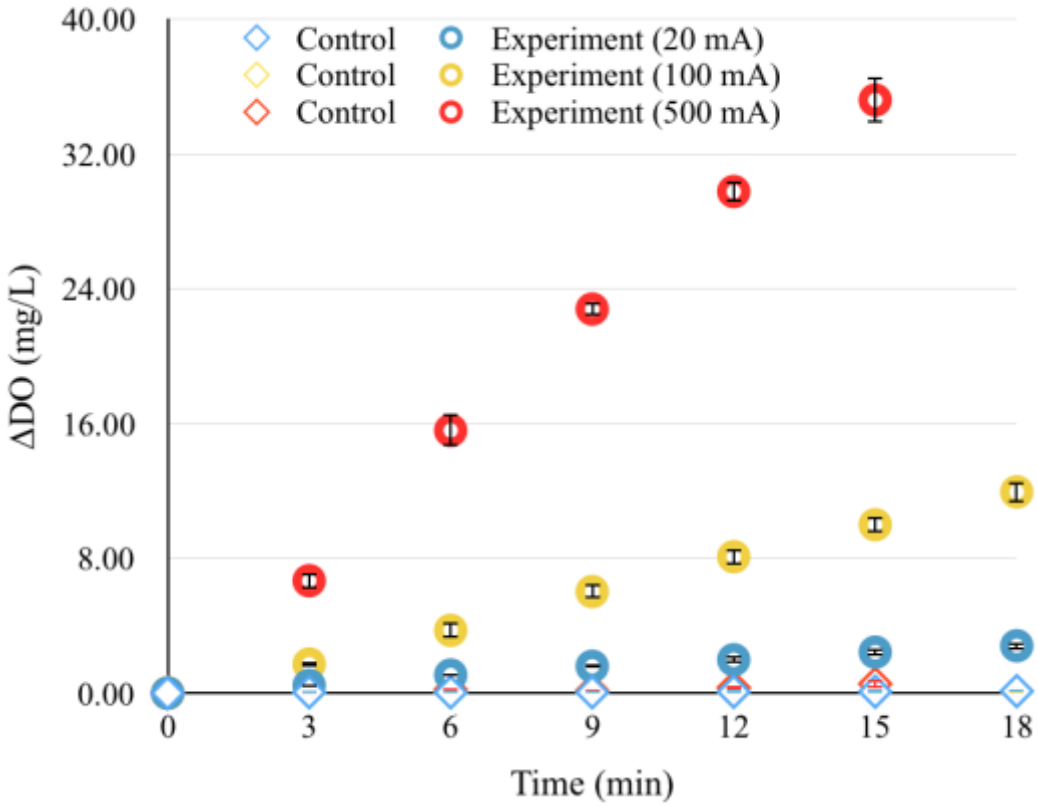

Figure 5.12 – *Increase in the DO concentration with time in the two-chamber design with gel membrane salt bridge, electrolysis of 0.2 M NaCl (aq) solution at 20, 100 & 500 mA. DO in water measured at the anode side. J= 5.5 mA/cm^2. $\Delta DO_{500\ mA}$= 938 µg/min (average).*

It is important to note that according to the DO sensor manual [115] the measurements may be affected by chlorine (Cl_2) evolution. Since the electrolyte has chloride (Cl^-) ions it is possible that Cl_2 gas is generated at the anode leading to a lower efficiency of the device. An analysis of the literature in gas evolution in water indicates that the Cl_2 evolution is the sole reaction occurring at higher current densities ranging from 100 to 1000 mA/cm^2 and therefore effort should be made to reduce the current density [116, 96]. Finally, the NaCl electrolyte also has a corrosive effect on the electrode which is more prominently observed at higher currents. Hence, to avoid future problems such as depending on a large surface area to exclusively generate O_2, it is of interest to investigate other strong supporting electrolytes that do not contain Cl^- and compare their performance with NaCl.

5.1.2 Supporting Electrolyte Selection

The electrolytic solution was prepared with three different supporting electrolytes to test the efficacy and efficiency to produce O_2. Both the effect of the supporting electrolyte on the electrode wear as well as its efficiency in O_2 generated was studied.

5.1.2.1 *Effect of the Supporting Electrolyte on the Robustness of the Electrode*

Various supporting electrolytes were investigated to identify the optimal one that not only generated O_2 with high efficiency but also preserved the shape and integrity of the electrode. The experimental setup consisted of the electro-chamber shown in Figure 5.13 filled with 400 mL of a supporting electrolyte, a gel membrane separator and SSM electrodes. The total surface area of the electrodes was increased to 205 cm^2 by attaching four sheets of thin SSM material so that a higher current can be applied.

The supporting electrolyte was prepared with a 0.2 molar concentration: 11.7 g/L of NaCl, 28.4 g/L of Na_2SO_4 and 8 g/L of NaOH were dissolved in DI water. SSM electrodes were placed in each chamber (four electrodes for each side) with an inter-electrode spacing of 14.5 cm. The electro-chamber was filled with 400 mL of the supporting electrolyte and a control beaker was filled with 90 mL of the same supporting electrolyte (Figure 5.13). The operating current was set at 2 A and was supplied nonstop for 30 min. The electric current density was 9.7 mA/cm^2. After 30 min, the electrodes were removed from the electrolysis-chamber and examined.

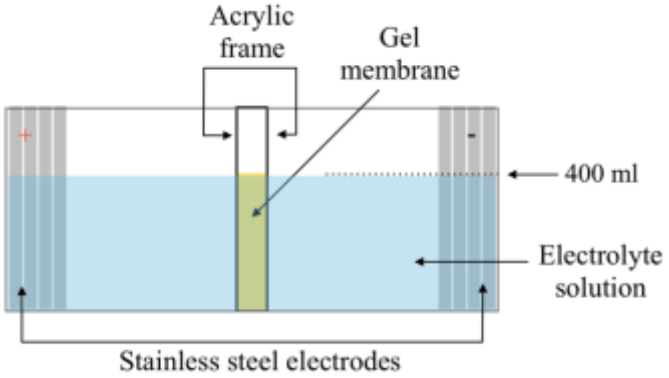

Figure 5.13 - *Illustration of different supporting electrolytes using four electrodes to increase the surface area.*

The images presented in Figure 5.14 show that various supporting electrolyte caused a differing magnitude of corrosive damage in the electrodes. The electrode degradation caused by the NaCl supporting electrolyte is shown in Figure 5.14(a). It was observed that the anode, was progressively consumed. This corrosion of the electrode was particularly visible at higher currents. The corrosion could be due to the production of Cl_2 gas which is a strong oxidising agent and can react with the iron (Fe) in the SSM to form Iron Chloride ($FeCl_2$). Note that hydrochloric acid (HCl) would not play any role in the degradation of the electrodes since Cl_2 formation is favoured over the production of HCl [133].

The electrode degradation caused by the Na_2SO_4 supporting electrolyte is shown in Figure 5.14(b). It was observed that the electrode at the anode resulted in a slight degradation of its bottom centre part. This could be due to the corrosion of stainless-steel in acidic conditions.

The effect of electrolysis in NaOH supporting electrolyte on the SSM is shown in Figure 5.14(c). It was observed that there was minimal to no degradation of the electrode in this electrolytic solution. It is known that the corrosion of stainless-steel is minimal in alkaline solution even with concentration NaOH solutions as the Fe forms iron hydroxides on the surface.

The supporting electrolytes, NaCl, Na_2SO_4 and NaOH, showed a temperature increase of 24ºC, 24.5ºC and 20ºC respectively. Note that the temperature change over time was nearly 4ºC lower for the NaOH supporting electrolyte compared to the other two salts. The differences in the temperature over time were expected because the literature shows that the conductivity of the three different salts used at the same concentration is as follows NaOH >NaCl >Na_2SO_4 [117]. Therefore, different resistive losses were produced.

Given that the electrodes were completely destroyed when using NaCl, this salt is not suitable for the design. The electrodes presented a slight damage when using Na_2SO_4 and did not present any damage when using NaOH. These two salts should be used to observe and compare their performances to generate O_2.

(a)

0.2 M NaCl

$\Delta T = 24^{o}C$

Before After

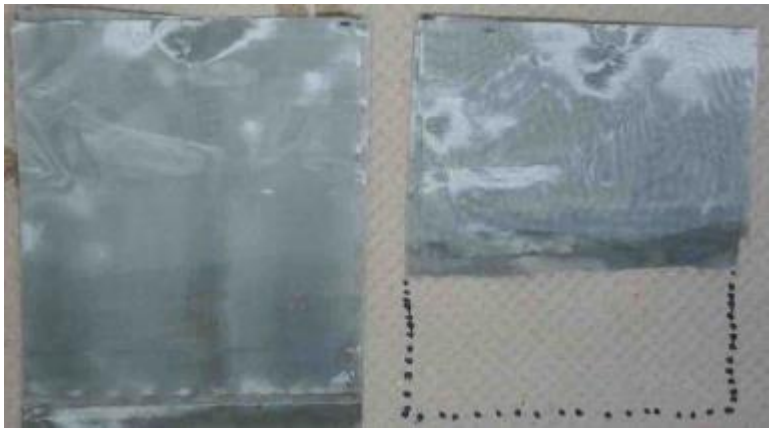

2.9 cm

Area immersed

Anode side

(b)

0.2 M Na_2SO_4

$\Delta T = 24.5^{o}C$

Before After

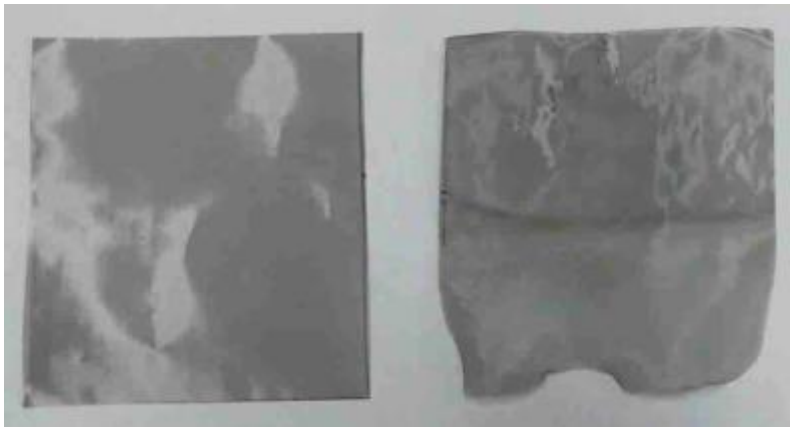

2.8 cm

Area immersed

Anode side

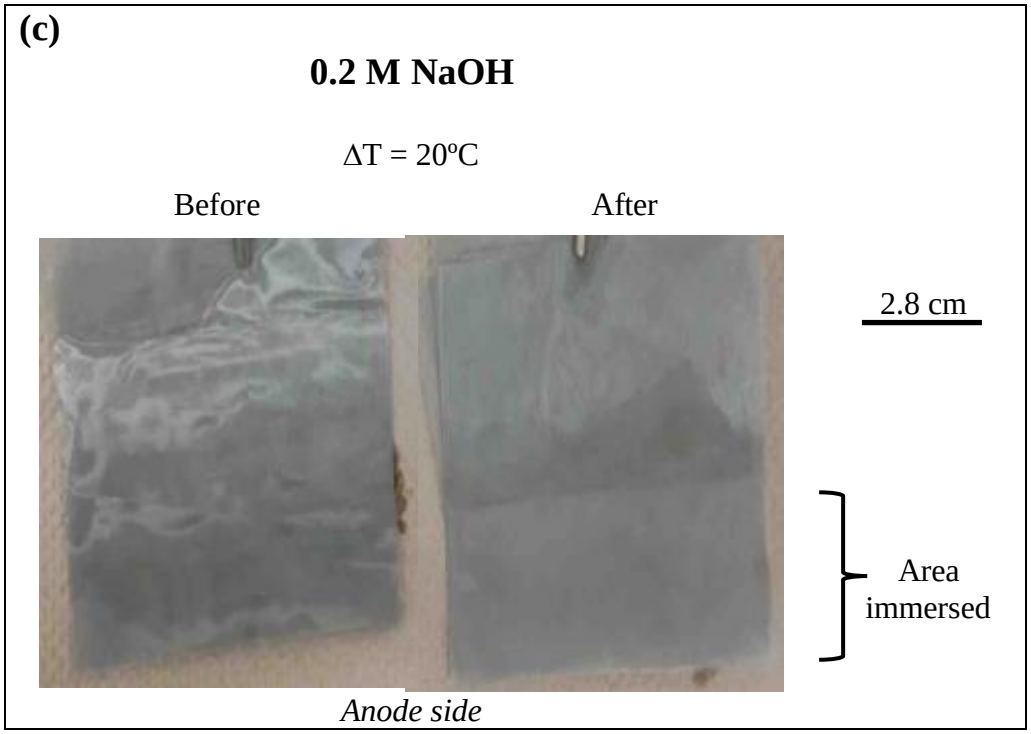

Figure 5.14 - *Effect of the supporting electrolyte on the degradation of the electrodes. Stainless-steel electrodes stood an electricity of 1800 C.*

5.1.2.2 *DO Produced Using Two Different Supporting Electrolytes*

NaOH and Na_2SO_4 with a 0.2 M concentration were used to prepare supporting electrolytes to test the efficacy and efficiency for producing O_2. The electro-chamber was filled with 400 mL of the supporting electrolyte; a control beaker was also filled with this electrolyte solution. The electrodes were placed in a vertical position having an inter-electrode spacing of 4 cm. The surface area of the electrodes on each side was 205 cm^2.A current of 2 A was supplied and readings were taken at the anode and control beaker every 3 min for 15 min. This experiment was repeated 3 times for each supporting electrolyte. The results are shown in Figure 5.15.

The initial concentration of DO for the Na_2SO_4 supporting electrolyte was found to be 6.8 mg/L. A potential of 15.3 ±0.1 V was required to apply a current of 2A which resulted in a resistive loss of 30.6 W. It was observed that upon application of the current, the DO concentration in the solution rapidly increased in the first 3 min after which it slowly reached a steady state. The DO increase was 37 mg/L which represents a ΔDO of 27.8 mg/L. The electrolyte solutions (Na_2SO_4 and NaOH) that served as the controls (no current applied) did not show a significant change in their initial DO content.

In the experiment with the NaOH supporting electrolyte, the initial DO concentration was found to be 5.9 mg/L. A potential of 12.5 ±0.3 V was required to apply a current of 2A which resulted in a resistive loss of 25 W. The increase in DO concentration in NaOH solution was found to be similar to the Na_2SO_4 solution with both supporting electrolytes achieving a maximum DO in water of 34.4 ±0.4 mg/L which represents an increase of 28 mg/L. No significant difference was found between the supporting electrolytes tested in terms of their O_2 generation performance (Figure 5.15).

As mentioned before, the DO reading is an indirect measure of the total O_2 being produced. Some of the O_2 generated escapes in the form of bubbles. However, the DO concentration is proportional to the O_2 generated and can be used as a representative marker. The results indicate that the amount of O_2 generated is sufficient to quickly saturate the water within 6 min. Any further O_2 that is generated will be evolved into the supernatant space and made available for oxygenation of blood if exposed via the oxygenator.

The DO measured in NaOH and Na_2SO_4 did not show a significant difference in the efficiency to produce O_2; therefore, the selection of the supporting electrolyte is solely based on how it affects

the durability of the electrode and the efficiency to supply the current. NaOH showed a better structural stability than Na_2SO_4; thus, NaOH is the salt of choice.

Now that the electrolyte solution has been chosen, the material of the electrodes and their placement were tested so that the efficiency of the electrolysis can be increased.

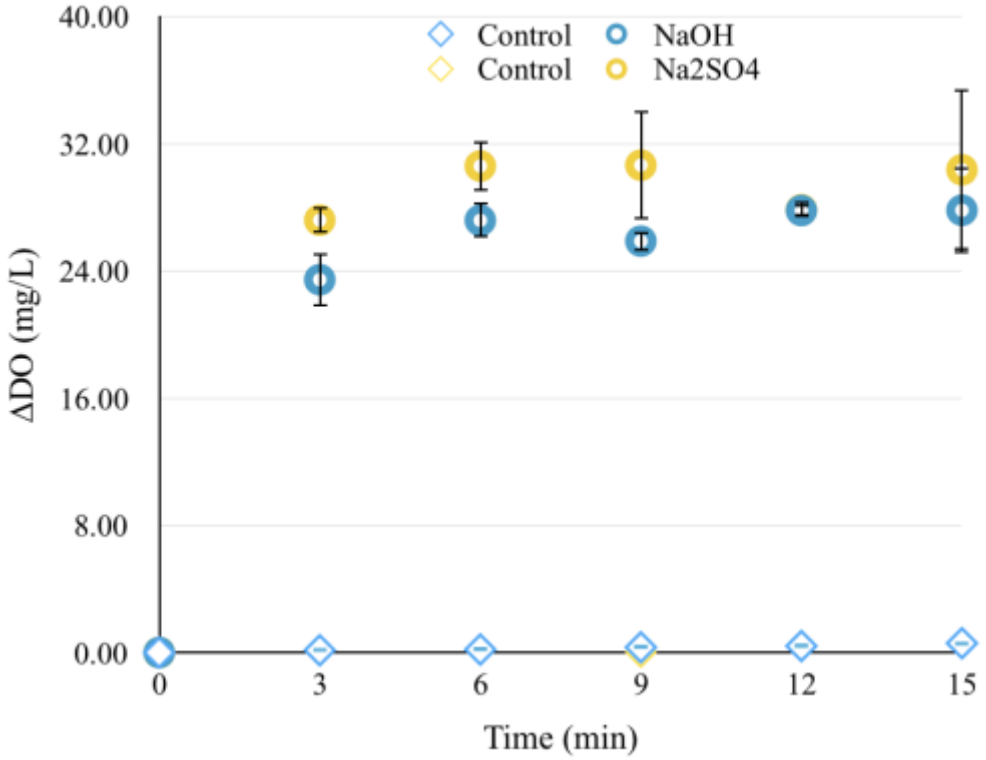

Figure 5.15 – *Increase in the DO concentration with time in the two-chamber design with gel membrane salt bridge, electrolysis of 0.2 M NaOH and 0.2 M Na_2SO_4 (aq) solutions. Performance of the supporting electrolytes to produce O_2. A current of 2 A is supplied to 0.2 M NaOH and 0.2 M Na_2SO_4 (aq) solutions. ΔDO=1.9 mg/min (within the first 6 min).*

5.1.3 Electrode Material

Two electrode materials, SSM and graphite sheet, were available in thin film form with high surface area that is suitable for use in the electrolyser. Both were tested to identify a robust electrode material and to compare their performances in efficiently generating O_2. A test of different electrode placements and inter-electrode spacing was then performed to improve the efficiency of the system.

5.1.3.1 *Effect of Graphite and Stainless-steel Electrodes*

Stainless-steel and graphite were chosen because both of them have a high conductivity [118]. Furthermore, both materials are low cost and readily available.

Graphite and stainless-steel were tested to compare the DO that both of them can generate in water, determine the voltage required and the temperature generated. The setup of the experiment was the same as shown in Figure 5.13 but instead of 4 electrodes, one electrode was used for each side of the electro-chamber. The inter-electrode spacing was 14.5 cm to force the system to use a higher voltage and observe if there were notable differences in the performance using stainless-steel and graphite. The electro-chamber was filled with 400 mL of 0.2 M NaOH aqueous solution. A current of 1.6 A was supplied for 5 min and the DO was measured afterwards. The procedure was repeated 3 times for each material.

It was observed that stainless-steel produced substantially more DO than graphite (Figure 5.16). Graphite and stainless-steel required a similar voltage (Figure 5.17); therefore, the increase in temperature was not significantly different ($p>0.05$).

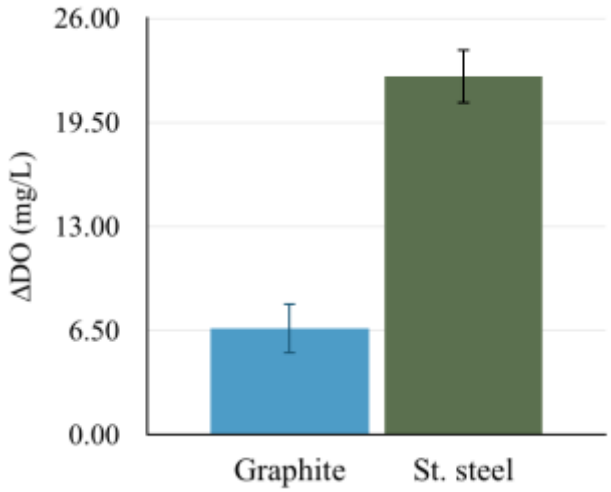

Figure 5.16 - *Increase in the DO concentration using stainless-steel and graphite electrodes, electrolysis of 0.2 M NaOH (aq) solution. Performance of the electrode material to produce* O_2. *I= 1.6 A supplied for 5 min.*

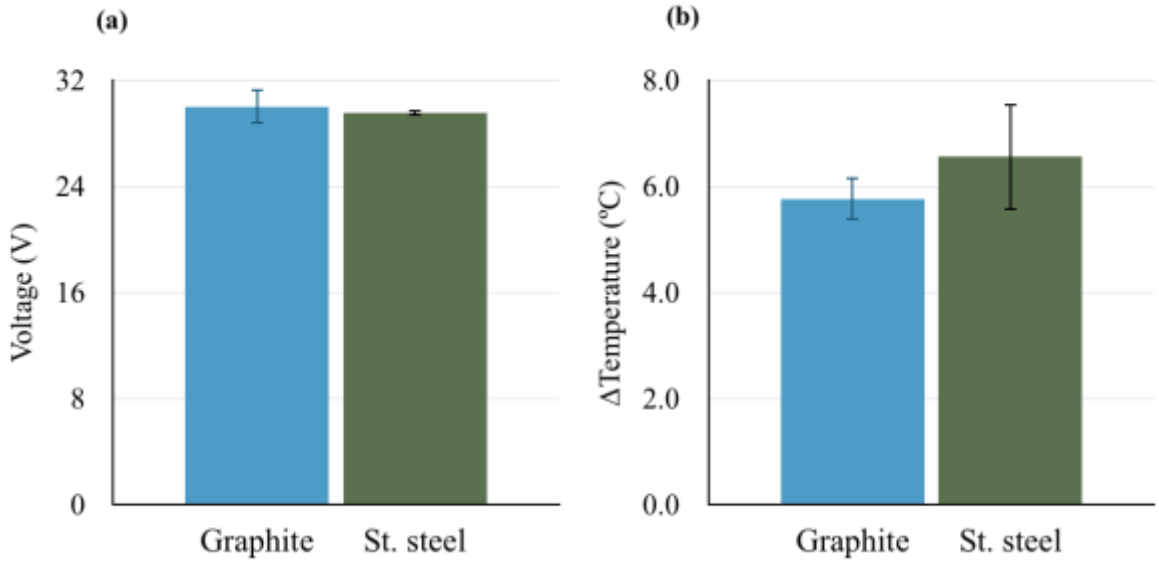

Figure 5.17 – *(a)Applied voltage to inject a current of 1.6 A using stainless-steel and graphite electrodes, (b) corresponding change in temperature (n=3). P>0.05.*

It was observed that after 5 min of running the experiment the graphite electrode showed a visible degradation; large pieces of the electrode that were visible to the naked eye was seen to fall off. Conversely, stainless-steel robustness was kept intact. The cathode and anode sides were observed under the microscope to identify the extent of the damage after 15 min of using these two different materials. It can be seen in Figure 5.18 that the graphite sheet showed a discoloration of the anode and the cathode. The anode turned into a lighter colour after 15 min of water electrolysis possibly because of reaction of the graphite with the O_2 being produced [118, 119]. The ΔDO measured after 5 min at the graphite anode was 6.5 mg/L, a production 3.4 times lower than that reached with the SSM electrode. The lower DO level with the graphite electrode can also be attributed to the reaction of the O_2 produced with carbon (C) in the electrode resulting in formation of carbon dioxide (CO_2). The cathode showed a disintegration associated with a swelling up of the carbon layers [120]. Clearly, graphite is not a suitable material to use with an alkali electrolyte such as NaOH because of the significant damage produced at both the anode and the cathode due to the production of H_2 and O_2. On the other hand, the use of stainless-steel resulted in no significant

damage of the mesh at the anode and cathode. Given the high degradation damage observed on the graphite electrode and the low production of O_2, stainless-steel was determined to be the material of choice.

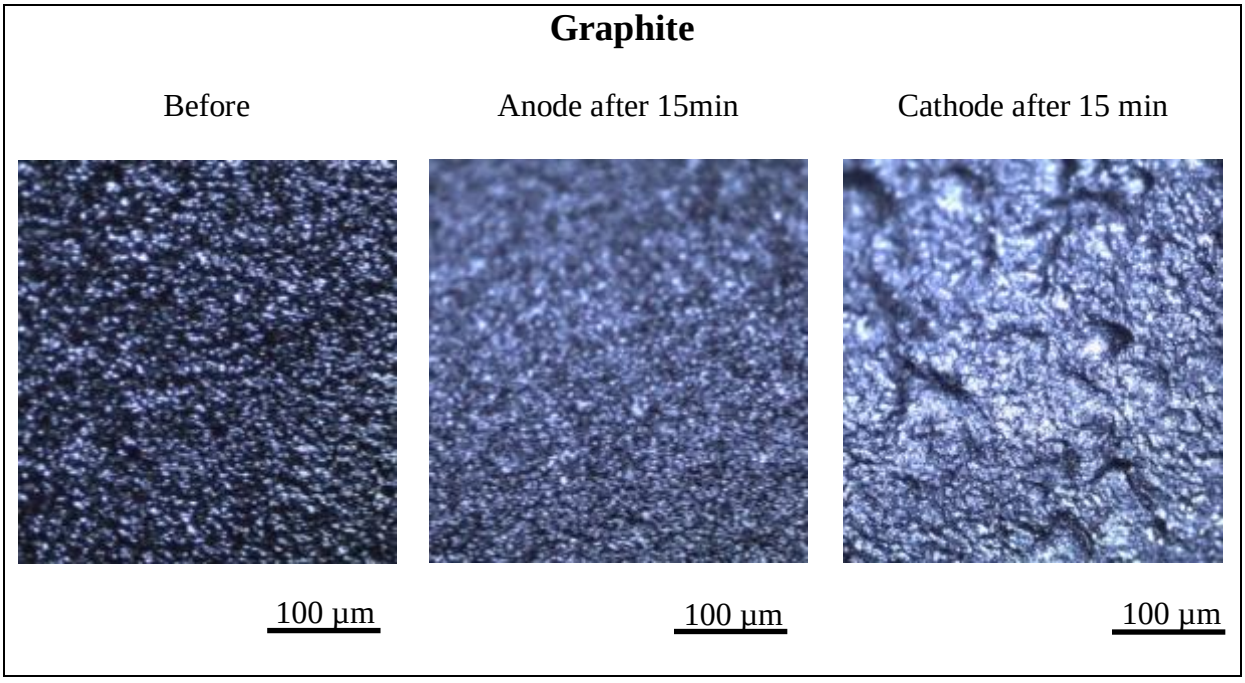

Figure 5.18 – *Microscopic images showing the damage to graphite electrodes at the end of 30 min, electrolysis of 0.2 M NaOH (aq) solution at 1.6 A.*

5.1.3.2 *Effect of the Electrode Placement*

The position of the electrode can potentially have an effect on the efficiency of O_2 generation in the electrolysis system. It also has an impact on the resistance of the system and hence the amount of Joule heating generated. It is generally desired to minimise the temperature increase as much as possible in order not to have any detrimental effects on the blood. Therefore, an optimal placement of the electrode such that the resistance is minimised is important.

Three electrode placements were proposed to improve the efficiency of O_2 production and reduce the resistive loss. The placements were horizontal with an inter-electrode spacing of 1 cm, vertical close to the separator with an inter-electrode spacing of 4 cm, and vertical far from the separator with an inter-electrode spacing of 14.5 cm (Figure 5.19).

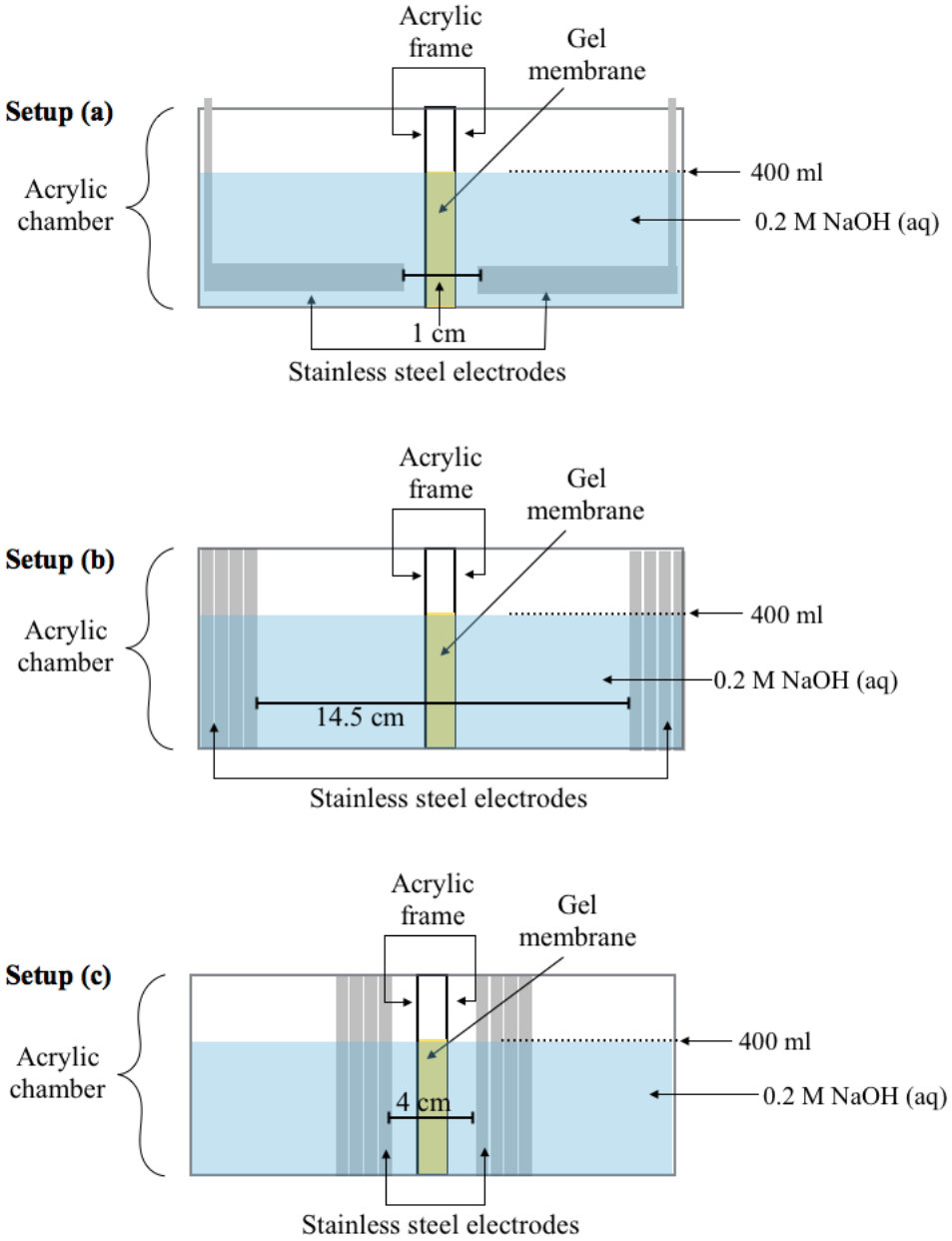

Figure 5.19 - *Diagram of the three different placements of the electrodes in the acrylic chamber.*

As shown in Figure 5.19, the acrylic chamber was filled with 400 mL of 0.2 M NaOH and four SSM electrodes were used on each side of the electro-chamber. A current of 2 A was supplied for 15 min and the DO measurements were taken every 3 min. This procedure was repeated 3 times for each electrode placement. Note that for setup (a) shown in Figure 5.19(a), the electrodes were held to the bottom of the chamber using two small pieces of acrylic previously glued on the facing walls with a distance away from the bottom of 5 mm. One side of the electrodes was cut off with dimensions of 1 cm by 7 cm to bring it above water so that it could be connected to the power supply. The surface area of this setup was 360 cm^2.The electrodes in setups (b) and (c) shown in Fig 5.19(b) and (c) were not cut off from any side. The surface area of these two setups was 205 cm^2. The results of the DO measurements with time are shown in Figure 5.20.

The O_2 production was the same for the different electrode placements proposed (Figure 5.20). The DO has the same trend in all cases, it plateaus out after 3 min suggesting that water reached oversaturation [121] and the O_2 production was being released to the atmosphere (Figure 5.20). The initial condition of DO in water was 6.2 mg/L and the maximum increase in DO was 34.2 mg/L which represents a ΔDO of ~28 mg/L.

The voltage required for setups (a), (b) and (c) were 12 ±0.2 V, 24.6 ±2.6 and 12.5 ±0.3 V, respectively (Figure 5.21(a)). Setup (b) had a higher resistance compared to setup (a) and (c), both of which had a similar resistance. Therefore, the resistive loss was higher on setup (b) causing a change of the temperature 1.5 times higher (~8ºC) compared to setup (a) and (c) (Figure 5.21(b)).

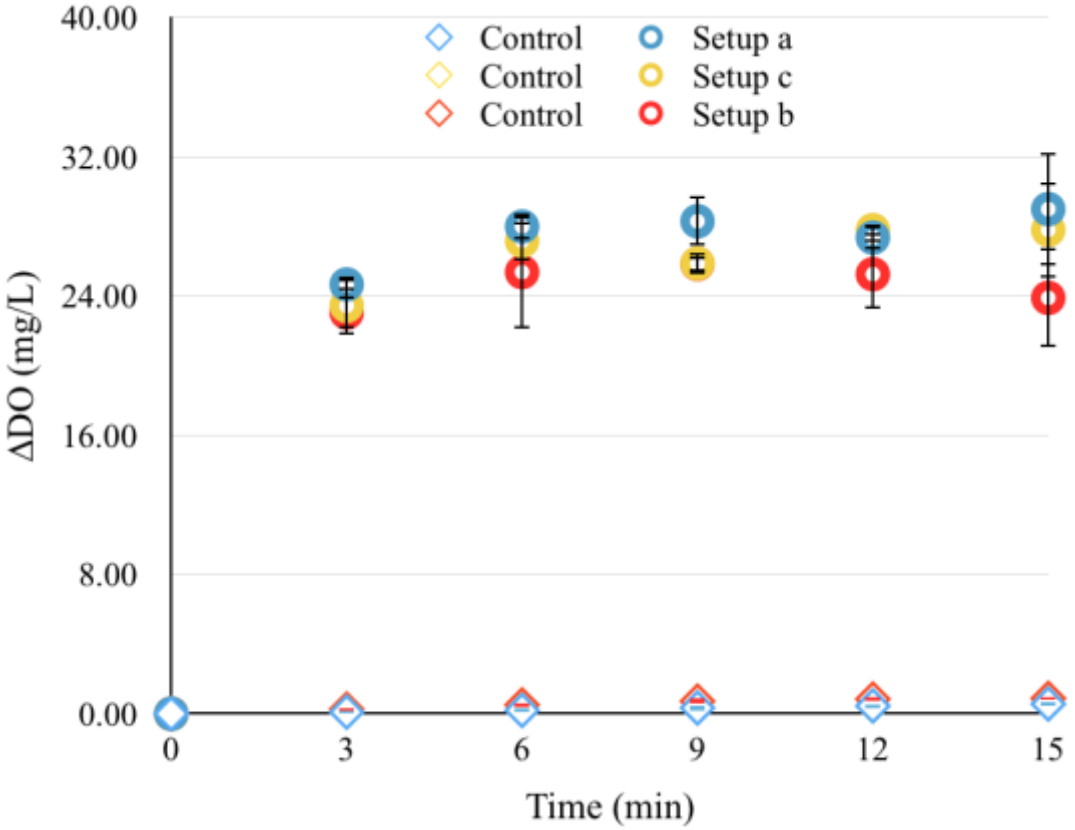

Figure 5.20 – *Increase in the DO concentration over time using the electro-chamber design, electrolysis of 0.2 M NaOH (aq) solution at 2 A. Electrode placement effect on the production of* O_2. *ΔDO=1.9 mg/min (within the first 6 min).*

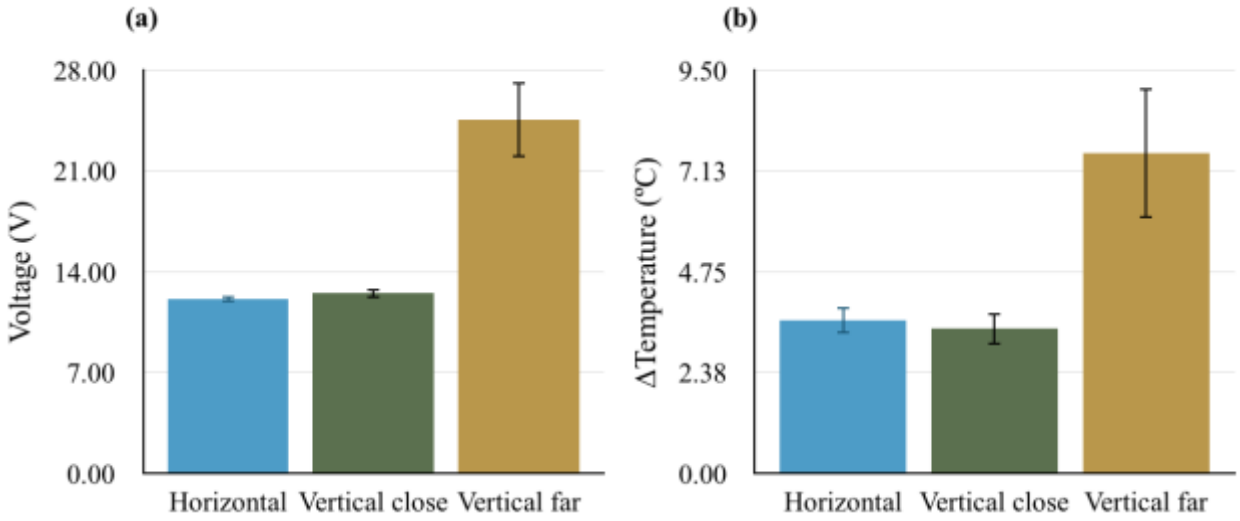

Figure 5.21 - *(a)Applied voltage to inject a current of 2 A using three different electrode placements, (b) corresponding change in temperature (n=3).*

The anode electrodes were observed under the microscope to determine whether one setup promoted more degradation than the other. It was found that a slight damage on the structure of the electrodes occurred during the experiments (Figure 5.22). An image analysis was performed using ImageJ software which showed that there was no significant change in structure. However, upon closer inspection, a deformation on the mesh wires was measured at the electrode after 15 min of electrolysis. Setup (a) showed a 2º deformation; setup (b) and (c) showed a slight deformation of less than 1º. This deformation was taken as an indication of that the electrode structure was being modified by the electrolysis process. It was then noted that setup (a), (b) and (c), had this deformation on the structure of the wires only in some areas of the electrode which suggests that the electrochemical reaction occurred on a fraction of the electrode surface. The entire area of the electrode was observed under the microscope and the areas where the deformation was more dominant were registered. Figure 5.23, summarises the aforementioned areas.

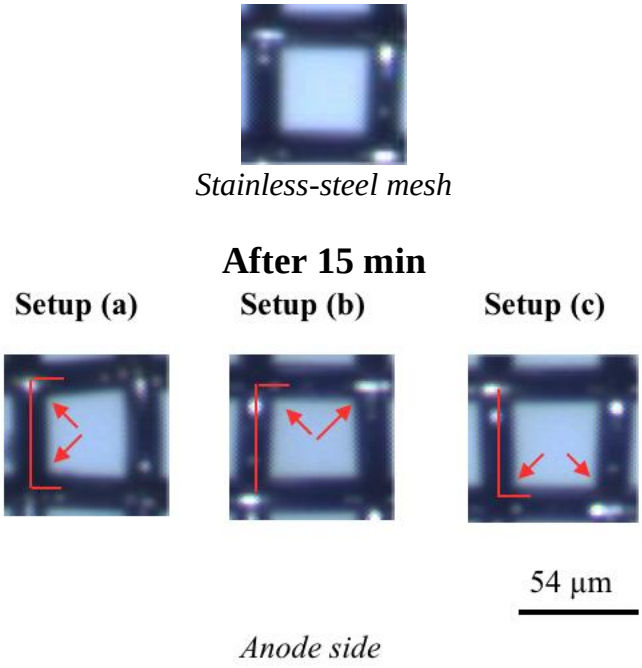

Figure 5.22 - *Magnified image of the SSM to show the changes on the mesh structure. The arrows indicate where the deformation is observed.*

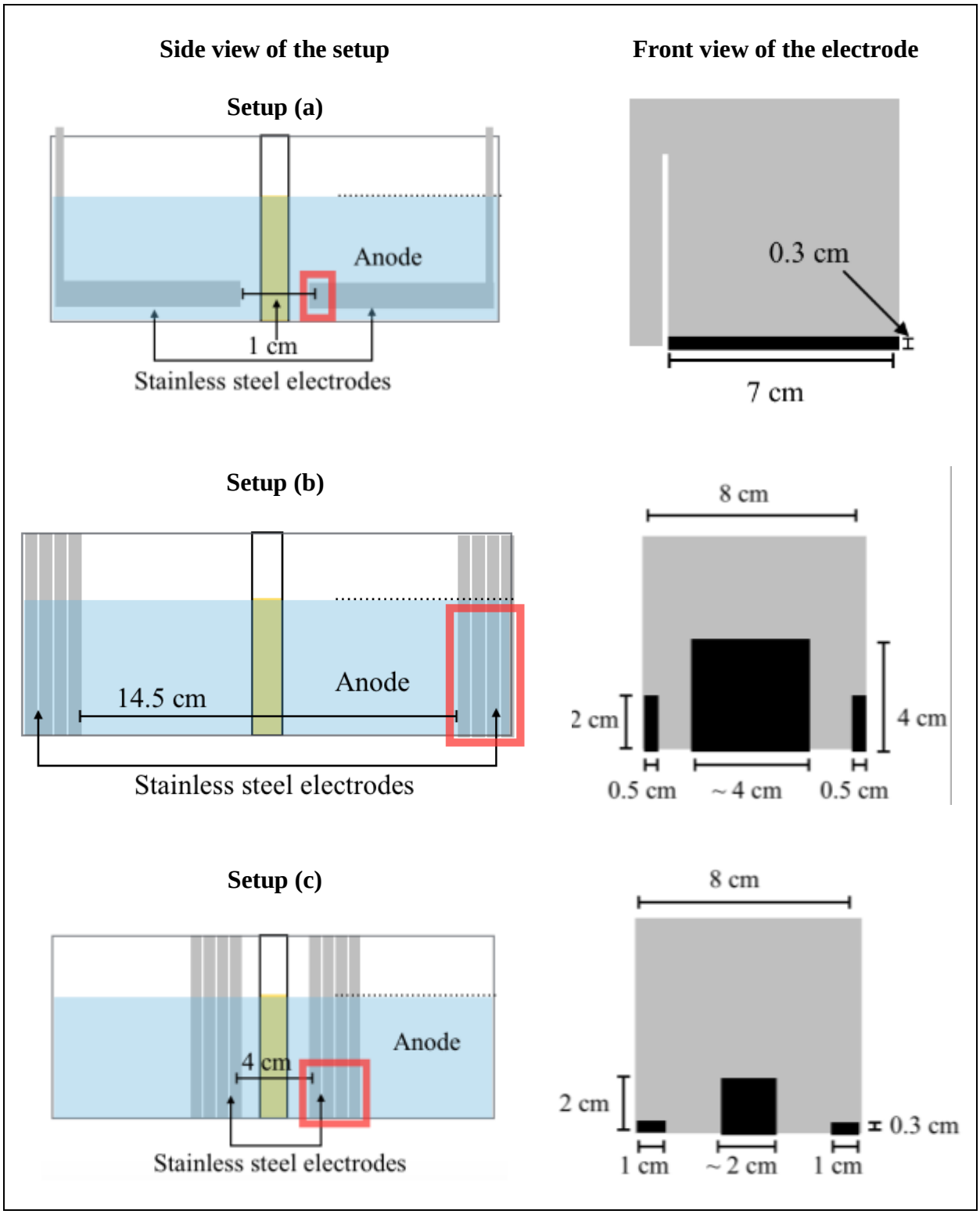

Figure 5.23 - *Illustration of the areas affected on the electrode by the electrode placement. Electrode reaction area is encircled in the setup (left side). A front view of the electrode and the reaction area is showed with detail on the right side. The dark spots (right side) indicate the degradation area of the electrode.*

Setup (a) – *Horizontal placement*

Dimensions of the electrode displayed on the image: 8 cm by 1.5 cm

Top view

Setup (b) – *Vertical far placement*

Dimensions of the electrode displayed on the image: 8 cm by 4 cm

Front view

Setup (c) - *Vertical close placement*

Dimensions of the electrode displayed on the image: 8 cm by 4 cm

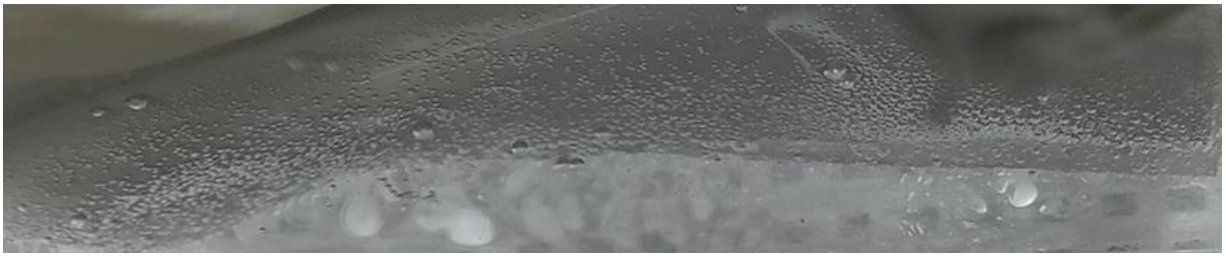

Top view

Figure 5.24 – *Bubble formation at the surface of the electrode using three different electrode placements.*

Figure 5.23 shows that a greater surface of the electrode was used with setup (b) compared to setup (a) and (c). Setup (a) showed that the surface where the reaction occurred was restricted to a very small area. Setup (b) and (c) showed to use a greater surface compared to setup (a). The electrode reaction area was then verified observing the bubble formation at the electrode.

Figure 5.24 shows the bubble formation with the three different setups used. Setup (a) had the bubbles being formed along the edge of the electrode and on a section of its left side (Figure 5.24(a)). Setup (b) and (c) show a homogeneous formation of bubbles along the surface of the electrode submerged in water (Figure 5.24(b) and (c)).

The O_2 production rate was consistent, and the current supplied was stable for all three setups indicating that the placement of the electrodes did not affect the efficiency of production of O_2. However, setup (a) showed a greater angular deformation of the wires in the mesh than that observed in setups (b) and (c). Furthermore, the bubble formation was predominant in a localised area of the electrode in setup (a) suggesting a faster rate of degradation of the electrode compared with setups (b) and (c). Thus, setup (a) is not suitable. Setup (c) showed a majority of its bubble formation and movement too close to the membrane separator suggesting that the integrity of the membrane may be compromised over time in setup (c). As a result, setup (b) was used. However, setup(b) suffered from a large inter-electrode distance resulting in a larger resistance and consequent Joule heating. This was avoided during further experiments by increasing the molar concentration of the solute, thus, reducing the resistance of the cell.

5.2 DISSOLVED OXYGEN IN WATER

This section presents two different experiments. The molar concentration of NaOH is increased to reduce the resistance and temperature of the water. The O_2 production is measured at different currents to generate a characterization curve of DO in water.

5.2.1 Effect of the Molar Concentration

Different molar concentrations were tested to observe the change in conductivity and the change in temperature of the system. NaOH with a molar concentration of 0.2M (8 g/L) and 0.5M (20 g/L) was prepared and 400 mL were poured in the electro-chamber. A control beaker was filled with 90 mL of the electrolyte solution. Four sheets of stainless-steel were attached to the anode and the cathode to have a surface area in contact with the supporting electrolyte of 205 cm^2. The supporting electrolyte was electrolysed with a current of 2 A for 18 min. The DO was measured at the anode at the beginning and end of the experiment. The experiment was repeated 3 times. The obtained values of DO, voltage and change in temperature are reported in Figure 5.25.

The initial condition of O_2 dissolved in water was 7.3 mg/L and 5.7 mg/L at 0.2M and 0.5 M concentrations, respectively. It was then seen that the change in the concentration of O_2 in water increased in the range of 28 mg/L after 18 min of electrolysis (Figure 5.25(a)). The potential required was 27.2 ± 2.9 V and 15.3 ±1.3V at 0.2 M and 0.5 M concentrations, respectively (Figure 5.25(b)). The temperature generated was 11 ± 2.6ºC and 5.1 ± 2ºC at 0.2 M and 0.5 M concentrations, respectively (Figure 5.25(c)).

Even though at a higher concentration of salt the water dissolves less O_2 [121], the DO measured was not significantly different for both molar concentrations. Unsurprisingly, the voltage required when using a 0.2 M solution was 1.5 times higher than with the 0.5 M concentration. Consequently, the change in temperature also increased as it was 2.4 times higher than that with the 0.5 M concentration. Therefore, 0.5M solution was chosen as the electrolyte as it had the least temperature increase.

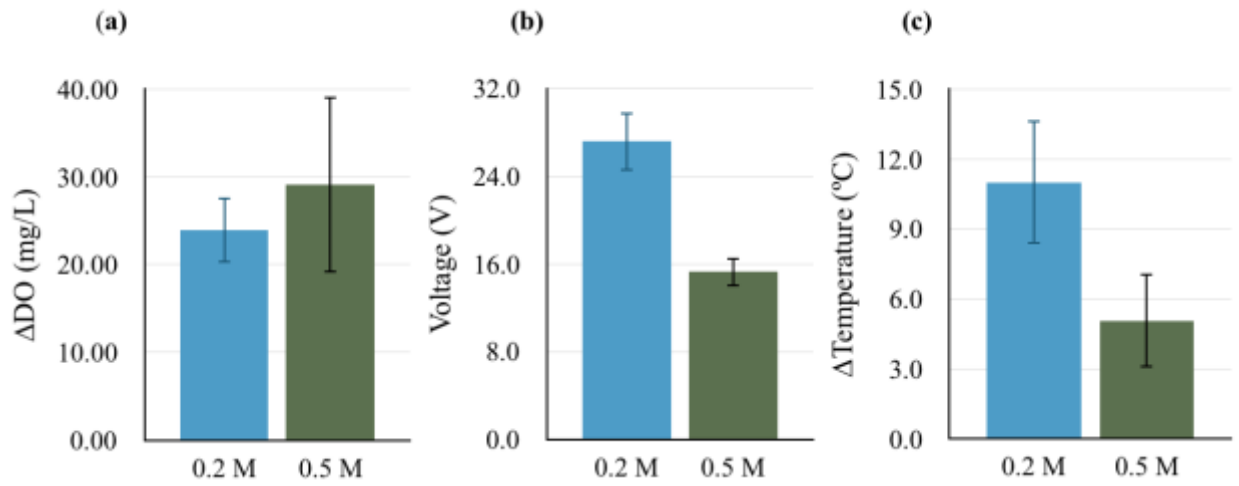

Figure 5.25 - *Effect of the molar concentration in the DO measured in water, change of voltage and temperature. Graphs show (a) the DO change at different molar concentrations, (b) the potential required to supply 2 A and (c) the temperature change after 18 min of electrolysis (n=3).*

5.2.2 Effect of the Current Supplied

A characterization of the production of gaseous O_2 by means of measuring the DO in water was performed to select the current that produced the desired rate of O_2 evolution. In the previous experiment, it was concluded that a higher molar concentration was needed to reduce the voltage and temperature while performing electrolysis. Thus, a 0.5 M concentration of NaOH was prepared as the supporting electrolyte. The chamber was filled with 400 mL and four electrodes were immersed in each side of the chamber 14.5 cm apart as shown in Figure 5.19 (b). The electrode surface area was 205 cm^2. A current of 1 A, 2 A and 3 A was supplied for 15 min and the readings were taken every minute. The experiment was repeated 3 times. The obtained values of DO, and temperature change and potential required are reported in Figure 5.26 and Figure 5.27, respectively.

The DO concentration increased rapidly and reached a plateau at 3 min for an applied current of 2 A and 3 A currents (Figure 5.26). However, in the case of an applied current of 1 A, the DO concentration reached a plateau only in the 6 min. (Figure 5.26). It was also visually observed that the generation of bubbles at 3 A was faster than that for 2 A resulting in more bubbles being generated. It is noted that the change in molar concentration positively affected the efficiency of the system decreasing the voltage needed; therefore, decreasing the temperature generated (Figure 5.27). The increase in temperature for the three currents supplied was nearly proportional to the power required on each of them.

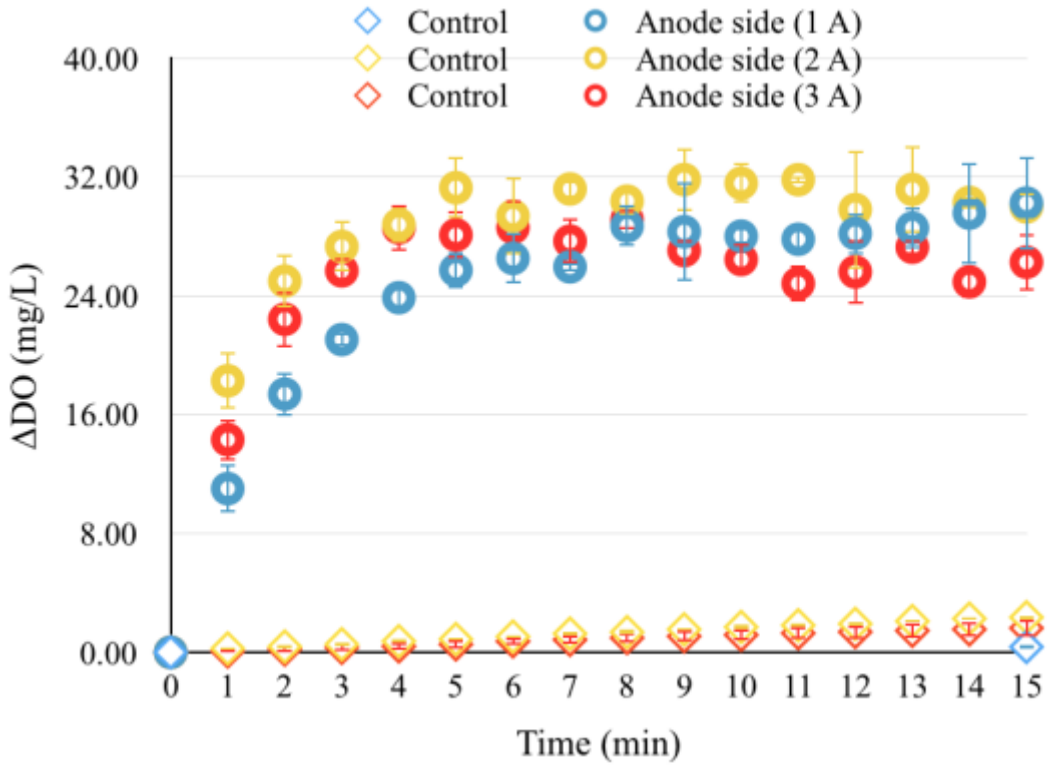

Figure 5.26 – *Increase in the DO concentration with time at different current levels using the electro-chamber design. Electrolysis of 0.5 M NaOH at 1, 2 & 3 A. Supporting electrolyte volume 400 mL. ~ΔDO= 2.8 mg/min (within the first 4 min) for 2&3 A.*

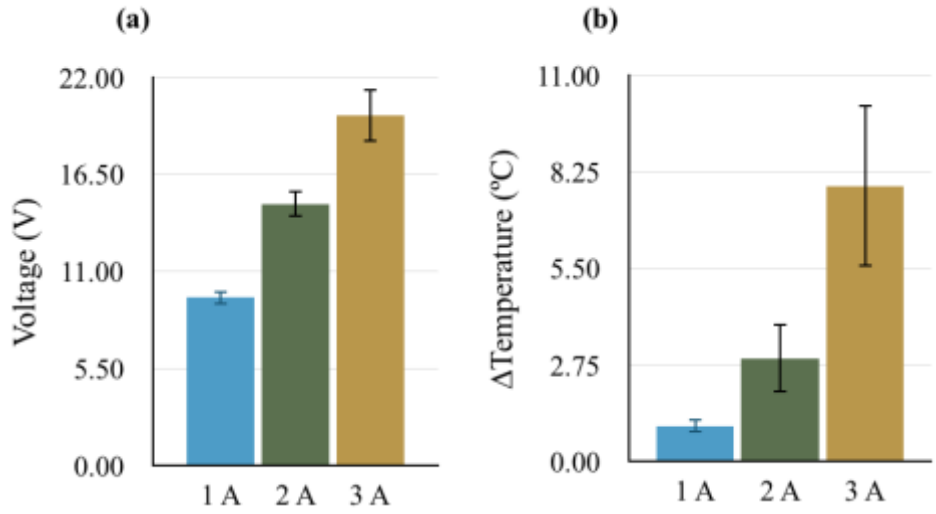

Figure 5.27 - *Effect of the different current levels on the change of voltage and temperature. Graphs show (a) applied voltage to inject a current of 1, 2 & 3 A (b) the corresponding change (n=3).*

It can be seen from the results that the measured DO concentration in the solution does not reflect the amount of O_2 being generated. The DO concentrations measured plateaus around nearly the same value which suggests the saturation concentration of O_2 in water was reached. This result indicates that at all the three current values the amount of O_2 is sufficient to saturate the water and the rest of the O_2 is evolved as gas bubbles which are released into the supernatant space and available for oxygenation purposes. The time to reach saturation (6 min in the case of 1 A vs 3 min in the case of 2&3 A) indicates that the rate of O_2 generation is slower for 1 A compared to higher currents. Thus, in-vitro oxygenation experiments need to be performed to determine the appropriate operating conditions suitable for sufficient blood oxygenation.

5.3 SOU IN-VITRO TESTING

This section first shows the results of PO and AO in-vitro experiments at molar concentration of 0.5 M and then a comparison in O_2 uptake performance with three different conditions is shown.

The supernatant space on the anode side of the electrolysis-chamber has a volume of 246 cm^3. This supernatant space is filled with air at normal ambient levels of ~21% O_2. In order to bring it up to enriched conditions, the electrolysis was started 30 min prior to any blood oxygenation experiment. For experiments performed in water (Figure 5.26), the DO measurement reached a plateau after 3 min of supplying 3 A which suggests that most of the O_2 produced is being released to the atmosphere after this period of time has been achieved. If one considers the first minute where most of the O_2 generated is taken up by the water as DO, the increase in DO concentration is equivalent to 5.7 mg (Figure 5.26). Therefore, assuming at least 5.7 mg of O_2 can be produced in a minute, it would require nearly 60 min to make fill the chamber with O_2 (1 atm) at 3 A. Since, some of the O_2 produced is not accounted in the DO measurements and since we do not need fully saturated condition by only enriched O_2, the chamber was pre-filled with O_2 for 30 min.

PO and AO were run at 0.5 M concentration to compare their performance in relation to the O_2 uptake. Bovine blood with SaO_2 of 51 ± 4% was loaded into 60 mL syringes (procedure in Chapter 4, Section 4.3.4). Further details on the PO procedure are explained in Chapter 4, Section 4.3.6.1. The blood flow rate was set at 3 mL/min. The supporting electrolyte was prepared in a concentration of 20 g/L and subsequently 400 mL were poured in the electro-chamber. The SSM electrode surface area was 205 cm^2. AO used a current of 3 A to produce O_2. The electro-chamber was prefilled with O_2 for 30 min so that the blood was exposed to an excess of O_2 environment (further details on the AO procedure are explained in Chapter 4, Section 4.3.6.2).

Blood samples exposed to air or enriched O_2 air were taken every 4 min for 16 min. The water and blood temperatures were also measured at the beginning and end of the experiments. These procedures were repeated 4 times. The results obtained for the increase in the blood oxygenation are shown in Figure **5.28**.

The AO showed a stable trend in the blood oxygenation. The PO also showed a steady trend. The AO and PO demonstrated an increase of blood SaO_2 to 69.5% and 55.9% which represents a ΔSaO_2 of 20.3% and 5.1%, respectively (Figure **5.28**). Thus, AO outperformed PO by 294%. AO compared to PO showed to be significantly different ($p<0.05$).

The AO required a potential of 15.2 ±0.5 V which represents a resistance of 5Ω and a resistive loss of 45 W. The initial temperature of water was 22.6ºC which showed to increase by 57.3ºC at the end of the experiment. This increase represents a temperature change of water of 34.7 ±5.5ºC. This higher temperature change measured on the in-vitro experiments compared to the water experiments was caused by the lid used to close the O_2 side of the chamber. Furthermore, the initial temperature of the blood was 19.4ºC and was found to increase to 32.8ºC which represents a change of 13.5 ±3.3ºC.

The hematocrit (Hct) measured with the micro-centrifuge showed that AO did not affect the Hct content. PO and AO had a Hct of 25.5± 0.3%. The average pressure drop through all the experiments was 50 mmHg which is within the desired range [23].

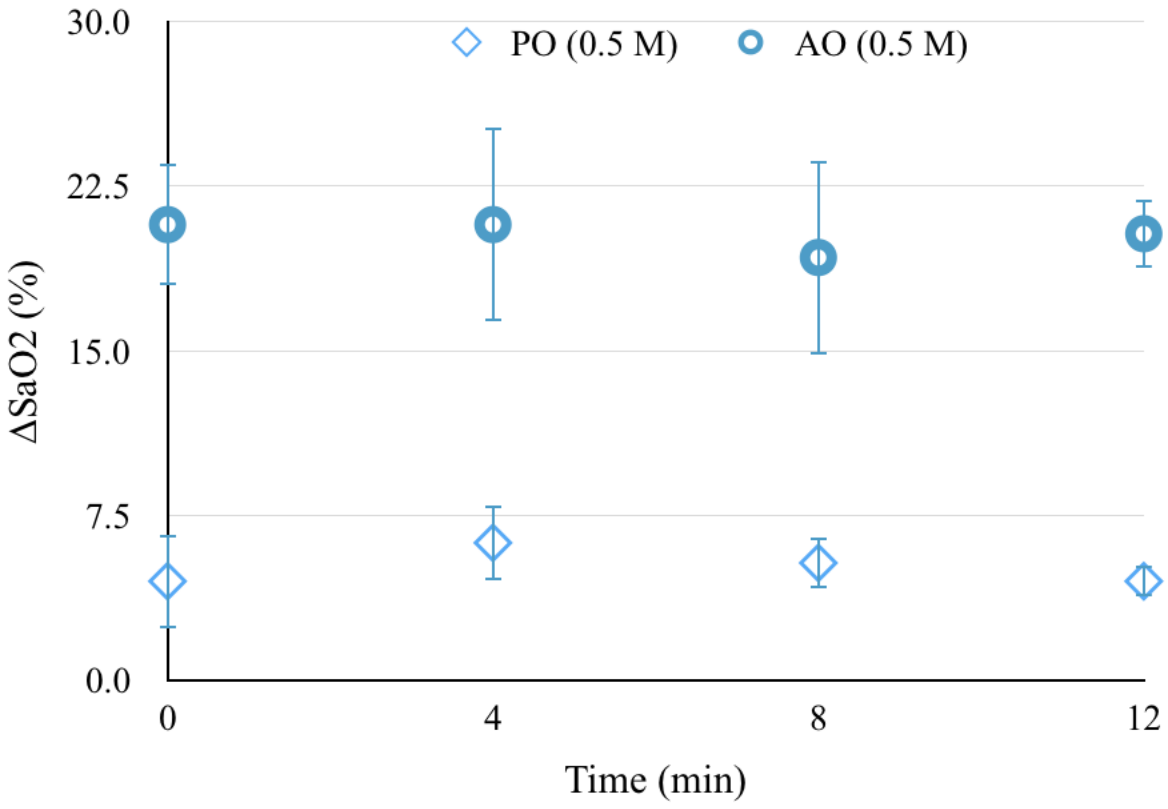

Figure 5.28 – *Increase in the blood oxygenation with time, electrolysis of 0.5 M NaOH (aq) solution at 3 A.*

The amount of O_2 that blood took up per minute is calculated using the following equation taken from [23],

$$\Delta Q_{O_2} = Qb \times (1.39 \times ctHb \times \Delta SaO_2 + 0.000031 \times \Delta pO_2) \quad \textbf{(5.3)}$$

Where Qb is the blood flow rate and ctHb is the total concentration of haemoglobin. The 1.39 [mL O_2/g Hb] is a theoretical constant of Hb O_2-carrying capacity and 0.000031 [mL O_2/mmHg/mL blood] is the solubility coefficient of O_2 in plasma [19].

The total concentration of Hb is calculated from the hematocrit content measured given by [109],

$$ctHb = 0.31 \times Hct \quad \textbf{(5.4)}$$

A molar concentration of 0.5M with a final temperature of the blood of 32.8ºC showed that the blood O_2 uptake for the AO resulted in being 67.5 µl/min, instead of 19.2 µl/min with the PO. The PO uptake reported here was similar to that found in other studies using the same oxygenator design [23]. AO showed that it is possible to oxygenate the blood by more than 20%, hence having a lung assist device that can support 67% of the partial oxygenation required for a preterm neonate [19].

This experiment clearly shows that enriched O_2 conditions can be created that will enhance the blood SaO_2 and the O_2 uptake in blood sufficient to raise the SaO_2 by ~ 20%. The initial setpoint of SaO_2 of the blood was ~50% which is below the expected saturation in venous blood of neonates which will be ~70%. In this context, the device provides significant oxygenation. There are several parameters that can be considered in improving the performance of the device and achieving 100% saturation.

a) The Hb content: bovine blood contains less proportion of packed cells [124] than human blood. Preterm neonates blood with mild to severe RDS have an average Hct of 45% [125]. In the in-vitro experiments performed, the average Hct measured with the micro-hematocrit centrifuge was 25.5% which translates to less oxy-haemoglobin bindings available. Therefore, if human blood were used for the in-vitro experiments, it would be 76.5% more packed RBCs, 6.9 g/dL more of Hb to bound to O_2. Thus, a greater blood SaO_2 could be achieved using human blood.

b) The SOU: blood might need to be exposed for a longer period to the O_2 enriched environment to uptake all the O_2 provided. Thus, lower flow rates or a SOU that provides

a greater gas exchange area are needed. The double-sided SOU mentioned by Matharoo [23] should be then tested.

c) The excess of the O_2 environment: the electro-chamber does not have a 100% O_2 environment inside it. A slight modification to the electro-chamber could be done to displace the air from the chamber while electrolysis is running.

In order to identify which of these factors would be significant the following experiment was conducted.

5.3.1 Oxygen Uptake in Air and in an Excess Oxygen Environments

Blood was exposed to an enriched O_2 environment using 100% O_2 to determine the amount of increase in blood SaO_2 under the same operating flow rates of blood.

A composite conventional SOU was placed inside an airtight acrylic chamber. The chamber was filled with 1 atm of 100% O_2 taken from a gas cylinder. Bovine blood with an initial SaO_2 of 62.3 ±3% was pumped through the SOU at a flow rate of 3 mL/min. Blood samples were taken at the beginning and end of the experiment. The procedure was repeated 3 times. The results obtained from PO (air) and AO (electrolysis) are plotted in Figure 5.29 and compared with compressed pure O_2 experiments taken from [126].

It is seen that the blood O_2 uptake was of 19.2 µl/min, 67.5 µl/min and 86.8 µl/min for PO, AO with electrolysis at 3 A current and AO in 100% O_2 environments, respectively (Figure 5.29). The O_2 uptake from AO was significantly different from the PO ($p<0.001$). Although, the average uptake for AO with 100% O_2 was better, AO with electrolysis was found to generate significant

amount of O_2 that produced an uptake approaching the 100% O_2 environment. This indicates that the O_2 concentration in the ambient does not reach 100% O_2. This could be due to the presence of air in the chamber prior to the generation of O_2. These results suggest that AO with electrolysis could be slightly improved further by either increasing the current applied or by enabling the chamber to be evacuated at the beginning of the O_2 generation process in order to remove the air present in the supernatant space so that a 100% O_2 environment can be achieved in the electro-chamber.

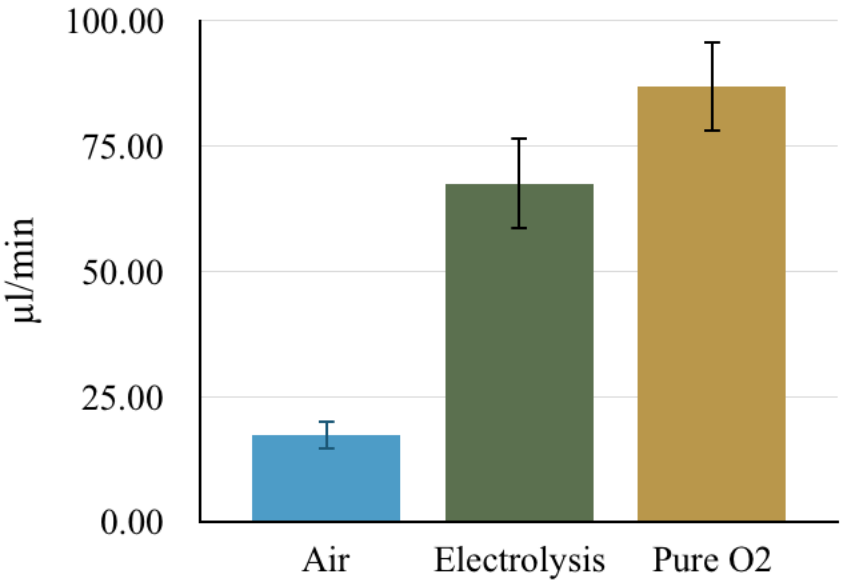

Figure 5.29 - *Oxygen uptake in air and O_2 excess environments.*

In this chapter, the design evolution of the electrolytic cell was presented. The results showed that the electrolytic cell separated into two containers with a thin gel membrane salt bridge allowed for better conductivity and increased production of O_2. Performance characterisation of different supporting electrolytes showed that NaOH had better structural stability and did not significantly affect the integrity of the stainless-steel electrode. The SOU in-vitro experiments demonstrated that AO with electrolysis enabled a greater O_2 uptake compared to PO. Although the concept of

electrolysing water to create a portable system seems promising, further work needs to be done on the efficiency and efficacy of the system so that the envisioned idea of a compact O_2 generator is cost-effective. The next chapter provides the conclusions of this project and gives future recommendations to further improve the performance of the system, so that the temperature increase is minimised and the blood O_2 uptake is increased.

CHAPTER 6

CONCLUSIONS

In this chapter, the key contributions of the work done in this thesis are summarised. Future work on improvements in the design of the electrolysis chamber is proposed to enhance the blood O_2 uptake and the efficiency on the O_2 production. In particular, the new design is targeted at decreasing the rise in temperature.

6.1 KEY CONTRIBUTIONS

The main contribution of this thesis is the development of an electrolysis-based system to produce O_2 in-situ and its demonstration in improving the O_2 uptake from a microfluidic oxygenator. The various components of the system such as the electrodes, electrolytic solution and the chamber design were optimized. The O_2 generator consisted of SSM electrodes and NaOH as the electrolyte supporting solution. The electrolysis chamber had inner dimensions of 16 cm x 8 cm x 6 cm to contain a volume of 400 mL. A current of 3 A was found to be sufficient to create an enriched environment and a significant change in the SaO_2 of the blood flowing through the oxygenator. The following were the key findings from the thesis.

1) NaCl, Na_2SO_4 and NaOH were supporting electrolytes tested using SSM electrodes. NaOH electrolyte solution did not affect the robustness of the electrode after electrolysis for 30 min at 2 A. Furthermore, NaOH had a better conductivity than the other two electrolytes showing lower rise in temperature, it rose ~4^{o}C less compared to the other two electrolytes.

2) Water experiments, using NaOH and a current of 3 A, showed that the DO in water reached a stable value in 3 min after the electrolysis process was started. The ΔDO increase found within the first minute of electrolysis was 5.6 mg O_2 which was twice the amount needed for 1 kg neonate.

3) Stainless steel and graphite sheets were electrodes tested with NaOH as the supporting electrolyte. It was observed that SSM was capable of increasing the DO concentration in water by 3.4 times as compared to graphite. At the same time, graphite showed degradation of its electrodes while stainless steel integrity was not affected.

4) The system was then tested in-vitro by flowing bovine blood across a composite conventional SOU. PO produced a change in blood SaO_2 of 5.1% at a flow rate of 3 mL/min. AO provided a change in SaO_2 of 20.3% at the same flow rate. The AO using electrolysis was found to have significantly improved the oxygenation of blood by providing with an enriched environment. Thus, outperforming PO by ~300%.

Furthermore, the system described is compact while providing adequate oxygenation of the blood. The consumption of the supporting electrolyte was insignificant proving that AO could run for long periods of time without the need for refilling the electrolysis chamber.

The properties of blood, including the pH and Hct, were not affected, however, the rise in temperature of the system led to an increase in the temperature of blood.

6.1.2 Additional Key Contributions

A mechanism to load syringes with blood and maintain the input setpoint of the O_2 level of blood at the inlet throughout the in-vitro experiments was developed. The technique proposed in this thesis involved first reducing the blood O_2 level as explained in Chapter 4, Section 4.3.3 followed by storing the container with the blood in the fridge. The blood was then loaded to a syringe using a peristaltic pump at the time of the experiment, where it was found that the increase in blood O_2 level was no more than 1% (Chapter 4, Section 4.3.4). Throughout the experiment (~40 min), the blood SaO_2 setpoint increased 1-2%.

6.2 RECOMMENDATIONS FOR FUTURE WORK

In this thesis, the production of O_2 was measured by measuring the DO in water and associated to the O_2 uptake by blood. Since some of the O_2 produced is not accounted for in the DO measurements because it is released into the atmosphere, it would be of interest to measure the O_2 concentration in the supernatant space. Thus, a correlation between the DO, the O_2 gas concentration in the chamber and the blood O_2 uptake can be made.

Furthermore, the generation of O_2 in-situ with an electrolysis-based system showed an improvement in blood oxygenation using a low cost system. Nonetheless, several issues need to be overcome for successful integration with the oxygenator. The main issue relates to heat generation and the size. A number of modifications such as reduction in inter-electrode space, increase in the area of the electrode, use of a more conductive electrode material, increase the molar concentration of the supporting electrolyte and use of air tight chambers can be considered in improve the performance.

A study needs to be performed on changes introduced by varying the inter-electrode spacing. A reduction in inter-electrode spacing would minimise the resistance, thus reducing the Joule heating. However, the critical inter-electrode spacing should be found, so the current density through the electrode is uniformly distributed. Furthermore, a heat exchanger could be added to the design to dissipate the heat generated within the system. A natural convection cooling system such as a heat spreader could be incorporated to the outside walls of the acrylic chamber. This method of passive cooling does not use a fan; therefore, the system can still be compact and no extra power is consumed. Moreover, the molar concentration of the solution can be increased to decrease the potential required to provide with 3 A to the system. Therefore, the Joule heating can be reduced. Finally, the use of more conductive materials to be utilised as electrodes can be explored. For instance, copper presents a greater conductivity (~40 times greater) than that of stainless steel. This greater conductivity would be expected to highly reduce the resistance and, thus, the potential required.

Once the temperature is controlled, the electrolysis-based system setup could be modified to force blood to uptake more O_2. The pressure in the electrolysis chamber, that encloses the SOU, could be increased to promote more blood O_2 uptake [22]. An airtight chamber, as the one shown in Figure 6.1, could be built with dimensions 16 cm by 8 cm by 10 cm that incorporates flanges to the design. The air in the chamber could be then replaced by the production of pure O_2 in-situ which would increase the pressure inside the chamber. Blood passing through an SOU immersed in the O_2 enriched environment with atmospheric pressure greater than one would be expected to reach full oxygenation.

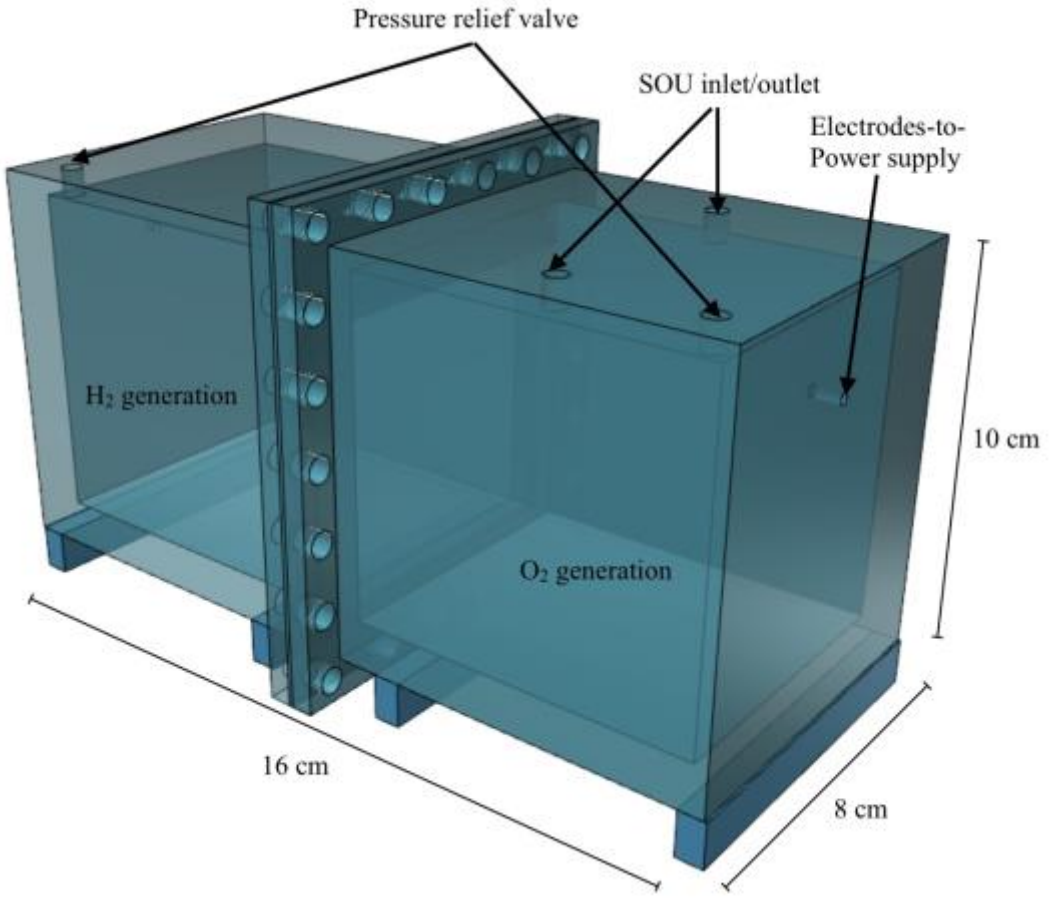

Figure 6.1 – *Modified electrolysis chamber.*

Alternatively, if the rise in temperature cannot be controlled with the aforementioned design, the electrolysis-based (O_2 generation) system could be separated from the oxygenation unit so that the temperature of blood does not change from its natural temperature. In this case, the chamber dimensions could be reduced creating an even more compact O_2 in-situ system. The inter-electrode spacing could also be reduced, therefore, reducing the resistance of the system. Moreover, air space could be smaller so that the volume of O_2 is easily moved towards the SOU connected by a PVC Tygon® tube to the electrolysis chamber. The SOU could also be modified so that a second inlet is added: one for blood and one for the O_2 generated in-situ with the electrolysis-based system. An alveolar chamber or O_2 chamber would then be required to separate blood from O_2 and restrict the O_2 from the atmosphere.

Additional to these aforementioned modifications of the cell a system with photovoltaic cells could be implemented so that the O_2 production does not depend on electricity. Thus, remote locations with minimal access to electrical power supply can also be benefit from this low cost and efficient oxygenator technology for preterm neonates. A commercially available solar cell that provides with 55 W [135] can be used to supply the 3 A required to produce the amount of O_2 needed for the SOU (114 mL/h) without interruption.

REFERENCES

[1] C. Metelo-Coimbra and R. Roncon-Albuquerque, "Artificial placenta: Recent advances and potential clinical applications," *Pediatr. Pulmonol.*, vol. 51, no. 6, pp. 643–649, 2016.

[2] R. J. Rodriguez, "Management of respiratory distress syndrome: an update.," *Respir. Care*, vol. 48, no. 3, pp. 279-86–7, 2003.

[3] American Lung Association, "Respiratory Distress Syndrome and Bronchopulmonary Dysplasia," pp. 111–116, 2008.

[4] C. P. Howson, M. V Kinney, L. McDougall, and J. E. Lawn, "Born too soon: preterm birth matters.," *Reprod. Health*, vol. 10 Suppl 1, no. Suppl 1, p. S1, 2013.

[5] H. Blencowe *et al.*, "Preterm birth-associated neurodevelopmental impairment estimates at regional and global levels for 2010.," *Pediatr. Res.*, vol. 74, no. S1, pp. 17–34, 2013.

[6] D. G. Sweet *et al.*, "European consensus guidelines on the management of neonatal respiratory distress syndrome in preterm infants - 2010 update," *Neonatology*, vol. 97, no. 4, pp. 402–417, 2010.

[7] D. G. Sweet *et al.*, "European consensus guidelines on the management of neonatal respiratory distress syndrome in preterm infants-2013 update," *Neonatology*, vol. 103, no. 4, pp. 353–368, 2013.

[8] N. Rochow *et al.*, "Artificial placenta - Lung assist devices for term and preterm newborns with respiratory failure," *Int. J. Artif. Organs*, vol. 36, no. 6, pp. 377–391, 2013.

[9] L. Lequier, "Extracorporeal life support in pediatric and neonatal critical care: a review.," *J. Intensive Care Med.*, vol. 19, no. 5, pp. 243–58, 2004.

[10] R. Veldhuizen, K. Nag, S. Orgeig, and F. Possmayer, "The role of lipids in pulmonary surfactant.," *Biochim. Biophys. Acta*, vol. 1408, no. 2–3, pp. 90–108, 1998.

[11] T. Stevens, "Surfactant replacement therapy," *Indian J. Pract. Pediatr.*, vol. 17, no. 1, pp. 52–55, 2007.

[12] A. Reininger *et al.*, "Surfactant administration by transient intubation in infants 29 to 35 weeks' gestation with respiratory distress syndrome decreases the likelihood of later mechanical ventilation: a randomized controlled trial.," *J. Perinatol.*, vol. 25, no. 11, pp. 703–8, 2005.

[13] N. S. Hakim and S. (Online Service), *Artificial organs*. 2009.

[14] A. Bougatef, "Neonatal Mechanical Ventilation Physiologic concepts," *Anaesthesia, Pain, Intensive Care Emerg. Med.*, pp. 73–81, 2005.

[15] M. J. Jeng, Y. S. Lee, P. C. Tsao, and W. J. Soong, "Neonatal air leak syndrome and the role of high-frequency ventilation in its prevention," *J. Chinese Med. Assoc.*, vol. 75, no. 11, pp. 551–559, 2012.

[16] S. Shankaran *et al.*, "Risk factors for early death among extremely low-birth-weight infants," *Am. J. Obstet. Gynecol.*, vol. 186, no. 4, pp. 796–802, 2002.

[17] N. Respiratory, *Manual of Neonatal Respiratory Care*, vol. 16, no. 2. 2001.

[18] J. a Potkay, "The promise of microfluidic artificial lungs.," *Lab Chip*, vol. 14, no. 21, pp. 4122–4138, 2014.

[19] W.-I. Wu *et al.*, "Lung assist device: development of microfluidic oxygenators for preterm infants with respiratory failure.," *Lab Chip*, vol. 13, no. 13, pp. 2641–50, 2013.

[20] R. P. Davis and G. B. Mychaliska, "Neonatal pulmonary physiology," *Semin. Pediatr. Surg.*, vol. 22, no. 4, pp. 179–184, 2013.

[21] P. Glass *et al.*, "Neurodevelopmental status at age five years of neonates treated with extracorporeal membrane oxygenation," *J. Pediatr.*, vol. 127, no. 3, pp. 447–457, 1995.

[22] T. a Nield, D. Langenbacher, M. K. Poulsen, and a C. Platzker, "Neurodevelopmental outcome at 3.5 years of age in children treated with extracorporeal life support: relationship to primary diagnosis.," *J. Pediatr.*, vol. 136, no. 3, pp. 338–44, 2000.

[23] H. Matharoo, "Oxygenating Unit of a Lung Assist Device for Term and Pre-Term Neonates with Respiratory Distress Syndrome," McMaster University, 2016.

[24] A. Manan, "Characterizing Gas Exchange and Assessing Feasibility of a New Lung Assist Device for Pre-Term and Term Neonates with Respiratory Distress Failure," 2013.

[25] N. Rochow *et al.*, "An integrated array of microfluidic oxygenators as a neonatal lung assist device: In-vitro characterization and in-vivo demonstration," *Artif. Organs*, vol. 38, no. 10, pp. 856–866, 2014.

[26] N. Rochow *et al.*, "Integrated microfluidic oxygenator bundles for blood gas exchange in premature infants," *Proc. IEEE Int. Conf. Micro Electro Mech. Syst.*, no. February, pp. 957–960, 2012.

[27] H. Turnbull, A. Conroy, R. O. Opoka, S. Namasopo, K. C. Kain, and M. Hawkes, "Solar-powered oxygen delivery: Proof of concept," *Int. J. Tuberc. Lung Dis.*, vol. 20, no. 5, pp. 696–703, 2016.

[28] M. B. Dobson, "Oxygen concentrators and cylinders," *Int. J. Tuberc. Lung Dis.*, vol. 5, no. 6, pp. 520–523, 2001.

[29] B. Ballisat and A. Hart, "Wrongly connected cylinder oxygen supply," *Anaesthesia*, vol. 69, no. 7, p. 791, 2014.

[30] R. a Malkin, "Design of health care technologies for the developing world.," *Annu. Rev. Biomed. Eng.*, vol. 9, pp. 567–87, 2007.

[31] F. Kelly and J. M. Donald, "Fire on intensive care caused by an oxygen cylinder," *Anaesth. News*, vol. 309, pp. 2012–2014, 2013.

[32] K. Chowdhury, "Fires in Indian hospitals: Root cause analysis and recommendations for their prevention," *J. Clin. Anesth.*, vol. 26, no. 5, pp. 414–424, 2014.

[33] U. Beckmann, D. M. Gillies, S. M. Berenholtz, A. W. Wu, and P. Pronovost, "Incidents relating to the intra-hospital transfer of critically ill patients. An analysis of the reports submitted to the Australian Incident Monitoring Study in Intensive Care.," *Intensive Care Med.*, vol. 30, no. 8, pp. 1579–1585, 2004.

[34] F. P. Smith, "Multiple deaths from argon contamination of hospital oxygen supply.," *J. Forensic Sci.*, vol. 32, no. July 1986, pp. 1098–1102, 1987.

[35] I. J. Gilmour, R. C. McComb, and R. J. Palahniuk, "Contamination of a hospital oxygen supply," *Anesth Analg*, vol. 71, no. 3, pp. 302–304, 1990.

[36] J. Weller, A. Merry, G. Warman, and B. Robinson, "Anaesthetists' management of oxygen pipeline failure: Room for improvement," *Anaesthesia*, vol. 62, no. 2, pp. 122–126, 2007.

[37] L. Mostert and A. R Coetzee, "Central oxygen pipeline failure," *South. African J. Anaesth. Analg.*, vol. 20, no. 5, pp. 214–217, 2014.

[38] K. M. Kovach *et al.*, "In-vitro evaluation and in-vivo demonstration of a biomimetic, hemocompatible, microfluidic artificial lung.," *Lab Chip*, vol. 15, no. 5, pp. 1366–75, 2015.

[39] M. W. Lim, "The history of extracorporeal oxygenators," *Anaesthesia*, vol. 61, no. 10, pp. 984–995, 2006.

[40] H. Iwahashi, K. Yuri, and Y. Nosé, "Development of the oxygenator: Past, present, and future," *J. Artif. Organs*, vol. 7, no. 3, pp. 111–120, 2004.

[41] N. W. Clowes GH Jr, Hopkins AL, "An artificial lung dependent upon diffusion of oxygen and carbon dioxide through plastic membranes.," *J. Thorac. Surg.*, vol. 32, pp. 630–637, 1956.

[42] J. A. Wegner, "Oxygenator anatomy and function," *J. Cardiothorac. Vasc. Anesth.*, vol. 11, no. 3, pp. 275–281, 1997.

[43] J. D. S. Gaylor, "Membrane oxygenators: current developments in design and application," *J. Biomed. Eng.*, vol. 10, no. 6, pp. 541–547, 1988.

[44] and C. M. M. Kay, Philip, *Techniques in Extracorporeal Circulation*, 4th ed. CRC Press, 2004.

[45] and L. H. E. J. Saxena, N. C., P. Hillyer, "Use of the spiral coil membrane oxygenator during open heart surgery in infants and children," *J. Cardiovasc. Surg. (Torino).*, vol. 18, no. 1, pp. 1–7, 1977.

[46] V. O. Björk, J. J. Sternlieb, and C. Davenport, "From the spinning disc to the membrane oxygenator for open-heart surgery.," *Scand. J. Thorac. Cardiovasc. Surg.*, vol. 19, no. 3, pp. 207–16, 1985.

[47] T.-K. Hung, "Transport and Flow Phenomena in a Microchannel Membrane Oxygenator," vol. 361, 1977.

[48] W. M. Zapol, T. Kolobow, J. E. Pierce, G. G. Vurek, and R. L. Bowman, "Artificial Placenta: Two Days of Total Extrauterine Support of the Isolated Premature Lamb Fetus," *Science (80-.).*, vol. 166, no. 3905, pp. 617–618, 1969.

[49] M. Cristina and A. Luigi, *Artificial Organs*. .

[50] R. H. Bartlett, "Extracorporeal life support: History and new directions," *Semin. Perinatol.*, vol. 29, no. 1, pp. 2–7, 2005.

[51] R. B. Hirschl, R. E. Schumacher, S. N. Snedecor, K. C. Bui, and R. H. Bartlett, "The efficacy of extracorporeal life support in premature and low birth weight newborns," *J. Pediatr. Surg.*, vol. 28, no. 10, pp. 1336–1341, 1993.

[52] and R. G. S. Federspiel, William J., "Lung, Artificial: Current Research and Future Directions," *Encycl. Biomater. Biomed. Eng.*, pp. 922–931, 2004.

[53] R. J. Gilbert *et al.*, "Computational and functional evaluation of a microfluidic blood flow device.," *ASAIO J.*, vol. 53, no. 4, pp. 447–455, 2007.

[54] J. K. Lee, H. H. Kung, and L. F. Mockros, "Microchannel technologies for artificial lungs: (1) theory.," *ASAIO J.*, vol. 54, no. 4, pp. 372–82, 2008.

[55] *Department MC Kung*, JK Lee*, HH Kung*, and LF Mockros*, "Microchannel Technologies for Artificial Lungs: (2) Screen-filled Wide Rectangular Channels," vol. 54, no. 4, pp. 383–389, 2009.

[56] L. M. JK Lee, MC Kung, HH KUng, "Microchannel Technologies for Artificial Lungs: (3) Open Rectangular Channels," *ASAIO J. NIH Public Access*, vol. 54, no. 4, pp. 390–395, 2008.

[57] K. A. Burgess, H. Hu, W. R. Wagner, and W. J. Federspiel, "Towards microfabricated biohybrid artificial lung modules for chronic respiratory support," pp. 117–127, 2009.

[58] J. A. Potkay and D. Ph, "a High Efficiency Micromachined Artificial Lung," pp. 2234–2237, 2009.

[59] D. M. Hoganson *et al.*, "Branched vascular network architecture: a new approach to lung assist device technology.," *J. Thorac. Cardiovasc. Surg.*, vol. 140, no. 5, pp. 990–995, 2010.

[60] J. a Potkay, M. Magnetta, A. Vinson, and B. Cmolik, "Bio-inspired, efficient, artificial lung employing air as the ventilating gas.," *Lab Chip*, vol. 11, no. 17, pp. 2901–2909, 2011.

[61] D. M. Hoganson, H. I. Pryor, E. K. Bassett, I. D. Spool, and J. P. Vacanti, "Lung assist device technology with physiologic blood flow developed on a tissue engineered scaffold platform.," *Lab Chip*, vol. 11, no. 4, pp. 700–707, 2011.

[62] A. J. Thompson, L. H. Marks, M. J. Goudie, A. Rojas-Pena, H. Handa, and J. A. Potkay, "A small-scale, rolled-membrane microfluidic artificial lung designed towards future large area manufacturing," *Biomicrofluidics*, vol. 11, no. 2, 2017.

[63] T. Kniazeva *et al.*, "Performance and scaling effects in a multilayer microfluidic extracorporeal lung oxygenation device," *Lab Chip*, vol. 12, no. 9, p. 1686, 2012.

[64] W. Wu *et al.*, "Development of Microfluidic Oxygenators as Lung Assisting Devices for Preterm Infants," *15th Int. Conf. Miniaturized Syst. Chem. Life Sci.*, no. January, pp. 550–552, 2011.

[65] T. Rieper, C. M??ller, and H. Reinecke, "Novel scalable and monolithically integrated extracorporeal gas exchange device," *Biomed. Microdevices*, vol. 17, no. 5, pp. 1–10, 2015.

[66] J. A. Potkay, "Reply to the 'Comment on "The promise of microfluidic artificial lungs"' by G. Wagner, A. Kaesler, U. Steinseifer, T. Schmitz-Rode and J. Arens, Lab Chip, 2016, **16** , DOI: 10.1039/C5LC01508A," *Lab Chip*, vol. 16, pp. 1274–1277, 2016.

[67] C. Higgins, "The use of heparin in preparing samples for blood-gas analysis.," *MLO. Med. Lab. Obs.*, vol. 39, no. 10, pp. 16–18, 20-23, 2007.

[68] R. Society and B. Sciences, "Ventures with an Artificial Placenta . I . Principles and Preliminary Results Author (s): L . Lawn and R . A . McCance Source : Proceedings of the Royal Society of London . Series B , Biological Sciences , Vol . 155 , Published by : Royal Society Stable," vol. 155, no. 961, pp. 500–509, 2017.

[69] B. Y. D. P. Alexander, H. G. Britton, D. A. Nixon, and D. P. Alexander, "Survival of the foetal sheep at term following short periods of perfusion through the umbilical vessels," *J. Physiol.*, pp. 113–124, 1964.

[70] T. Kniazeva, J. C. Hsiao, J. L. Charest, and J. T. Borenstein, "A microfluidic respiratory assist device with high gas permeance for artificial lung applications," *Biomed. Microdevices*, vol. 13, no. 2, pp. 315–323, 2011.

[71] and W. J. K. SenGupta, Amarendra, Howard P. Taylor, "An artificial placenta designed to maintain life during cardiorespiratory distress," *ASAIO J.*, vol. 10, no. 1, pp. 63–65, 1964.

[72] Y. Kuwabara *et al.*, "Development of Extrauterine Fetal Incubation Sys tern Using Extracorporeal Membrane Oxygenator," vol. 11, no. 3, pp. 224–227, 1987.

[73] Y. Kuwabara *et al.*, "Artificial Placenta : Long-Term Extrauterine Incubation of Isolated Goat Fetuses," vol. 13, no. 6, pp. 527–531, 1989.

[74] N. Unno *et al.*, "Development of an Artificial Placenta : Survival of Isolated Goat Fetuses for Three Weeks with Umbilical Arteriovenous Extracorporeal Membrane Oxygenation," vol. 17, no. 12, pp. 996–1003, 1993.

[75] M. Sakata, K. Hisano, M. Okada, and M. Yasufuku, "A new artificial placenta with centrifugal pump: long-term total," pp. 1023–1031, 1998.

[76] J. Arens *et al.*, "NeonatOx: A Pumpless Extracorporeal Lung Support for Premature Neonates," *Artif. Organs*, vol. 35, no. 11, pp. 997–1001, 2011.

[77] B. W. Gray *et al.*, "Development of an Artificial Placenta IV," *ASAIO J.*, p. 1, 2012.

[78] Y. Miura *et al.*, "Novel modification of an artificial placenta: pumpless arteriovenous extracorporeal life support in a premature lamb model.," *Pediatr. Res.*, vol. 72, no. 5, pp. 490–4, 2012.

[79] B. Bryner *et al.*, "An extracorporeal artificial placenta supports extremely premature lambs for 1 week," *J. Pediatr. Surg.*, vol. 50, no. 1, pp. 44–49, 2015.

[80] "Maquet Quadrox-i Neonatal." [Online]. Available: https://www.maquet.com/int/products/quadrox-i-neonatal-and-pediatric/.

[81] "CAPIOX FX 05 Baby." [Online]. Available: https://www.terumo-cvs.com/products/ProductDetail.aspx?groupId=1&familyID=801&country=1.

[82] "Dideco D100." [Online]. Available: http://www.livanova.sorin.com/file/view-1559.action.

[83] J. Dingley, D. Williams, P. Douglas, M. Douglas, and J. O. Douglas, "The development and evaluation of a non-pressurised, chemical oxygen reaction generation vessel and breathing system providing emergency oxygen for an extended duration," *Anaesthesia*, pp. 1464–1470, 2016.

[84] T. C. Blakeman *et al.*, "Evaluation of Oxygen Concentrators and Chemical Oxygen Generators at Altitude and Temperature Extremes," vol. 181, no. c, 2017.

[85] K. R. Ward, G. S. Huvard, M. McHugh, R. R. Mallepally, and R. Imbruce, "Chemical oxygen generation," *Respir. Care*, vol. 58, no. 1, pp. 184–195, 2013.

[86] M. A. Machado, D. A. Rodriguez, Y. Aly, M. Schoenitz, E. L. Dreizin, and E. Shafirovich, "Nanocomposite and mechanically alloyed reactive materials as energetic additives in chemical oxygen generators," *Combust. Flame*, vol. 161, no. 10, pp. 2708–2716, 2014.

[87] A. G. Catto *et al.*, "An evaluation of oxygen systems for treatment of childhood pneumonia," *BMC Public Health*, vol. 11, no. Suppl 3, p. S28, 2011.

[88] T. Duke *et al.*, "Improved oxygen systems for childhood pneumonia: a multihospital effectiveness study in Papua New Guinea," *Lancet*, vol. 372, no. 9646, pp. 1328–1333, 2008.

[89] K. Kinoshita, *Electrochemical oxygen technology*. John Wiley & Sons, 1992.

[90] E. Zoulias and E. Varkaraki, "A review on water electrolysis," *Tcjst*, vol. 4, no. 2, pp. 41–71, 2004.

[91] D. R. Crow, *Principles and applications of electrochemistry*. CRC Press, 1994.

[92] B. L. Bursten, *Brown LeMay Bursten ®*. 2004.

[93] K. Zeng and D. Zhang, "Recent progress in alkaline water electrolysis for hydrogen production and applications," *Prog. Energy Combust. Sci.*, vol. 36, no. 3, pp. 307–326, 2010.

[94] J. M. Oldham, Keith, "Fundamentals of electrochemical science," Elsevier, 2012.

[95] C. Neagu, H. Jansen, H. Gardeniers, and M. Elwenspoek, "Electrolysis of water: An actuation principle for MEMS with a big opportunity," *Mechatronics*, vol. 10, no. 4, pp. 571–581, 2000.

[96] J. E. Bennett, "Electrodes for Generation of Hydrogen a N D Oxygen From Seawater," vol. 5, pp. 401–408, 1980.

[97] R. P. Viswanath, "A patent for generation of electrolytic hydrogen by a cost effective and cheaper route," *Int. J. Hydrogen Energy*, vol. 29, no. 11, pp. 1191–1194, 2004.

[98] "The Oxygenator." [Online]. Available: http://www.keepfishalive.com/pro-livewell-flush-mount.php.

[99] J. A. Senkiw, "Flow-through oxygenator," US 7670495 B2, 2010.

[100] "Livewell oxygenator generator." [Online]. Available: http://oxyedge-chum.com/oxygen-generator/electrolysis-type/.

[101] G. Chen, "Electrochemical technologies in wastewater treatment," *Sep. Purif. Technol.*, vol. 38, no. 1, pp. 11–41, 2004.

[102] M. McLachlan, D. MacKay, and P. H. Jones, "A conceptual model of organic chemical volatilization at waterfalls," *Environ. Sci. Technol.*, vol. 24, no. 2, pp. 252–257, 1990.

[103] L. A. Woodbury, "A Sudden Mortality of Fishes Accompanying a Supersaturation of Oxygen in Lake Waubesa, Wisconsin," *Trans. Am. Fish. Soc.*, vol. 71, no. 1, pp. 112–117, 1942.

[104] W. Butler and J. H. Coste, "Seasonal Variations in the Dissolved Oxygen Content of the Water of the Thames Estuary," *Biochem. J.*, vol. 17, pp. 49–58, 1923.

[105] U. P. Prec, "Supersaturation of Oxygen in Acidic," vol. 23, pp. 619–621, 1978.

[106] J.G. De Mey and P.M. Vanhoutte, "Heterogeneous Behavior of the Canine Arterial and Venous Wall Importance of the Endothelium," *Circ. Res.*, vol. 51, pp. 439–447, 1979.

[107] G. B. Richerson, "Serotonergic neurons as carbon dioxide sensors that maintain ph homeostasis," *Nat. Rev. Neurosci.*, vol. 5, no. 6, pp. 449–461, 2004.

[108] J. Deptula, M. Valleley, K. Glogowski, J. Detwiler, J. Hammel, and K. Duncan, "Clinical Evaluation of the Terumo Capiox ® FX05 Hollow Fiber Oxygenator with Integrated Arterial Line Filter," pp. 220–225, 2009.

[109] D. U. H. S. C. L. M. D. Laboratory, "IL GEM 3000 AND 682 CO-OXIMETER," 2015.

[110] J. Viskupicova *et al.*, "Effect of high glucose concentrations on human erythrocytes in-vitro," *Redox Biol.*, vol. 5, pp. 381–387, 2015.

[111] K. D. McClatchey, *Clinical laboratory medicine*. Lippincott Williams & Wilkins, 2002.

[112] A. H. Jobe and E. Bancalari, "Bronchopulmonary Dysplasia," *Am. J. Respir. Crit. Care Med.*, vol. 163, pp. 1723–1729, 2001.

[113] M. E. Rollie, G. Patonay, and I. M. Warner, "Deoxygenation of solutions and its analytical applications," *Ind. Eng. Chem. Res.*, vol. 26, no. 1, pp. 1–6, 1987.

[114] P. Dürre, *Handbook on clostridia*. CRC press, 2005.

[115] YSI, "YSI 550A Handheld Dissolved Oxygen and Temperature System, Service Manual." 2003.

[116] H. K. Abdel-Aal, S. M. Sultan, and I. A. Hussein, "Parametric study for saline water electrolysis: Part II-Chlorine evolution, selectivity and determination," *Int. J. Hydrogen Energy*, vol. 18, no. 7, pp. 545–551, 1993.

[117] Dow Water & Process Solutions, "FILMTECTM Reverse Osmosis Membranes, Technical Manual," 2011.

[118] and J. W. Ralls, Kenneth M., Thomas H. Courtney, *Introduction to materials science and engineering*. Wiley, 1976.

[119] T. Heinrich, "The oxidation of carbon in electrolytes at normal temperature," *Trans. Faraday Soc.*, vol. 34, 1938.

[120] J. O. Besenhard and H. P. Fritz, "Cathodic reduction of graphite in organic solutions of alkali and NR4+ salts," *J. Electroanal. Chem.*, vol. 53, no. 2, pp. 329–333, 1974.

[121] F. Environmental, "'Dissolved Oxygen.' Fundamentals of Environmental Measurements," 2013. [Online]. Available: http://www.fondriest.com/environmental-measurements/parameters/water-quality/dissolved-oxygen/.

[122] J. González-Alonso and J. A. L. Calbet, "Reductions in systemic and skeletal muscle blood flow and oxygen delivery limit maximal aerobic capacity in humans," *Circulation*, vol. 107, no. 6, pp. 824–830, 2003.

[123] B. W. Gray *et al.*, "Development of an artificial placenta V: 70 h veno-venous extracorporeal life support after ventilatory failure in premature lambs," *J. Pediatr. Surg.*, vol. 48, no. 1, pp. 145–153, 2013.

[124] M. Reynolds, "Plasma and blood volume in the cow using the T-1824 hematocrit method," *Am. J. Physiol.*, vol. 173, no. 3, pp. 421–427, 1953.

[125] L. E. Orme and P. Brady, "Effective pulmonary bood flow in preterm infants with and without respiratory distress:," vol. 52, no. 2, 1973.

[126] M. Dabaghi, "Unpublished data of the composite conventional SOU exposed to pure oxygen."

[127] A. J. Bloom, H. A. Mooneyt, O. Bjorkmanj, and J. Berryj, "Materials and methods for carbon dioxide and water exchange analysis," *Plant Cell Environ.*, vol. 3, no. 5, pp. 371–376, 1980.

[128] G. J. C. G. M. Bosman, J. M. Werre, F. L. A. Willekens, and V. M. J. Novotný, "Erythrocyte ageing in-vivo and in-vitro: Structural aspects and implications for transfusion," *Transfus. Med.*, vol. 18, no. 6, pp. 335–347, 2008.

[129] J. M. Zhao, C. S. Clingman, M. J. Närväinen, R. A. Kauppinen, and P. C. M. Van Zijl, "Oxygenation and hematocrit dependence of transverse relaxation rates of blood at 3T," *Magn. Reson. Med.*, vol. 58, no. 3, pp. 592–597, 2007.

[130] and C. R. H. Skeggs Jr, Leonard T., Jack R. Leonards, "Artificial Kidney. II. Construction and Operation of an Improved Continuous Dialyzer.*," *Proc. Soc. Exp. Biol. Med.*, vol. 72, no. 3, pp. 539–543, 1949.

[131] W. S. Haworth, "The Development of the Modern Oxygenator," *Ann. Thorac. Surg.*, vol. 76, no. 6, 2003.

[132] D. W. Ballentyne, *A dictionary of named effects and laws in chemistry, physics and mathematics*. Springer Science & Business Media, 2012.

[133] H.-W. Lin, R. Cejudo-Marín, A. W. Jeremiasse, K. Rabaey, Z. Yuan, and I. Pikaar, "Direct anodic hydrochloric acid and cathodic caustic production during water electrolysis.," *Sci. Rep.*, vol. 6, no. 20494, pp. 1–4, 2016.

[134] S. Chien, S. Usami, R. J. Dellenback, and M. I. Gregersen, "Shear-dependent in rheology deformation blood of erythrocytes of human," *Am. J. Physiol.*, vol. 219, no. 1, pp. 136–142, 1970.

[135] S. panel Store, "Photovoltaic cells." [Online]. Available: http://www.solarpanelstore.com/solar-power/small-solarpanels/solarland_standard_modules/solarland5512.html.

[136] The National Hydrogen Association, "Hydrogen: Similar but Different," pp. 9–10.

APPENDIX

APPENDIX A

A.1 FABRICATION

A.1.1 Composite Conventional SOU Fabrication

A.1.1.1 *PDMS Degas Process*

1. Mix silicon elastomer base and curing agent (10:1 by mass ratio) for 1 minute.
2. Place the plastic beaker in the vacuum desiccator. Turn on the vacuum pump and make sure the valve is opened so that the extraction of gases can be done.
3. After 3 min close the valve so that the desiccator is closed to the pass of air. Turn off the pump.
4. Slightly open the valve until a hissing sound is perceived. Then, stop opening the valve.
5. Let the PDMS sit for 15 min in the chamber.
6. If, after 15 min, a lot of bubbles still present, then repeat step 4 and wait for another 5 min.
7. When the PDMS is clear of bubbles remove it from the chamber.

A.1.1.2 *Composite Membrane Fabrication*

8. Preheat the furnace at 100ºC.
9. Cut off a stainless-steel mesh (Asada Hardmesh® *MS-400/19* – DynaMesh) sizing 8X8cm. Make sure the mesh does not have any wrinkles or loose wires that might perforate the PDMS membrane.
10. Load a small syringe with PDMS.
11. Use a silicon wafer with an anti-adhesive coating (Bytac® FEP Film General Purpose with Vinyl Back – US Plastics Corp.®).

12. Turn on the spin coater and introduce the recipe (save the recipe in step 1). The recipe is as follows: 4000 rmp, 5 sec of ramp, and 40 sec of dwell time.
13. Clean both sides of the wafer with IPA.
14. Place the clean wafer in the spin coater. Center it with the chuck.
15. Turn on the vacuum pump and open the compressed air line.
16. Push 1ml of the PDMS to the center of the wafer. Close the lid of the spin coater and start the spin coating process.
17. Once the spinner stops, take off the lid. Gently deposit the stainless-steel mesh on the wafer. Carefully push the mesh against the wafer.
18. Cure the PDMS at 100ºC for 3 min.
19. Then, cut off the protruding corners of the mesh.
20. Take the wafer to the spinner and center it to the chuck.
21. Repeat step 9 and 11.
22. Cover the composite membrane with a KimWipe and store it in a petri dish.

A.1.1.3 *Air Plasma Bonding*

23. Preheat the furnace at 80ºC
24. Clean the composite membrane and the vascular network side using compressed air.
25. Position both parts of the SOU on a non-conductive surface. Use the handheld corona treater (BD20-AC – Electro-Technic Products ®) to treat the two parts of the SOU.
26. The wire electrode must be as close as possible to the surface (but not touching it) so that plasma production is stable and the sparkling is reduced.
27. Turn on the power and gently move back and forth the wire electrode trying to expose all the area facing the wire. Repeat the slow movement for 30sec.

28. Right away, start treating the second surface on the same way as in point 4.
29. Then, softly press together both surfaces being cautious that the membrane is fully covering the vascular network. Keep pressing the whole bonded area for a minute or so.
30. Next, place the SOU in the furnace at 80ºC and leave it overnight.
31. Carefully peel off the membrane and the device itself from the wafer.
32. Cover the membrane side with a KimWipe and store it in a petri dish.

A.1.2 Agarose Gel Filter Paper Membranes

1. Cut the required filter paper membranes.
2. Cut some plastic wrap and extend the plastic on the bench.
3. Prepare 1 M KNO_3 using deionized water.
4. Mix 2% of agar powder into 1 M KNO_3.
5. Put a glass beaker with the mixture in the microwave for 1 minute or until the agar is melted. A temperature of up to 85ºC needs to be reached to melt the agar.
6. Put the glass beaker in a preheated (200ºC) hot plate with a magnetic stirrer to maintain the agar melted.
7. Mix the solution at 130 rpm to keep it homogeneously hot.
8. Dip in the membranes (one at a time) and place the membrane on top of the plastic wrap.
9. Use a microscope slide to gently push into the pores the agarose gel. Create a smooth surface removing any gel excess using the glass slide.
10. Repeat the process for the other paper membranes.
11. Once all the gel membranes are fabricated wrap them in the plastic and store them in the fridge for up to three weeks.

A.2 EXPERIMENTAL SETUP

A.2.1 Setting Blood Oxygen Level

1. Fix the setup as shown in Figure 4.6**.**
2. Use Parafilm® M to cover the mouth of the outlet bottle. Poke the film to introduce a Tygon® PVC tube down to the bottom of the bottle. Use transparent tape to cover most of the film and hole made.
3. Calibrate the peristaltic pump.
4. Take the bottle with blood out of the refrigerator. Add 3 units/ml of Heparin and 1.5 mmol/L of glucose to the blood. Gently spin around the container to allow the blood to mix properly. Put in a stir bar.
5. Repeat step 2 for the inlet bottle.
6. Place the inlet bottle on the magnetic stirrer. Fix the mixing at a slow, gentle speed.
7. Let the 95% N_2-5% CO_2 mixture fill the hollow fibre oxygenator. Twist the knob until it is fully opened (approximately 20 bar).
8. A 3-way valve is located at the outlet of the oxygenator but before the collecting bottle. Turn the valve so that the collecting path is closed and the blood comes out at to the sampling beaker.
9. Start pumping the blood at 5 ml/min. Take the first sample after 5 min and place it in the gas analyzer (GEM Premier 3000 - Instrumentation Laboratory).
10. After obtaining the reading change the flow rate accordingly (e.g. decrease the flow to reduce the SaO_2 in blood).
11. Repeat step 10 as many times as needed.
12. Start collecting the deoxygenated blood when the desired SaO_2 is obtained.

13. Once the process is finished, tightly close the collecting container, and store the deoxygenated blood in the refrigerator.

A.2.2 Cleaning of the Hollow Fibre Oxygenator

The coagulation cascade of blood roughly starts when the peristaltic pump is stopped. Hence, the importance to flush the blood away of the HFO right after finishing the deoxygenation of blood.

The cleaning process has several steps, and it could vary from one day to three days of cleaning (Figure A. 1). For the first two stages, the setup was essentially the same as for the deoxygenation process, but cold water was pumped and compressed air supplied instead of blood and N_2CO_2 gas mixture, respectively.

The first step was to pump water at the maximum flow rate that the pump could sustain (Figure A. 1(**a)**). Water was used to try to remove as much blood as possible before the clots of blood were formed. Once the blood was not leaving a taint anymore, pressurised air was incorporated into the water flow (Figure A. 1 (**b)**). The bubbles formed served to scrub inside the fibres to detach any clot formation. Finally, the setup was changed moving the HFO into a 37ºC precision water bath (Thermo ScientificTM 2825) and rinsing it out with an enzymatic cleaner to remove the remaining clots (Figure A. 1 (**c)**). The enzymatic cleaner broke down the proteins, so the clots stood a better chance to be flushed out; 10 ml of cleaner was diluted in 1L of water. Enzymatic solution and compressed air were pumped into the inlet of the oxygenator overnight (8 to 12 h). Later, if more cleaning was required, the enzymatic solution was replaced approximately every 8 hours; and was continuously pumped until cleansed.

1. Fix the setup(a) as shown in Figure A. 1 (a).
2. Pump cold water at the maximum flow rate that the peristaltic pump can supply.
3. If no more stained water with a bloody colour is visible, stop the pump and change to setup(b) (Figure A. 1 (b)).
4. Open the compressed air knob to 20 bar and start pumping cold water (in that order) at the maximum flow rate.
5. After an hour or so when no more blood is being scrubbed out, stop the pump and close the compressed air knob. Change to setup(c) (Figure A. 1 (c)).
6. Fill up half of the bath chamber with water and turn on the system fixed at 37ºC.
7. Dilute 10 ml of enzymatic cleaner in 1 L of water. Place the beaker in the water bath.
8. Bring in the hollow fibre oxygenator to the water bath. Make the proper connection to the compressed air line and enzymatic solution, and screw them onto side 1 of the oxygenator.
9. Repeat step 4 (instead of water, enzymatic solution runs through the system).
10. Clean the fibres for 8 hours or leave running the setup overnight.
11. Stop the pump and close the compressed air knob (in that order).
12. Change the connections direction. Connect the compressed air and the enzymatic solution lines to side 2 of the oxygenator.
13. Replace the enzymatic cleaner solution for a new one. Repeat step 7.
14. Repeat step 9 to 12 as many times until the hollow fibres are completely clean or close to being fully clean (e.g. blood clots present in just a few fibres).

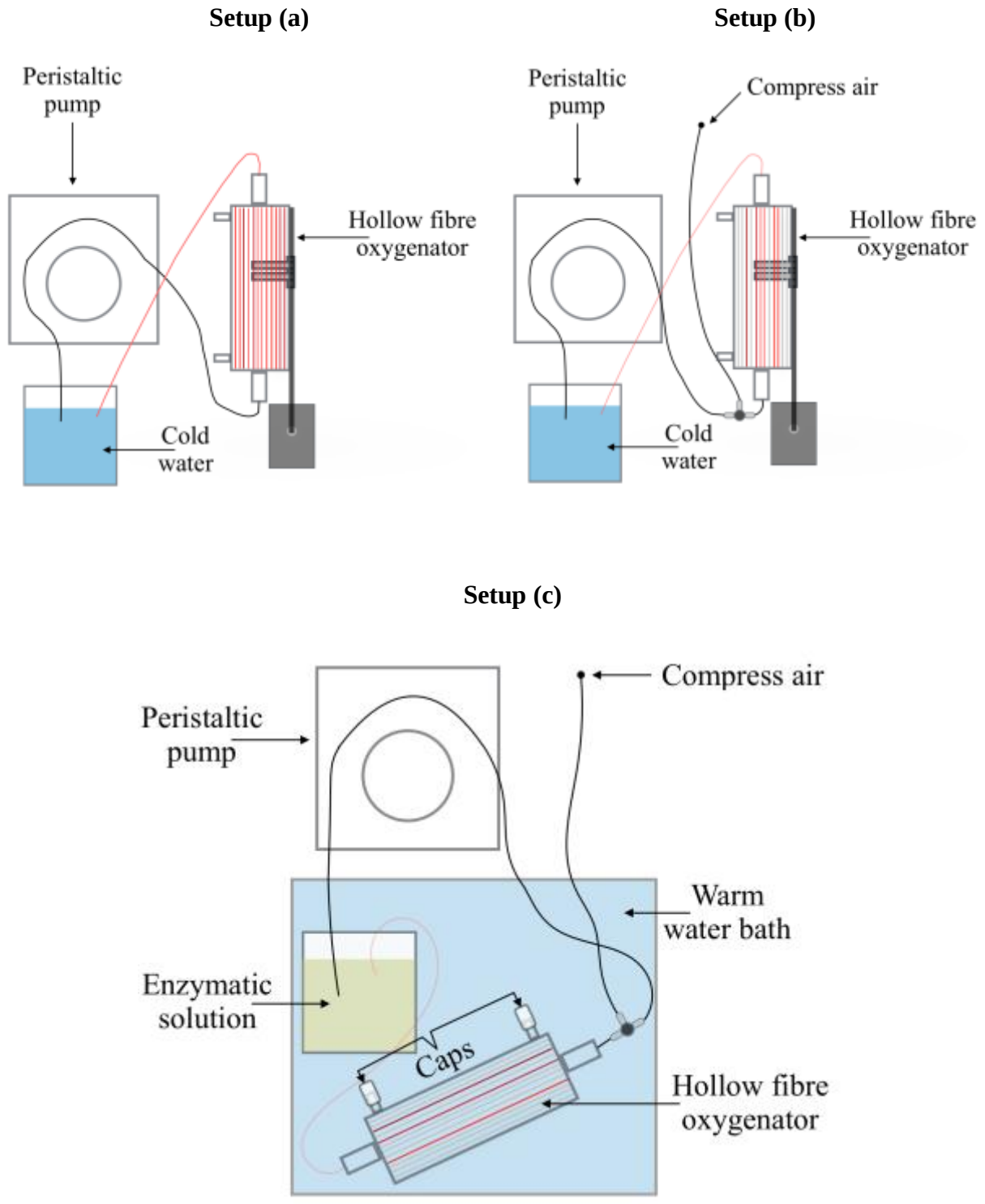

Figure A. 1 - *Schematic for the hollow fibres cleansing. The cleansing order was (a), (b) & (c), respectively. (a)&(b) water was pumped until no more blood came out. (c) compressed air and enzymatic solution were pumped until the HFO was visibly clean.*

A.3 TESTING

A.3.1 Hydraulic Resistance Test

1. Calibrate the peristaltic pump. Then, set it at the maximum flow rate.
2. Prepare a water and food colouring mixture. Use approximately 8 droplets for 50ml of water.
3. Place the inlet tube of the peristaltic pump in the beaker and connect the outlet tube to the pressure transducer.
4. Connect the outlet of the transducer to the inlet of the SOU. Make sure the SOU is at the same level as the transducer.
5. The outlet of the SOU goes back to the beaker.
6. Fill a syringe with 3 ml of water and connect it to the back of the transducer.
7. Connect the transducer wire to the pressure monitor. Turn on the pressure monitor.
8. Fill up the whole system with the mixture. Once it is filled, stop the pump.
9. On the pressure monitor select “ART” and press “zero”. When the arterial pressure indicates “0” start pumping the mixture through the system.
10. Run the test for 5min at the maximum flow rate. Keep track of the fluctuations in the pressure drop. It should not vary that much.
11. After 5min write down the pressure drop and the flow rate of that specific SOU.
12. Dismount the SOU and carefully remove the mixture using tap water. Stop when almost all the food colouring is gone.
13. Cover the membrane of the SOU with a KimWipe and store the SOU in a petri dish.

A.3.2 Hematocrit Measurement

1. Take a small sample with a syringe.
2. Fill the capillary tube (Plastic Microhematocrit Tubes - StatSpin™ SafeCrit™) with the blood making sure that no air gaps are formed.
3. Seal one side of the tube with vinyl plastic putty (Capillary Tube Sealant - Leica Microsystems Critoseal™), placed it in the micro-hematocrit rotor, and screw-on the transparent lid.
4. Insert the rotor in the centrifuge (Microhematocrit Centrifuge - StatSpin® CritSpin™) and start the centrifuge process.
5. Use the digital reader (Digital Hematocrit Reader - Beckman Coulter StatSpin™) to measure the packed red cells.

A.3.3 Variables that Affect the Oxygen Uptake in Blood

In this section, experiments were designed to assess the O_2 uptake behaviour so blood age and tubing permeability to O_2 could be taken into account for the in-vitro experiments. Two experiments were proposed: analysing the transfer of O_2 through the tubing used and observing the change in the haemoglobin (Hb) content in the RBCs over 2 weeks.

A.3.3.1 Effect of PVC Tygon® Tube in Blood Oxygenation

It is well known that one of the PVC characteristics is its low permeability to gases [127]. A verification of the O_2 transferred due to the tubing was tested at a low flow rate. Blood was pumped across a PVC Tygon® tube to evaluate how much O_2 was transferred to the blood.

Bovine blood with an average SaO_2 of 55% was loaded into a 60 ml syringe. A syringe pump was used with a flow rate of 1.5ml/min to give the blood more residence time in the tube. The length of the tube was 36 cm with a priming volume of 3.66 ml. Right after the syringe, a control station was set up and the sample being affected by the tube was taken at the end of the tube (Figure A. 2).

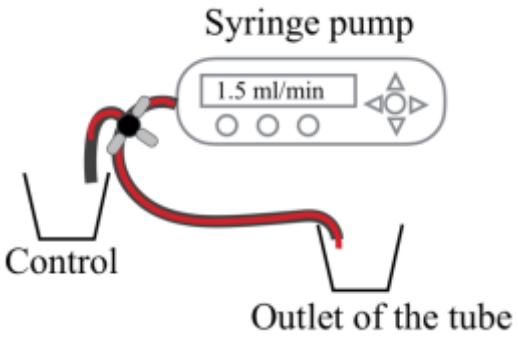

Figure A. 2 - *Setup to measure the O_2 content in blood to test the gas transfer due to the tubing used.*

The results showed that the saturation of O_2 did not change over time. Therefore, the ΔSaO_2 should be taken merely as the blood O_2 uptake from the SOU when running in-vitro experiments.

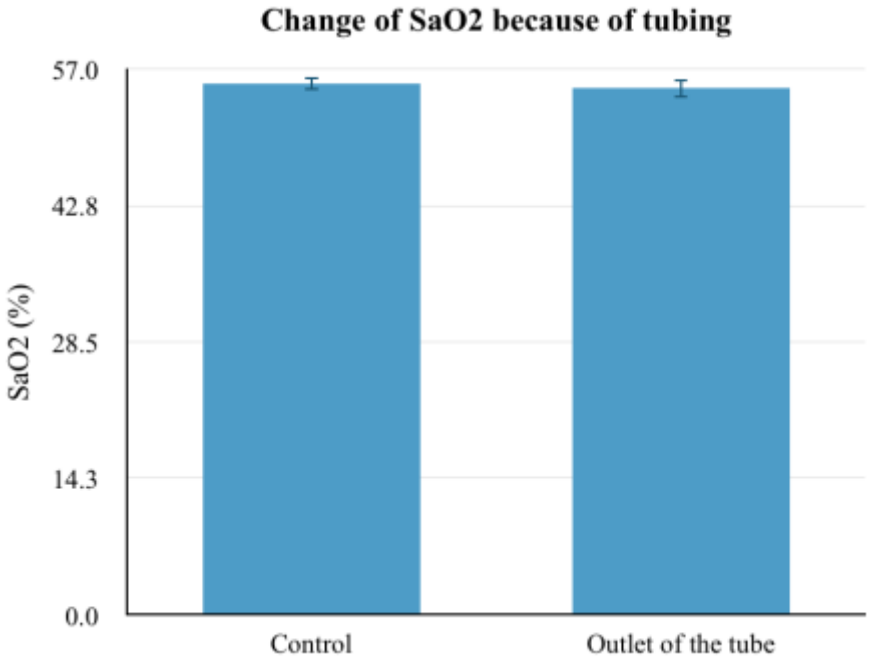

Figure A. 3 - *Change on O_2 concentration in blood because of PVC Tygon® tube.*

A.3.3.2 Effect of Blood's Age on the Oxygen Uptake

It is well known that the proteins and cells in the blood start to decay over time including the lysis of RBCs which contain the Hb that binds to O_2 [128]. The lysis of blood directly reduces the capacity of free O_2 to bind to the available haemoglobin. Experiments with blood were performed on day 2, 8 and 15 to assess how the freshness of the blood affects the Hb content.

The experiment consisted of running a PO (procedure explained in Chapter 4, Section 4.3.6.1) on day 2, 8 and 15 starting the count from the day the blood was received. Three sets of experiments were run for each day. The setup was the same as the one mentioned on Section 4.3.6 for the PO.

The graph below (Figure A. 4) shows that there is a statistically significant reduction in Hb content in the RBCs after the first week has passed. The decrease in Hb content when comparing it with day 2 is closer to 3.3% for the first week and almost 5% by week two. Therefore, every week the RBCs are losing their capacity to bind with free O_2 affecting, to a certain extent, the uptake of O_2. Consequently, during the course of this experiment, blood is considered fresh only within the first week to prevent any divergence that might be caused when trying to oxygenate the blood. Hence, in-vitro experiments were performed within the first 7 days upon receiving of the blood.

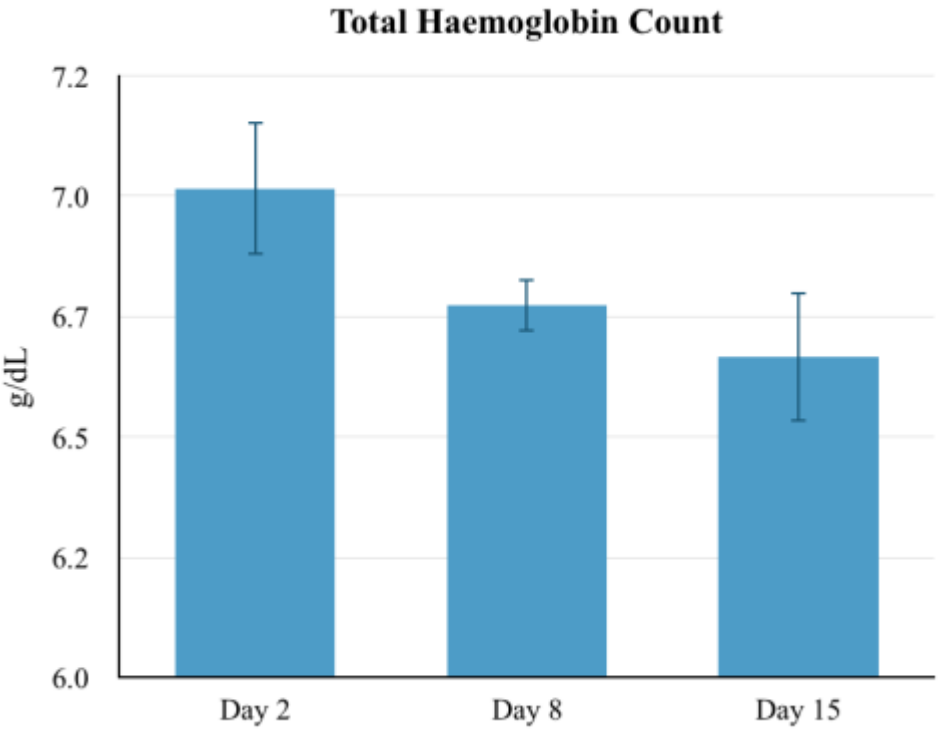

Figure A. 4- *Change of haemoglobin count over 2 weeks.*